

Trauma, 9e >

Chapter 19: Diagnostic and Interventional Radiology

Scott D. Steenburg

KEY POINTS

KEY POINTS

- Imaging is a critical adjunct to the comprehensive evaluation of the trauma patient.
- Imaging protocols specific to blunt and penetrating trauma victims should be clearly defined and operationalized to enhance rapid imaging and patient throughput.
- Modern computed tomography (CT) technology and imaging protocols allow for high-resolution imaging of any body part.
- Advanced imaging exams, such as extremity and neck CT angiography, can now be integrated as a part of the initial imaging evaluation of the trauma patient.
- Multiphase CT can provide important information regarding the presence and character of vascular lesions, including active bleeding and solid organ pseudoaneurysms.

INTRODUCTION

Obtaining reliable clinical history and a physical examination may be challenging in the acute trauma patient. Thus imaging can provide timely and helpful information about these patients and identify injuries that otherwise may not be readily recognized. Imaging can be used to assist in injury prioritization and patient triage, as well as guiding the trauma surgeon toward any number of management choices. Despite the advanced imaging technology available in a modern trauma center, it is important to recognize that imaging alone cannot be used to make management decisions in isolation; that is, the surgeon must treat the patient based on an experienced integration of their clinical assessment and diagnostic images.

Practical variables that affect imaging strategies include the proximity of available imaging technology to the resuscitation area, the technical capabilities of the imaging equipment, the experience and availability of radiology technologists performing these imaging procedures, and timely access to expert interpretation and reporting.

Imaging is typically initiated in the trauma bay and integrated as a part of the clinical survey. However, it should reflect the needs of each individual patient. Hemodynamically unstable patients should be resuscitated prior to imaging according to accepted guidelines and recommendations, with some exceptions for image-guided endovascular hemostasis techniques in select scenarios (eg, resuscitative endovascular balloon occlusion of the aorta [REBOA]). To enhance efficiency, imaging should be obtained based on the acute needs for accurate information that can be used to direct treatment of the patient. Close cooperation and open communication between all major stakeholders, including emergency medicine physicians, traumatologists, consultants, nurses, imaging technologists, and radiologists, are essential to optimize any imaging assessment and provide superior patient care.

A single chapter alone cannot reasonably teach interpretation of diagnostic images. Instead, a general overview of trauma imaging strategies is provided. In addition, reflecting current trends in the modern trauma center, an emphasis on advanced computed tomography (CT) technology and capabilities, focusing on select high-yield and common clinical scenarios, is presented.

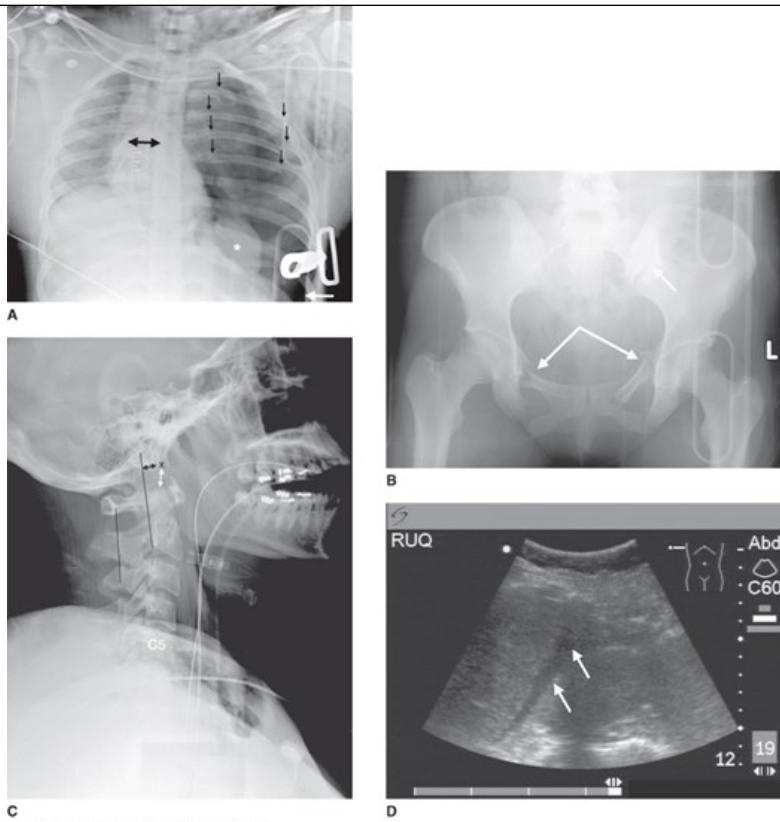
INITIAL IMAGING FOR THE ASSESSMENT OF BLUNT TRAUMA

Trauma Series

Imaging of the trauma patient is integrated as a part of the secondary clinical survey in the resuscitation suite. The goal of the initial imaging studies is to identify life-threatening, but clinically occult, injuries that require emergent intervention prior to any further imaging, such as an unstable pelvic fracture, hemopneumothorax, or malpositioned/misplaced support lines and tubes.¹ Anteroposterior (AP) supine chest and AP supine pelvis radiographs are typically performed as a part of this initial assessment, if clinical evaluation alone is deemed insufficient (Fig. 19-1). A single-view, cross-table, horizontal beam cervical spine radiograph can be obtained to evaluate for gross cervical malalignment but should not be used to exclude all fractures of the cervical spine (see later section).

FIGURE 19-1

Trauma series. This 27-year-old unrestrained left rear seat passenger sustained multiple injuries in a high-speed side-impact crash. (A) Anteroposterior (AP) recumbent chest radiograph shows hyperexpanded and hyperlucent left hemithorax with deep sulcus sign (short white arrow) and rightward mediastinal shift (double-ended arrow) due to left tension pneumothorax. Short black arrows show multiple displaced rib fractures. Asterisk shows irregularity of left hemidiaphragm, which strongly suggests herniation of abdominal contents through left diaphragmatic laceration. (B) AP pelvis radiograph shows lateral-compression-type pelvic ring disruption consisting of bilateral iliopubic and ischiopubic ramus and left sacral fractures (long arrows) with sacroiliac joint disruptions (short arrow). (C) Cross-table lateral cervical spine radiograph is grossly normal to C5. Therefore, this constitutes a nondiagnostic study. Craniocervical alignment should be assessed and may be easily overlooked. Dens–basion distance (white double-ended arrow) is normally no greater than 12 mm. Posterior axial line represents cephalad extension of posterior cortex of C2 body (and is normally no more than 12 mm posterior or 4 mm anterior to basion) (black double-ended arrow). Anterior atlantodens interval is normally no greater than 3 mm in adults and 5 mm in children (8 years and younger). Laminar point of C2 (laminar points are most anterior extent of neural canal margin of lamina) should be within 1.5 mm of line connecting laminar points of C1 and C3. (D) Coronal image of right upper quadrant (RUQ) from focused abdominal sonography for trauma (FAST) shows free intraperitoneal fluid in anterior subhepatic (Morison's) space (arrows), compatible with hemoperitoneum.



Source: David V. Feliciano, Kenneth L. Mattox, Ernest E. Moore: Trauma, Ninth Edition
Copyright © McGraw Hill. All rights reserved.

The trauma resuscitation ABCD strategy may be extended to this trauma series. Verification of the integrity of the airway (and other tubes and lines) should occur on the chest radiograph. Radiographic pulmonary opacities associated with hypoxemia include pulmonary contusions, aspiration pneumonitis, and atelectasis (including collapse due to aspirated dental or foreign debris). Tension pneumothorax and hemothorax are typically detected on clinical examination, whereas clinically occult pneumothoraces or hemothoraces are commonly shown by chest x-rays as a deep sulcus sign and generalized hemithoracic opacification, respectively. Other injuries, such as rupture of the hemidiaphragm, flail chest, pneumopericardium, and pneumomediastinum and hemomediastinum, may be diagnosed or at least suggested by initial x-ray findings. Hemodynamic instability may arise from any number of causes, including extraperitoneal hemorrhage from pelvic ring disruption or hemoperitoneum from solid organ injuries. Biomechanically unstable disruptions of the pelvic ring are almost always shown on AP radiographs and may be associated with injuries to the bladder and urethra. In addition, pelvic x-rays may show hip dislocations and fractures of the acetabulum and proximal femur.

Although used less commonly, a technically adequate (C1–T1) lateral x-ray of the cervical spine is a limited examination but may provide helpful information in the setting of a cervical spine fracture/dislocation or other gross malalignment and may confirm that spinal shock from a vertebral fracture is the cause of unexplained hypotension.

Focused Assessment with Sonography in Trauma

Focused assessment with sonography in trauma (FAST) is performed as part of the secondary survey in victims of torso trauma to identify fluid accumulations in the chest and abdomen. These abnormal fluid collections serve as a proxy for significant internal injury. The ultrasound probe is used to search for fluid in the pericardial sac, both upper abdominal quadrants, and the intraperitoneal recesses in the pelvis adjacent to the bladder. Scanning is optimally performed in two orthogonal planes (eg, longitudinal and transverse) and may also be used to detect a hemothorax or a pneumothorax immediately superior to the perihepatic and perisplenic views. In patients who have severe hemodynamic compromise or obvious hemorrhagic shock, FAST can establish the abdomen as a source of hemorrhage within a few seconds. It is important to recognize that FAST is a limited anatomic examination and, as such, the identification of intraparenchymal and retroperitoneal injuries is not a goal, but certainly occurs. FAST is widely available, inexpensive, and noninvasive; uses no ionizing radiation; is portable; and can be repeated serially with little additional time and effort. Commercially available handheld real-time imaging devices are technically adequate to perform FAST.

FAST is uniformly accurate for the detection of intraperitoneal fluid with moderately large volumes greater than 400 cm³ (at smaller volumes, accuracy varies with user experience).²⁻⁴ Unfortunately, isolated hepatosplenic injuries with minimal or no hemoperitoneum represent as many as one-third of solid organ injuries.^{5,6} Fortunately, small isolated intraparenchymal lesions with less than 250 mL of intraperitoneal blood often do not require endovascular or surgical intervention (liver <1%, spleen <5%).⁷ False-positive interpretation of FAST images can result from improper machine settings (gain), sonolucent perinephric fat (which is rarely sonolucent in both axial and coronal scanning planes), fluid-filled bowel and bladder, various types of fluid-filled intra-abdominal cysts, physiologic fluid (especially in females), or preexisting nontraumatic free fluid (ascites). A final false-negative scenario outlines a negative pericardial window despite the underlying presence of a cardiac injury secondary to ejection of the blood out of the pericardial sac via an adjacent rent in the pleura or diaphragm.

The FAST does, however, require operator training and experience for reliable performance and interpretation, which may limit its value. In addition, FAST lacks value in patients with preexisting nontraumatic ascites, bowel and mesenteric injuries, injuries to the retroperitoneum, subcutaneous emphysema, and hemoperitoneum due to pelvic fractures. Although a systematic review of the literature would not support the use of FAST as a replacement for diagnostic peritoneal lavage (DPL) and CT in blunt abdominal trauma, many trained surgeon-sonographers use it on a daily basis with great accuracy.⁸

Hemodynamically stable patients who have suffered trauma with a clinical presentation suspicious for injuries, even in the setting of a positive FAST scan, are candidates for intravenous contrast-enhanced CT of the abdomen and pelvis to identify or exclude internal injuries.

COMPREHENSIVE IMAGING FOR BLUNT POLYTRAUMA

Blunt polytrauma victims are triaged based on the physical examination, initial imaging assessment, and hemodynamic status to the operating room, intensive care unit, or angiography suite for ongoing resuscitation. Some remain in the trauma center for completion of secondary and tertiary clinical surveys and advanced targeted imaging. Typically, this consists of CT for clinically appropriate imaging (eg, head, neck, chest, abdomen, pelvis, and lower extremities) for hemodynamically stable patients. Subsequently, conventional x-rays of the extremities may be obtained. Less severely injured individuals may take a slightly different route with conventional x-rays preceding CT and directed at abnormalities found by clinical examination or prior imaging.

There has been recent increased utilization of the “pan scan” or other variations of whole-body CT imaging techniques as a method of screening patients for clinically unsuspected injuries or to further define injuries identified or suspected on physical examination and initial imaging. This paradigm advocates rapid acquisition of high-resolution thin collimation images to include CT of any or all body parts, including the extremities in some instances. Some literature suggests that integrating whole-body CT as a part of the comprehensive evaluation of the trauma patient decreases morbidity and mortality.^{9,10} Employing this strategy provides excellent anatomic coverage with high accuracy for the detection and exclusion of injuries and is most frequently used in high-volume facilities with considerable imaging resources and expertise.

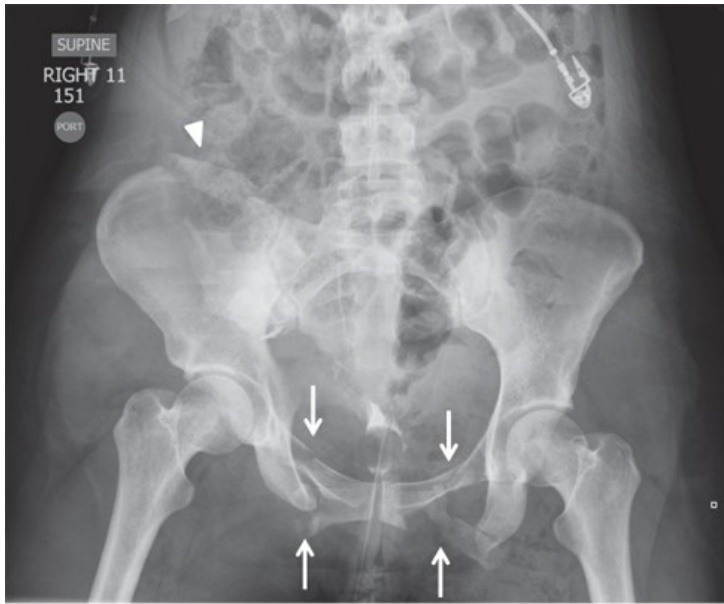
Multidetector Computed Tomography

The widespread availability of multidetector CT (MDCT) scanners has revolutionized the way that trauma patients are imaged.¹¹⁻¹³ Modern MDCT scanners, particularly those with 16 or more detector rows, acquire imaging data at submillimeter slice thickness. Because of this isotropic spatial resolution, two-dimensional (multiplanar) images in any arbitrary plane can be reconstructed with the same resolution as the axial images. Three-dimensional images with surface shading and cinematic rendering approximate that of anatomic specimens. Some of the newest software packages can reconstruct CT raw data sets to generate “virtual” radiographs (Fig. 19-2).

FIGURE 19-2

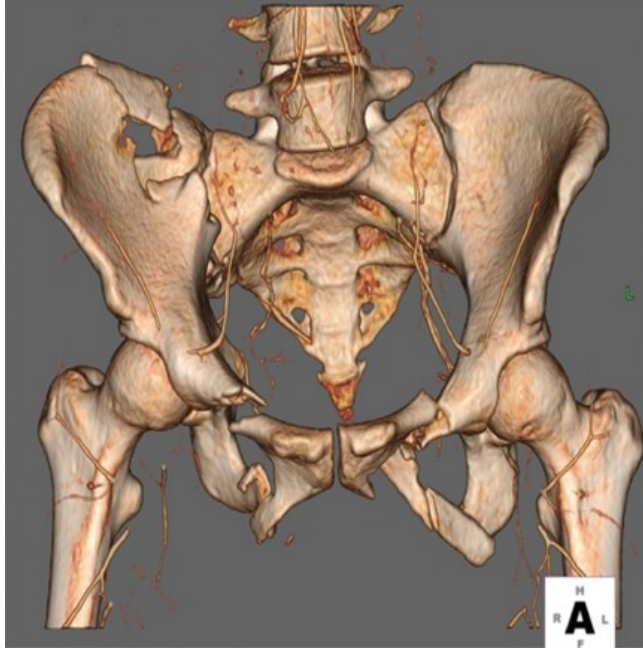
Advanced computed tomography (CT) imaging depicting pelvic and acetabular fractures. (A) Anteroposterior (AP) frontal radiograph of a 34-year-old female following a motorcycle crash. There is a highly disorganized pelvic ring disruption with fractures of the superior and inferior pubic rami (arrows) indicating a lateral compression force vector. There is also a comminuted fracture of the right iliac crest (arrow head). Notice the vertical height difference indicating a vertical shear mechanism of injury in addition to lateral compression. (B) Three-dimensional image with surface detail from the same patient nicely displays the bony fractures and their relationships to one another, with overlying soft tissue, bowel gas, and stool no longer a limiting factor. (C) AP frontal radiograph of a 74-year-old male with a left acetabular fracture (arrow) following a fall from standing height. The

patient has L4–L5 posterior fixation hardware as well as a pain pump reservoir (arrowhead) overlying the left ilium. (D) A “virtual” pelvic radiograph on the same patient as in C, generated using the raw data from a subsequently performed pelvic CT. Notice that the pain pump reservoir has been partially removed from the image.



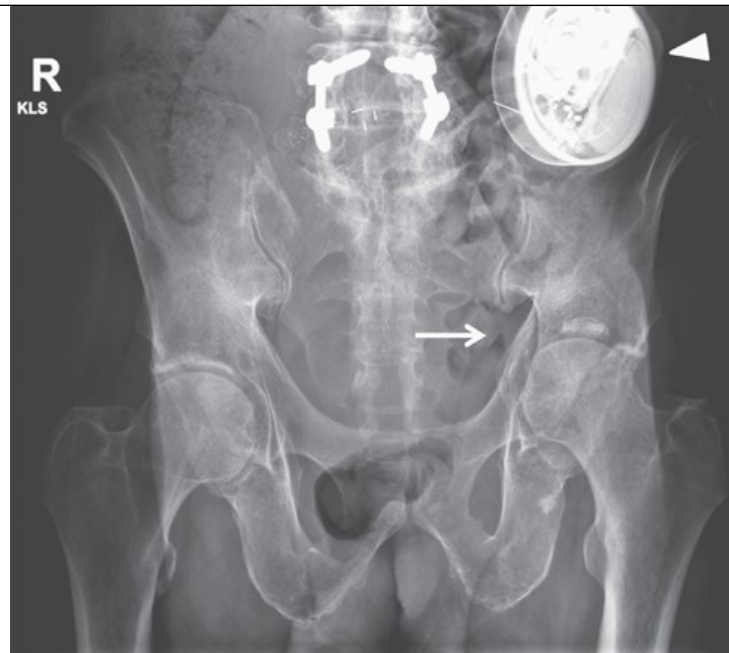
A

Source: David V. Feliciano, Kenneth L. Mattox,
Ernest E. Moore: Trauma, Ninth Edition
Copyright © McGraw Hill. All rights reserved.



B

Source: David V. Feliciano, Kenneth L. Mattox,
Ernest E. Moore: Trauma, Ninth Edition
Copyright © McGraw Hill. All rights reserved.

**C**

Source: David V. Feliciano, Kenneth L. Mattox,
Ernest E. Moore: Trauma, Ninth Edition
Copyright © McGraw Hill. All rights reserved.

**D**

Source: David V. Feliciano, Kenneth L. Mattox,
Ernest E. Moore: Trauma, Ninth Edition
Copyright © McGraw Hill. All rights reserved.

This, coupled with rapid intravenous contrast injection and increased table speed, allows for even shorter scan times as well as imaging large portions of the body during multiple phases of vascular and organ enhancement. As a result, patients can be scanned from the cranial vertex to feet in only a few seconds.^{14,15} Reconstructions of any scanned body part, including the face, thoracolumbar spine, pelvis, and extremities, can be generated in multiple planes, thus reducing unnecessary repeat scanning. The previous practice of focused, specialized imaging of the face and spine can be abandoned. As such, individual repeat thin-section imaging of parts of the body in addition to the CT survey is superfluous, increases ionizing radiation unnecessarily, and increases time away from the resuscitation area.

Instead of sending all of the submillimeter thin-section data to a picture archiving and communication system (PACS) for review (which can be quite

time consuming, despite improved image transfer time), the thinner slices are stacked together so that maximum useful information can be extracted without overwhelming the reviewer with high image volume. It is typical for images through the chest, abdomen, and pelvis to be reconstructed at 2- to 5-mm slice thickness in axial, sagittal, and coronal planes, although any slice thickness can be prescribed and tailored to local preferences. It is common practice for the axial images to be reconstructed using thicker slices (eg, 3–5 mm), with sagittal and coronal images reconstructed using thinner slices (eg, 1.5–3 mm) to provide finer spatial resolution of the pelvis and spine. Specific soft tissue and/or bone reconstruction algorithms can be applied to the CT raw data, again supplanting redundant focused imaging. Open communication with the radiology team is strongly encouraged so that optimal image quality and the imaging needs of the trauma surgeon and patient can be achieved. Consistency and familiarity with the scanning process and the image reconstructions can help improve patient throughput once a standard trauma CT survey is agreed upon, thus decreasing patient time away from the trauma care area.

In the era of “as low as reasonably achievable” (ALARA), there is concern regarding the radiation doses that trauma patients receive given the younger demographic of trauma patients, as well as the need for additional or repeat imaging for monitoring. Although dose reduction in CT is achievable, multiple studies have demonstrated cutoffs for minimum dose and noise levels for maintaining image and diagnostic quality in a variety of clinical settings. In the setting of trauma, it is essential to balance dose reduction with diagnostic quality given the potential for significant morbidity and mortality resulting from missed diagnoses in this patient population.

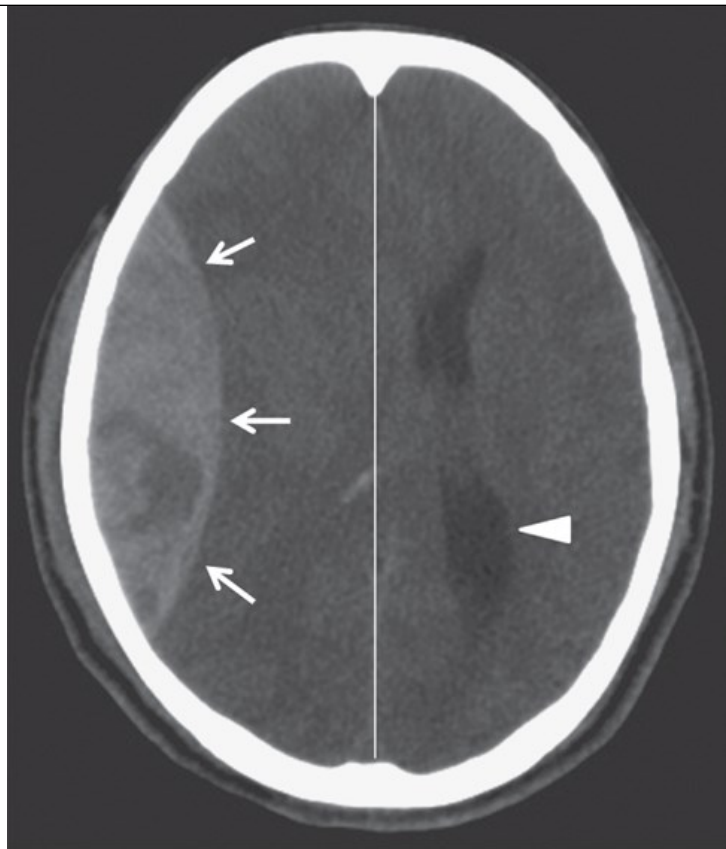
There are a number of radiation dose reduction techniques available. Aside from only scanning what is deemed necessary, there have been many technologic advances that have resulted in substantial radiation dose reduction delivery to the patient while maintaining diagnostic image quality. Inherently high-contrast structures, such as the bones and lungs, lend themselves well to dose reduction. Z-axis dose modulation can be employed to automatically reduce delivered dose through less dense parts of the body (eg, through the lungs), thus only using the dose necessary to maintain diagnostic image quality. Back-end computational methods for image reconstruction from the raw data can be used to reduce image noise, thus providing the potential to reduce radiation dose while maintaining desired image quality.

Computed Tomography of the Head

Axial noncontrast CT scanning remains the reference standard in patients with acute craniocerebral trauma, guiding initial decisions regarding clinical management.^{16,17} Indications for CT of the head include the following: (1) objective evidence of closed injury to the brain, including decreased level of consciousness; (2) cranial or facial deformity; (3) hemotympanum; or (4) evidence for leakage of cerebrospinal fluid (Figs. 19-3, 19-4, 19-5). Clinical criteria reliably predict significant intracranial injury and help determine which patients will require CT scanning of the head. In children, significant intracranial injury is extremely unlikely in any child who does not exhibit at least one of the following high-risk criteria: (1) evidence of significant skull fracture; (2) altered level of alertness; (3) neurologic deficit; (4) persisting vomiting; (5) scalp hematoma; (6) abnormal behavior; or (7) coagulopathy.¹⁸ More generically, minor trauma to the head may lead to surgically important injuries to the brain, and liberal utilization of CT is appropriate among individuals who have sustained “high-risk” mechanisms. These clinical criteria are not as reliable in the elderly patient.¹⁹

FIGURE 19-3

Epidural hematoma. (A) Axial computed tomography (CT) using brain windows shows epidural hematoma (arrows), associated midline shift (white line), and leftward deviation of the left lateral ventricle (arrowhead). (B) Axial CT at level of the suprasellar cistern and brain windows shows epidural hematoma (arrow) and obliteration of the basal cisterns due to uncal herniation (arrowhead).

**A**

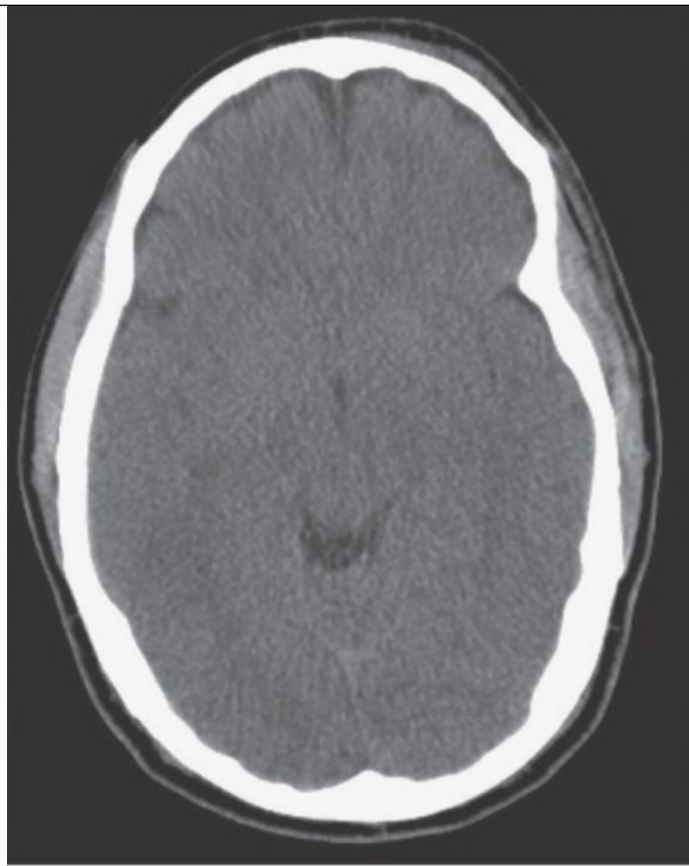
Source: David V. Feliciano, Kenneth L. Mattox,
Ernest E. Moore: Trauma, Ninth Edition
Copyright © McGraw Hill. All rights reserved.

**B**

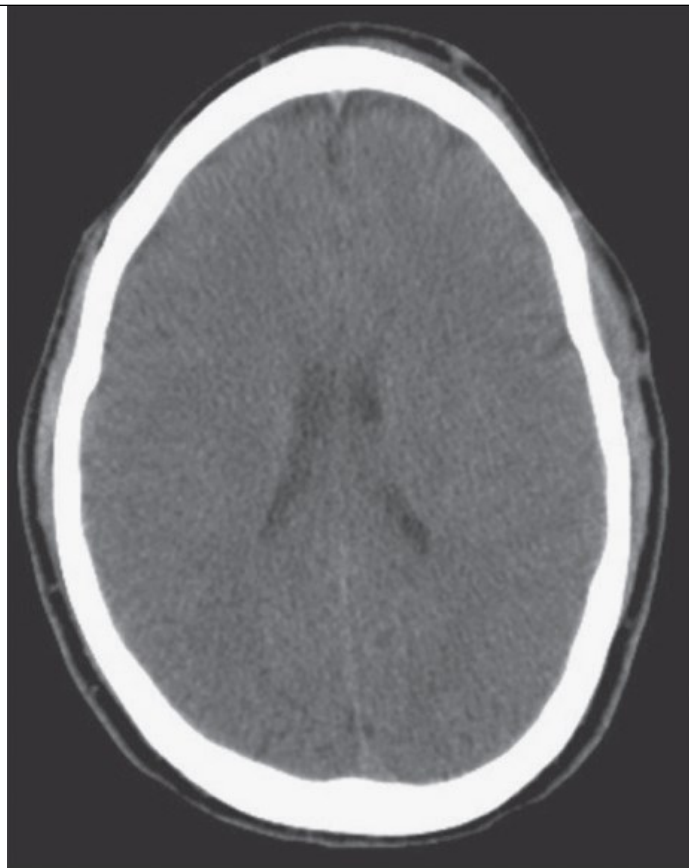
Source: David V. Feliciano, Kenneth L. Mattox,
Ernest E. Moore: Trauma, Ninth Edition
Copyright © McGraw Hill. All rights reserved.

FIGURE 19-4

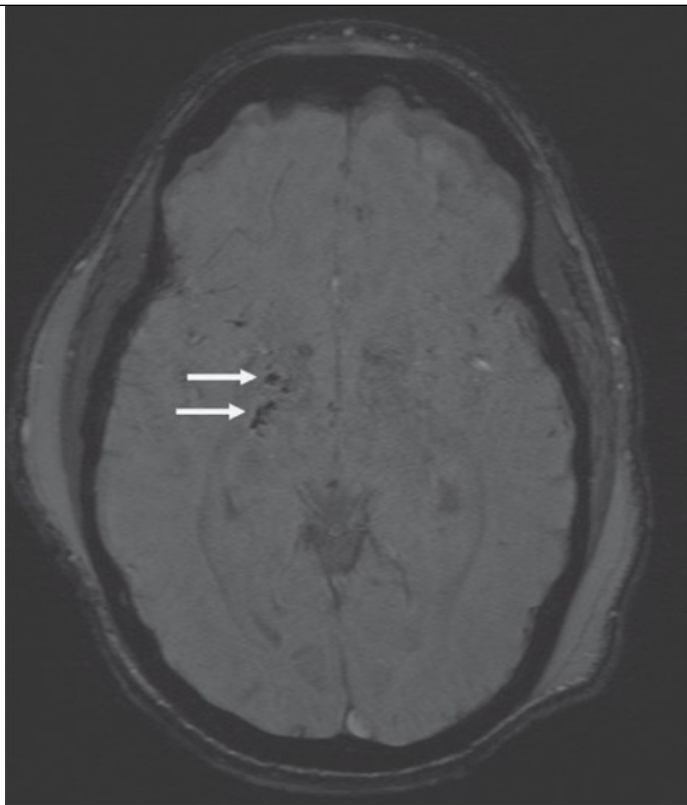
Blunt head injury: axonal shear injury. A 24-year-old helmeted male following a high-speed motorcycle collision. Admission axial noncontrast computed tomography (CT) at level of the third ventricle (**A**) and lateral ventricles (**B**) demonstrates no significant abnormality. The patient's neurologic status did not improve; therefore, brain magnetic resonance imaging (MRI) was performed 25 hours after admission (**C**, **D**). Axial MRIs at the same levels as **A** and **B** using gradient echo (GRE) sequences (which are highly sensitive for blood products) demonstrated numerous hemorrhagic foci throughout the brain, concentrated in the right basal ganglia (**C**) and the gray-white junction (**D**) (arrows).

**A**

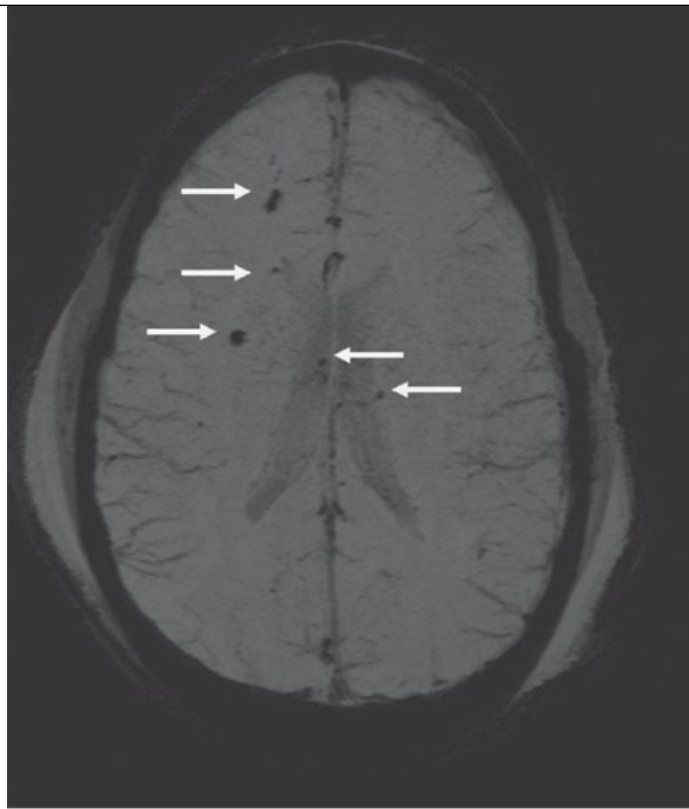
Source: David V. Feliciano, Kenneth L. Mattox,
Ernest E. Moore: Trauma, Ninth Edition
Copyright © McGraw Hill. All rights reserved.

**B**

Source: David V. Feliciano, Kenneth L. Mattox,
Ernest E. Moore: Trauma, Ninth Edition
Copyright © McGraw Hill. All rights reserved.

**C**

Source: David V. Feliciano, Kenneth L. Mattox,
Ernest E. Moore: Trauma, Ninth Edition
Copyright © McGraw Hill. All rights reserved.

**D**

Source: David V. Feliciano, Kenneth L. Mattox, Ernest E. Moore: Trauma, Ninth Edition
Copyright © McGraw Hill. All rights reserved.

FIGURE 19-5

Patterns of herniation. (A) Axial computed tomography (CT) at level of suprasellar cistern shows extensive subarachnoid hemorrhage extending from lateral aspect of suprasellar cistern (1), into the Sylvian fissure (2), circumferentially about brainstem and perimesencephalic cistern (3), along tentorium (4), and interpeduncular cistern (5). Entrapment of lateral ventricles is shown as dilatation of temporal horns (white arrows). Brainstem appears relatively lucent and heart shaped, with pointed inferior portion of heart due to “beaking” of mesencephalon due to upward herniation. (B) Subfalcine shift. Axial CT of another patient at level of lateral ventricles shows marked leftward subfalcine shift (white double arrow), quantified as distance from midline (vertical white line) connecting the anterior and posterior portions of the sagittal sinus (which tend not to shift due to their fixed relation to calvarium) to the interventricular septum. Note a right-sided holohemispheric subdural hematoma with hematocrit level (white arrow). (C) Uncal herniation. Axial CT of the same patient as in B at the level of middle cranial fossa again shows right-sided subdural hematoma (white arrow) with associated right uncal herniation (arrowhead). Enlargement of the left temporal horn (notched white arrow) is compatible with obstruction of the cisternal system.

**A**

Source: David V. Feliciano, Kenneth L. Mattox,
Ernest E. Moore: Trauma, Ninth Edition
Copyright © McGraw Hill. All rights reserved.

**B**

Source: David V. Feliciano, Kenneth L. Mattox,
Ernest E. Moore: Trauma, Ninth Edition
Copyright © McGraw Hill. All rights reserved.

**C**

Source: David V. Feliciano, Kenneth L. Mattox,
Ernest E. Moore: Trauma, Ninth Edition
Copyright © McGraw Hill. All rights reserved.

Head CT images are traditionally acquired using a conventional “step and shoot” axial technique. Most modern MDCT scanners, however, have the capability of scanning the head using helical acquisition, as used for other body parts, and can thus reconstruct head CT images in both sagittal and coronal planes. Traditionally, axial images are reconstructed at 5-mm slice thickness using both bone and soft tissue algorithms and are viewed using bone windows and at least two different soft tissue windows (including “brain” and “blood” window settings).

CT scanning is highly sensitive and specific for the detection of extra- and intra-axial hemorrhage, mass effect and midline shift, soft tissue injuries to the scalp and globes, and fractures to the calvarium, skull base, bony orbits, and paranasal sinuses. In patients with diffuse axonal injury, however, CT may even be normal and discordant between the severity of the clinical brain injury and radiographic findings (Fig. 19-4). On a cautionary note, skull fractures that are aligned in the plane of scanning may easily elude detection, and review of multiplanar reconstruction (MPR) images or the scout views used to plan the CT study of the head may alert the clinician to such fractures. Except for medicolegal imaging of pediatric nonaccidental trauma (child abuse), conventional x-rays of the skull are usually not necessary.²⁰

Computed Tomography of the Maxillofacial Skeleton

Indications for specific facial CT scans include the following: (1) deformity or instability of the maxillofacial structures found by physical examination; (2) deformity, opacification, or fracture of the periorbital or paranasal sinus shown on head CT; and (3) clinical evidence for leakage of cerebrospinal fluid (Fig. 19-6). The mnemonic LIPS-N (lip lacerations, intraoral lacerations, periorbital contusions, subconjunctival hemorrhage, or nasal lacerations) provides a helpful tool during clinical examination of trauma patients given the high association between LIPS-N lesions and facial fractures.²¹

Fortunately, physical examination is highly sensitive for selecting which patients need maxillofacial CT imaging.²² Absence of paranasal or periorbital sinus fluid on CT (the “clean sinus” sign) generally excludes surgically important injury to the maxillofacial skeleton, with only very rare exceptions.²³

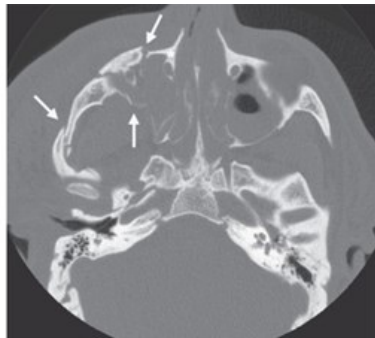
FIGURE 19-6

Facial fracture: zygomaticomaxillary complex (ZMC) fracture with associated naso-orbito-ethmoid (NOE) complex fracture. This 54-year-old male

sustained a blow to the face in a motorcycle crash. (A) Anteroposterior (AP) scanogram shows loss of symmetry to orbital volumes, with elliptoid enlargement of right orbit. Associated indistinctness of orbital floor and lateral maxillary sinus walls is also present. Opacification of right maxillary sinus is shown. (B) Axial computed tomography (CT) image at the level of zygomatic arches shows depression and overriding apposition of impacted zygomatic arch fracture (lateral white arrow), posterolateral maxillary sinus wall disruption (posterior arrow), and segmental comminuted fracture of anterior maxillary wall (anterior arrow). Medial to this anterior arrow is the base of the nasofrontal process of the maxilla with a fractured nasolacrimal duct just posterior to it. Internal rotation of the nasofrontal process of the maxilla and associated fracture of the nasolacrimal duct are not portions of ZMC fracture and represent an associated NOE complex fracture. (C) Coronal CT reformation shows separation of right frontozygomatic suture (lateral and superior arrow), disruption of orbital floor (white arrow projected over orbit), and lateral maxillary wall (inferior white arrow). (D) Sagittal CT reformation shows associated vertical fracture of right ascending ramus of mandible, with anterior subluxation at temporomandibular joint (white and black arrows, respectively). (E) Three-dimensional CT reformation gives an overview of complex fracture of zygomaticomaxillary region and right mandibular fracture. It is important to note that spatial resolution is lost with three-dimensional reformations, although spatial comprehension is often improved. (F) Three-dimensional CT reformation shows depression of right zygomatic arch and loss of projection of the right zygoma (flat cheek).



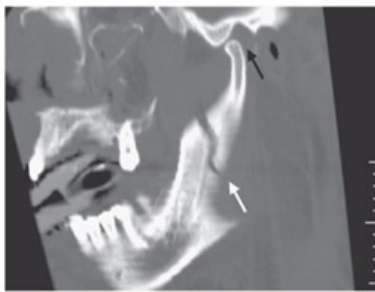
A



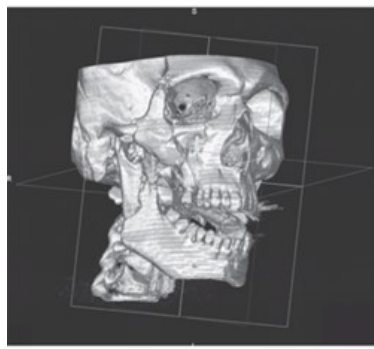
B



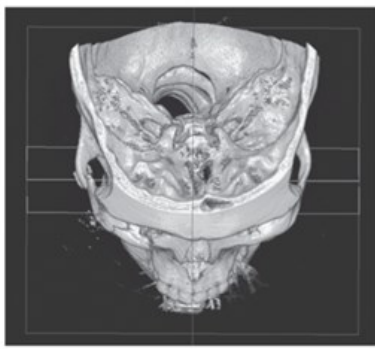
C



D



E



F

Source: David V. Feliciano, Kenneth L. Mattox, Ernest E. Moore: Trauma, Ninth Edition
Copyright © McGraw Hill. All rights reserved.

Images of the face are acquired using helical scanning technique and are reconstructed in the axial, sagittal, and coronal planes at 1- to 2-mm slice thickness, typically using both soft tissue and bone reconstruction algorithms. Helical acquisition with MDCT technology can be used to generate three-dimensional (3D) surface-rendered images of the bones, which can be quite helpful in determining the type of facial fracture patterns, particularly for patients with highly comminuted and disorganized high-energy midface smash fracture patterns. This technique provides valuable

information on spatial relationships and is particularly useful in planning operative treatment.^{24,25} However, axial and two-dimensional reformations best portray defects in soft tissue, interposition of osseous fragments, and herniations of soft tissue (eg, orbital floor blowout fractures) and are best for quantifying size of fractures.^{26,27} It is important to recognize that some institutions do not routinely include the mandible as a part of the maxillofacial CT scan protocol; thus, open communication with the radiology team is important in order to include the relevant anatomy for evaluation.

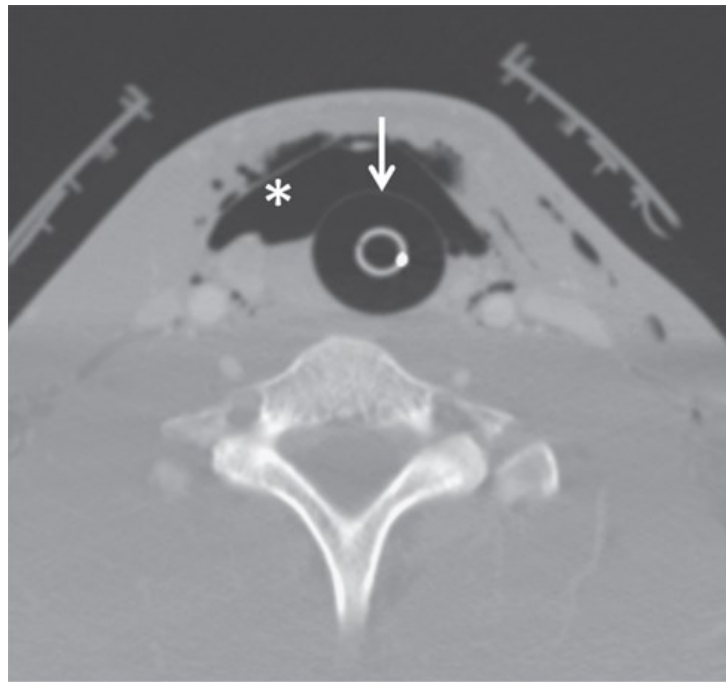
Radiation reduction techniques for CT continue to evolve; however, maxillofacial CT can still deliver significant radiation to the orbits and to the soft tissues of the neck (eg, thyroid), which is an important consideration when imaging children in particular.²⁸

Imaging for Soft Tissue Injuries of the Neck

Clinical findings for blunt injury to the aerodigestive tract are nonspecific but include subcutaneous crepitus, hemoptysis, hoarseness, neck pain, and abrasions or hematomas (eg, from the shoulder harness of a three-point restraint; Figs. 19-7 and 19-8). X-ray findings include parapharyngeal or precervical emphysema, soft tissue swelling, or fracture of the larynx or hyoid bone on the lateral image of the cervical spine. Soft tissue injuries are inadequately evaluated using radiography; hence CT is the accepted imaging standard for imaging this area.

FIGURE 19-7

Tracheal, soft tissue, and vascular neck injuries. (A–D) This is a 21-year-old male motorcyclist with a “clothesline injury,” resulting in tracheal transection, as well as a complex cervical vascular injury and neck muscle injuries. (A) Axial and (B) sagittal computed tomography (CT) images using lung windows reveal an endotracheal balloon inflated in a tracheal defect (arrows). There is surrounding cervical emphysema (asterisk). (C) Sagittal CT image using soft tissue windows reveals a complex injury of the carotid bulb (arrow) and proximal internal carotid artery (arrowhead). There is an associated neck soft tissue injury manifested by fluid in the muscular defect (asterisk). (D) Axial CT image through the chest using lung windows reveals pneumomediastinum (black arrow) resulting from inferior extension of cervical emphysema. There is extensive right greater than left bilateral aspiration (black asterisk). (E) Axial CT from a 36-year-old male who was hit in the neck with a hockey puck reveals a fracture of the midline (triangle) and right side (arrow) of the thyroid cartilage. The patient was intubated due to immediate voice changes and to protect the airway.



A

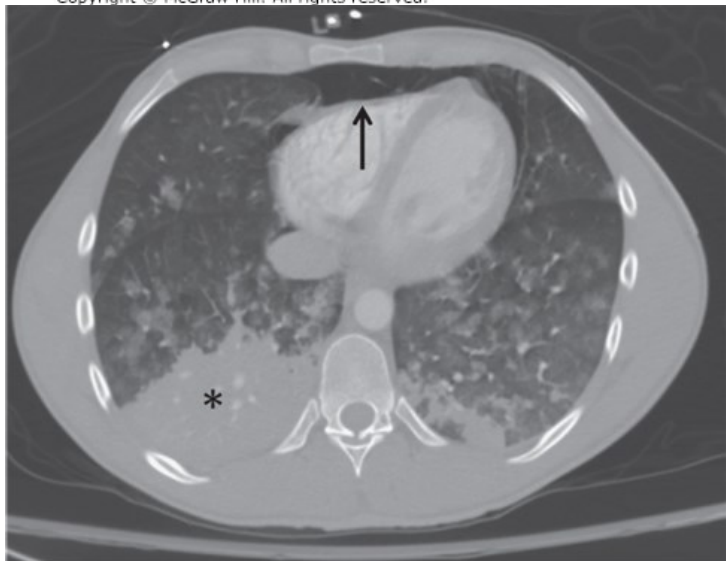
Source: David V. Feliciano, Kenneth L. Mattox,
Ernest E. Moore: Trauma, Ninth Edition
Copyright © McGraw Hill. All rights reserved.

**B**

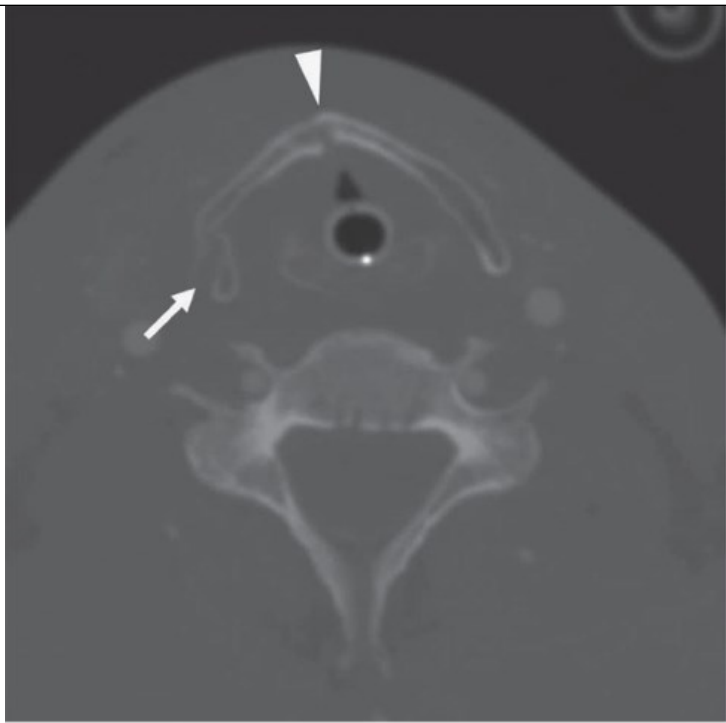
Source: David V. Feliciano, Kenneth L. Mattox,
Ernest E. Moore: Trauma, Ninth Edition
Copyright © McGraw Hill. All rights reserved.

**C**

Source: David V. Feliciano, Kenneth L. Mattox,
Ernest E. Moore: Trauma, Ninth Edition
Copyright © McGraw Hill. All rights reserved.

**D**

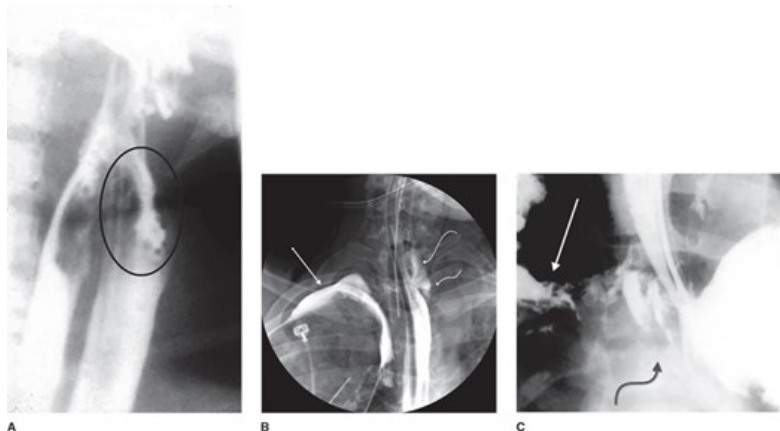
Source: David V. Feliciano, Kenneth L. Mattox,
Ernest E. Moore: Trauma, Ninth Edition
Copyright © McGraw Hill. All rights reserved.

**E**

Source: David V. Feliciano, Kenneth L. Mattox, Ernest E. Moore: Trauma, Ninth Edition. Copyright © McGraw Hill. All rights reserved.

FIGURE 19-8

Esophageal injuries. (A) Gunshot wound in zone II of the neck of a teenager. Barium extravasation directly enters the airway from a high laryngoesophageal fistula (circled). (B) Gunshot wound traversing zone I into the right chest. Barium swallow shows leak on both the left side of the cervical esophagus (curved arrows) and the right thoracic esophagus (straight arrow). (C) A 27-year-old male sustained a low transverse mediastinal gunshot wound entering left and exiting right. Gastrograffin esophagram shows leak into the right chest (straight right arrow) and into the peritoneal cavity (curved black arrow).



A Source: David V. Feliciano, Kenneth L. Mattox, Ernest E. Moore: Trauma, Ninth Edition. Copyright © McGraw Hill. All rights reserved.

MDCT of the neck with intravenous contrast can not only be used to evaluate for upper aerodigestive tract injuries, but can also be used to simultaneously evaluate the cervical vasculature and spine (see later). Images are routinely reconstructed in three planes using both soft tissue and bone algorithms.

CT is often most helpful in the evaluation of laryngotracheal injuries when physical examination and endoscopy are technically difficult (Fig. 19-7E).²⁹ A

careful search for direct signs of a laryngotracheal injury, manifested by focal defects, guides the need for intervention for debridement and mucosal closure. Soft tissue gas may be focal adjacent to the site of injury, but larger defects, particularly if the patient is under positive-pressure ventilation, can result in massive soft tissue emphysema extending into the skull base and head superiorly or into the mediastinum and beyond inferiorly.³⁰ CT can assist in the grading of laryngotracheal injuries but tends to understage injuries compared to endoscopy or open exploration. The most common injuries are those to the thyroid cartilage, which typically occur within 2 to 3 mm of the anterior crest of the two lateral laminae. Comminuted fractures of the laminae generally result from higher energy and direct impact injuries to the larynx and are more commonly associated with thyrocricoid dislocation. In addition, CT can demonstrate subluxations and dislocations of the arytenoid cartilage. Most tracheal disruptions are in the membranous portion of the trachea and can heal with conservative therapy. Soft tissue emphysema immediately adjacent to the trachea suggests an injury in this location but, again, could be massive in volume and anatomic distribution. A search for a fracture of a tracheal ring is often fruitless unless the fracture is displaced. Coronal reformations through the trachea may show separation (vertical diastasis between tracheal rings) of the trachea compatible with more serious grades of injury.

Blunt esophageal injuries are very uncommon, but when they do occur, they are most often observed in the proximal third of the esophagus. However, a penetrating injury to the esophagus is more common and may involve any portion of the esophagus. Any focal gas adjacent to the esophagus, without an obvious airway source, should raise the possibility of an injury, particularly if a wound tract extends up to or through the region of the esophagus.

If there is a concern for an esophageal injury, contrast esophagography, endoscopy, or both should be performed. Both tests have a sensitivity of 80% to 90%, but this increases to approximately 95% when both examinations are performed.^{31,32} As a result, clinicians must use their level of suspicion to determine which of these tests (or both) to employ. Iso-osmolar water-soluble contrast material is the preferred *initial* contrast agent of choice for suspected esophageal injuries because it is less toxic to the lungs if aspirated and is better tolerated if leaked into the mediastinum or peritoneum. Unfortunately, iso-osmolar contrast material is less dense on fluoroscopy, with the potential to miss subtle injuries. Barium sulfate is easier to see but can be irritating to the soft tissues if an esophageal injury is present and should be used after initial water-soluble esophagography is negative. Gastrografin should be avoided because of its hyperosmolarity and because it can cause life-threatening pulmonary edema if aspirated.

Esophagography performed on patients who are awake and able to cooperate with the examination is performed as any other esophagram, but with the contrast agent modifications as described earlier. Performing esophagography in intubated and/or sedated patients is technically challenging and often limited despite maximal efforts on the part of the radiology team. A nasogastric tube is necessary to perform this examination on obtunded, intubated, and/or sedated patients. The patient is placed in reverse Trendelenburg position (10–20° as tolerated) with the fluoroscopy table floor board in place. The radiologist manipulates the nasogastric tube to the distal esophagus and, under real-time fluoroscopic surveillance, injects the contrast agent in an attempt to achieve full distention of the esophagus. The contrast is then immediately aspirated, and the nasogastric tube is repositioned more proximally. This process is repeated to evaluate all segments of the esophagus. Care should be taken to avoid overdistention of the proximal esophagus, which can result in reflux and aspiration, even in intubated patients. Rapid imaging is necessary, with fluoroscopic cineradiographs obtained at 2 to 3 frames per second.

IMAGING OF CERVICAL VASCULAR INJURIES

Neck CT angiography (CTA) with MDCT has a sensitivity of 90% to 100% for blunt cervical vascular injuries and is, therefore, the imaging test of choice in patients without indications for immediate surgery or catheter angiography. Neck CTA can be performed as its own stand-alone examination (as in the setting of penetrating neck injuries), added on to the standard trauma CT protocol, or integrated as a part of a single-pass whole-body CT trauma protocol.^{33–37} Neck CTA protocols vary widely based on local preferences and mechanism of injury (ie, blunt vs penetrating). Positioning of the patient's arms is an important consideration when integrating neck CTA into the imaging evaluation of these patients, as increased image noise and decreased image quality will result when the arms are included in the scanned region.³⁷ Optimal cervical arterial opacification can be obtained following either a timing bolus or using a fixed scan delay. These images are reconstructed at 1- to 3-mm slice thickness from the aortic arch to the skull base (or to the cranial vertex if needed), with MPR reconstructed in axial, sagittal, and coronal planes. Coronal maximum-intensity projections (MIPs) are particularly helpful for visualizing the cervical vasculature but should not be relied upon for evaluation of the vertebral arteries due to volume averaging effects and the potential for a missed injury. Liberal use of a dedicated 3D volume viewing station for manipulation of the data set is strongly encouraged, as it is often the case that a cervical vascular injury may be best visualized and displayed using nontraditional planes.

Catheter angiography is indicated emergently in patients with an expanding cervical hematoma; active extravasation from the nose, mouth, or ears; or

a cervical bruit in individuals younger than 50 years old.³⁸ Angiography is not only a diagnostic test in symptomatic blunt carotid and vertebral artery injuries, but is also a therapeutic tool as it allows for rapid utilization of endovascular therapy for bleeding and identifies patients at risk for embolic stroke.^{39,40} The sensitivity of duplex Doppler US is inadequately low (38.5%) for directly depicting vascular injuries in the neck and is, therefore, not a primary tool for evaluation of the cervical vasculature.⁴¹ Existing literature for the use of magnetic resonance angiography (MRA) demonstrates limited sensitivity for cervical vascular injuries compared to CTA and catheter angiography.⁴² This, in addition to the technical and practical limitations of MRI in the setting of trauma, limits the utility of magnetic resonance imaging (MRI)/MRA in the acute setting.

BLUNT CERVICAL VASCULAR INJURIES

Blunt carotid and vertebral injuries (Fig. 19-9A–C) are now known to be much more common than previously appreciated, occurring in 1% to 3% of screened asymptomatic patients.³⁵ Vascular imaging of the neck is warranted in injury patterns associated with a high risk of blunt injury to the carotid and vertebral arteries, including the following: fracture of the cervical spine (especially involving C1–C3, involving the transverse foramina, or extension into the foramen magnum), neurologic deficits not explained by findings at brain imaging, new-onset Horner syndrome, high-energy facial fractures (Le Fort II or III), fracture of the skull base involving the foramen lacerum, or soft tissue injury in the neck (neck belt sign and “hangings” sufficient to cause central anoxia).^{39,43} It should be noted, however, that approximately one-fifth of patients with blunt cervical vascular injuries do not have these classically described risk factors and thus may elude detection if selective screening is employed.⁴⁴

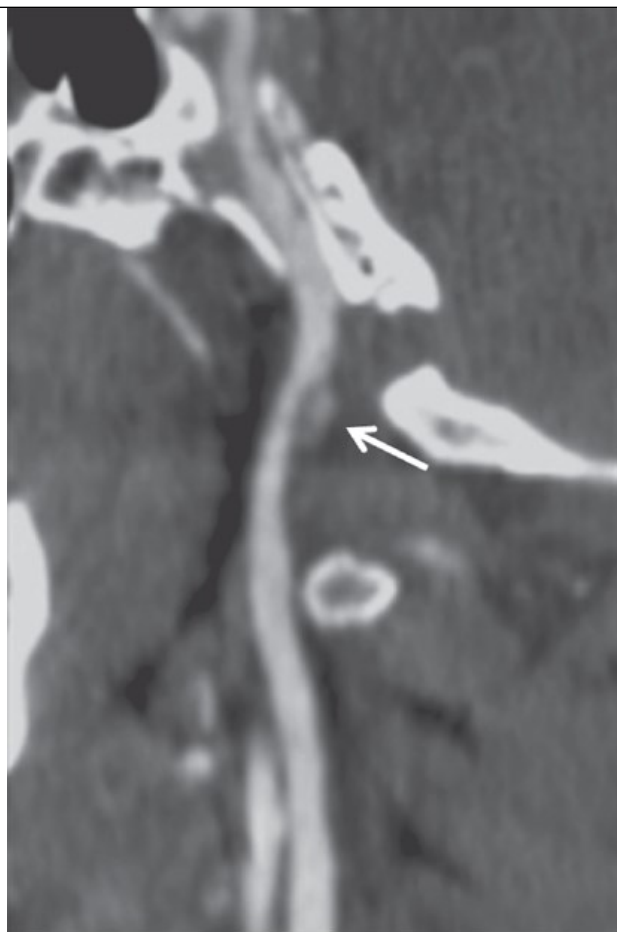
FIGURE 19-9

Cervical vascular injuries. (A) A 24-year-old female involved in a high-speed motor vehicle collision. Admission axial computed tomography (CT) image demonstrates an intimal flap in the distal internal carotid artery (arrow) that is actually a pseudoaneurysm seen best on the sagittal image (B). The patient was treated conservatively. (C) Repeat neck CT angiography 20 days after injury reveals an enlarging pseudoaneurysm (arrow). (D) A 24-year-old male with common carotid artery and tracheal injuries following a dog attack. The right common carotid artery is not opacified (arrow) due to injury and subsequent thrombosis. A tracheal defect (arrowhead) is present, along with extensive cervical emphysema. (E) The extent of the cervical emphysema (arrows) is best seen on the scout image with gas extending inferiorly into the mediastinum (arrowheads).



A

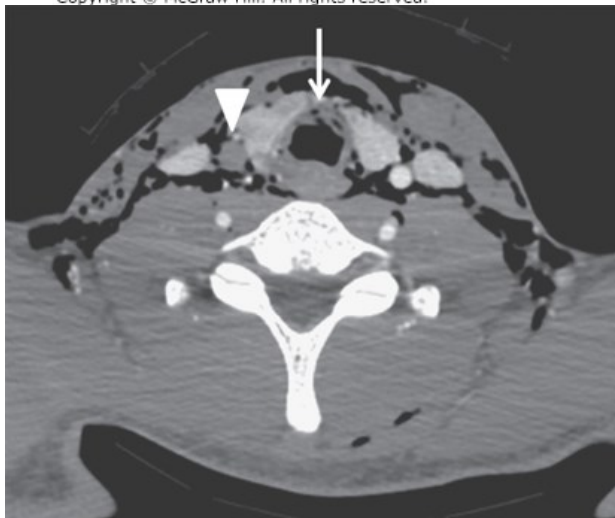
Source: David V. Feliciano, Kenneth L. Mattox,
Ernest E. Moore: Trauma, Ninth Edition
Copyright © McGraw Hill. All rights reserved.

**B**

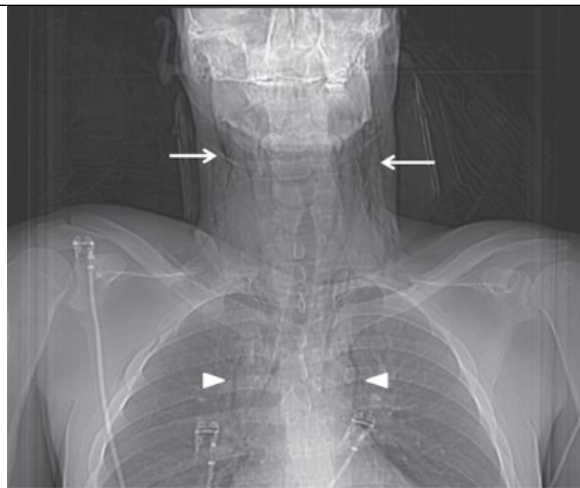
Source: David V. Feliciano, Kenneth L. Mattox,
Ernest E. Moore: Trauma, Ninth Edition
Copyright © McGraw Hill. All rights reserved.

**C**

Source: David V. Feliciano, Kenneth L. Mattox,
Ernest E. Moore: Trauma, Ninth Edition
Copyright © McGraw Hill. All rights reserved.

**D**

Source: David V. Feliciano, Kenneth L. Mattox,
Ernest E. Moore: Trauma, Ninth Edition
Copyright © McGraw Hill. All rights reserved.

**E**

Source: David V. Feliciano, Kenneth L. Mattox, Ernest E. Moore: Trauma, Ninth Edition
Copyright © McGraw Hill. All rights reserved.

PENETRATING NECK INJURIES

Penetrating injuries to the neck are associated with high morbidity and mortality, primarily due to injuries of the cervical vasculature, upper aerodigestive tract, and spine. As such, any patient with “hard” signs of a cervical vascular injury (eg, expanding pulsatile hematoma, active bleeding from the wound, hemorrhagic shock) or compromise or injury of the upper aerodigestive tract or airway (eg, stridor, hoarseness) requires urgent intervention by individuals with experience managing such injuries. Neck CTA has proven highly useful in identifying and excluding injuries that require intervention and can significantly reduce the rate of nontherapeutic cervical explorations for patients without indications for immediate surgery or intervention⁴⁵⁻⁴⁸ (Fig. 19-9D-E). In addition, it can be used to determine trajectory and identify direct signs of vascular injury. When patients are stable or asymptomatic, immediate CTA has great value in excluding injury, in detecting vascular injuries that can be treated nonoperatively by embolization or insertion of a stent or stent graft, and in facilitating surgical exploration.

There has been a shift away from mandatory evaluation of the neck with surgery and other invasive tests based on the zonal wound location toward a “no zone” selective approach with CTA evaluation of the neck.⁴⁹ Many factors must be considered when approaching the patient with a penetrating wound to the neck, including the mechanism of injury (high vs low energy), the number and location of surface wounds, hemodynamic and neurologic status, and the likelihood of injury. Gunshot wounds can result in significant soft tissue cavitation that may result in direct or indirect vascular injuries. In addition, fragments of bone and metal frequently cause artifacts in the area, which make interpreting a CT difficult. Catheter angiography (particularly digital subtraction angiography) is extremely useful for the evaluation of the carotid and vertebral arteries when they are partially obscured by beam hardening artifact from metallic bullet fragments.

Neck zonal anatomy is an important consideration for patients with “hard” clinical signs of significant internal injury; however, it should be noted that clinically significant internal injuries may be present in a zone differing from that of the physical examination and that penetrating wound tracts may extend beyond the neck into the skull base, cranial vault, mediastinum, or upper thorax. Zone III, above the angle of the mandible extending to the skull base, is difficult to assess clinically and to explore operatively. There are numerous vessels at risk, including the internal carotid artery, the external carotid artery and branches, the vertebral artery, and the accompanying veins. Thus, imaging plays a vital role in these patients. Neck CTA can be used to evaluate these vessels, but a low threshold for catheter angiography should be maintained for patients with possible injuries in zone III. Selective internal and external carotid arteriography, vertebral arteriography, and four-vessel intracranial arteriography all play important roles in detecting and evaluating zone III vascular injuries. Indeed, arteriography is so valuable for the evaluation and treatment of bleeding in this zone that aggressive steps to resuscitate the unstable patient and control bleeding by packing are warranted to allow angiography to proceed. Most vascular injuries in zone III are best managed by an experienced interventional radiology service.

Zone II, between the inferior margin of the angle of the mandible and cricoid cartilage, is more easily and reliably evaluated by physical examination. If the common carotid artery or the internal jugular vein requires repair, operative exposure is relatively simple and unobstructed. Thus, little imaging is

necessary after penetration when “hard” signs of a vascular injury are present. The detection and treatment of vascular injuries in asymptomatic patients are more controversial.

Zone I is the area between the cricoid cartilage and the sternal notch. Structures here include the brachiocephalic vessels, trachea, and esophagus. Vascular injuries in this zone may result in rapid exsanguination, and as a result, symptomatic patients may undergo urgent exploration without imaging.

IMAGING OF THE SPINE

Imaging of spinal trauma often begins with simple radiography to evaluate for biomechanically unstable injuries, such as burst fractures and dislocations. It is critical to note that adequate radiographs of the spine may be technically difficult to obtain, may have limited quality in obtunded or immobilized patients, and may not detect all fractures. A meta-analysis of the sensitivity of radiography for cervical spine fractures by Holmes and Akkinenpalli⁵⁰ documented a pooled sensitivity of 52%, compared to 98% for cervical spine CT. Thus, the decision to image with radiography or CT must be made based on the mechanism of injury and the likelihood of a spinal fracture and must be balanced with the possibility of other more life-threatening injuries. If an abnormality is identified on conventional x-rays, CT and/or MRI can be used to further characterize the injury for planning of treatment and provide information on the patient’s prognosis.

Conventional Radiographs of the Spine

Validated clinical prediction rules (ie, National Emergency X-Radiography Utilization Study Group [NEXUS] and the Canadian Cervical Spine Rule) for adults and older children (≥ 10 years old) can reliably identify trauma victims who need imaging of the cervical spine.^{51,52} In essence, oriented asymptomatic individuals without findings on a physical examination following trauma do not require subsequent imaging. Imaging of the thoracic and lumbar spine following blunt trauma is indicated when patients present with one or more of the following: (1) signs or symptoms of local injury (pain, tenderness, interspinous step-off); (2) depressed level of consciousness, including intoxication; (3) acute myelopathy or radiculopathy referable to the thoracolumbar spine; and (4) major distracting injury, including concomitant injuries to the cervical spine.^{53,54}

A cross-table lateral cervical spine radiograph is often obtained in the setting of acute trauma, although its use is declining due to the easy availability of MDCT and relative lack of sensitivity compared to CT. Single-view lateral cervical spine films may not reveal a significant percentage of fractures. In fact, a study by Brohi et al⁵⁵ in 2005 reported a sensitivity of 39.3% and a sensitivity of 51.7% for single lateral view radiography evaluating unstable cervical injuries. This same study reported the sensitivity, specificity, and negative predictive value of CT to be 98.1%, 98.8%, and 99.7%, respectively.⁵⁵ The standard three-view cervical spine series includes an AP open-mouth odontoid view (an AP image of the craniocervical junction), an AP view of the subdental cervical spine, and a lateral view of the cervical spine that extends down to the C7-T1 interspace. To supplement these three views, a swimmer’s lateral image (one arm elevated above the head and the other arm in caudal traction) is often obtained to better visualize the cervicothoracic junction, and bilateral oblique views are obtained to evaluate the facet joints. The addition of these supplemental images adds time and radiation exposure and may still be technically limited, despite maximum effort on the part of the x-ray technologist and the patient.

Given the differences in the incidence of injury to the cervical spine in children and the differences in their distribution (far more common in the upper cervical spine) relative to adults, an examination limited to frontal and lateral views is generally acceptable.⁵⁶ In infants 0 to 4 years of age and in children 5 to 9 years of age, AP, lateral, and open-mouth views are satisfactory. All patients age 10 and over require a minimum of three views to as many as five or six views to adequately survey the cervical spine. Clinical decision rules developed for adults cannot be reliably applied to children.

Films of the thoracic and lumbar spine are usually obtained as separate sets of frontal and lateral projections. The upper thoracic spine may require the addition of a swimmer’s lateral view, if one has not been previously obtained as part of a cervical spine series. In general, if pathology is identified, then further evaluation with CT is indicated to further define the fracture pattern and to identify potential adjacent spinal injuries.

Technically inadequate examinations of the cervical or thoracic spine may be due to lack of visualization of the cervicothoracic junction or overlying arms due to upper extremity injuries. It is necessary to see the top of T1 on the cervical spine and the bottom of C7 on radiographs of the thoracic spine. A careful count of the vertebral bodies on the frontal examination to establish the correct levels is recommended to avoid wrong level surgery and is based on the number of rib-bearing (thoracic) and non-rib-bearing (lumbar) vertebrae. On the lateral images, it is important to look at the corners of the vertebral bodies, especially the anterior superior corner, which is affected in approximately 90% of all vertebral body fractures. On the

frontal images, it is most important to evaluate the adjacent end plates for continuity, the lateral margins of the vertebrae, the posterior elements for pathologic interspinous and interpedicular widening, and horizontal lucencies that would suggest horizontal soft tissue and/or osseous disruption of a flexion-distraction-type injury.

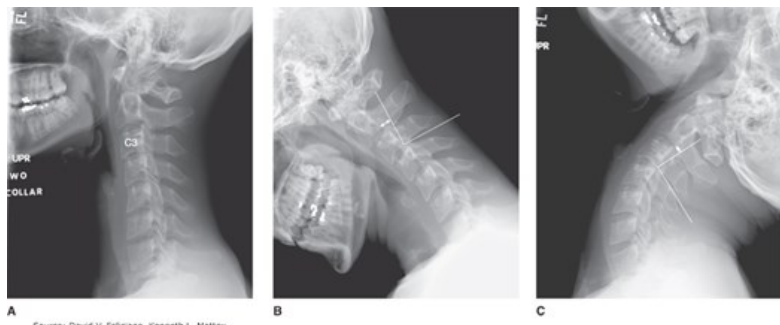
One of the common errors made in evaluating the cervical spine is mistaking developmental variations for pathology. Common variations at the craniocervical junction include the following: (1) fusion of C1 to the occiput (which may be partial or complete); (2) failure of fusion or development of the posterior elements of C1; (3) pseudospreading of C1 relative to C2, which may mimic Jefferson burst fractures (most common in the 0- to 4-year age range, but may be seen up through puberty); (4) pseudosubluxation of C2 on C3 in pediatric patients, which can be recognized as normal by a normal C1-C3 spinolaminar line; and (5) os odontoideum (an anomalous bone that replaces all or part of the dens but is not attached to the C2 body).

Flexion and Extension Cervical Spine Radiographs

Flexion and extension radiographs may be used to assess for potential ligamentous instability in patients who are completely alert and who have normal x-rays but exhibit posterior midline tenderness (Fig. 19-10). Some centers have recommended the use of passive (guided by the physician) flexion and extension studies using fluoroscopy, and although this may be appropriate in very limited circumstances in the hands of physicians with considerable experience, the published data are not sufficiently strong to warrant generalization.

FIGURE 19-10

Flexion-extension radiograph: cervical spine showing subtle instability at C2-C3. This 24-year-old male bicyclist was struck by a car from behind, and posterior midline tenderness of upper cervical spine was palpated. (A) Upright lateral out-of-collar radiograph shows loss of usual cervical lordosis without focal kyphosis or translation. Precervical soft tissues are normal. (B) Upright lateral flexion radiograph of cervical spine shows no gross interspinous widening or loss of parallelism of facet joint. Reference lines are drawn from posteroinferior corner of C3 to most inferior aspect of C3 spinous process. Perpendicular to that line from posteroinferior corner, a line is used as a reference for translation of C2 relative of C3, as demonstrated by double-arrowed line. (C) Upright lateral extension radiograph of cervical spine again shows no gross widening of anterior disk space. Using same reference for translation of C2 on C3, 2.5 mm of difference at C2-C3 disk space is demonstrated between flexion and extension, compatible with partial, dynamic instability.



A Source: David V. Feliciano, Kenneth L. Mattox, Ernest E. Moore: Trauma, Ninth Edition. Copyright © McGraw Hill. All rights reserved.

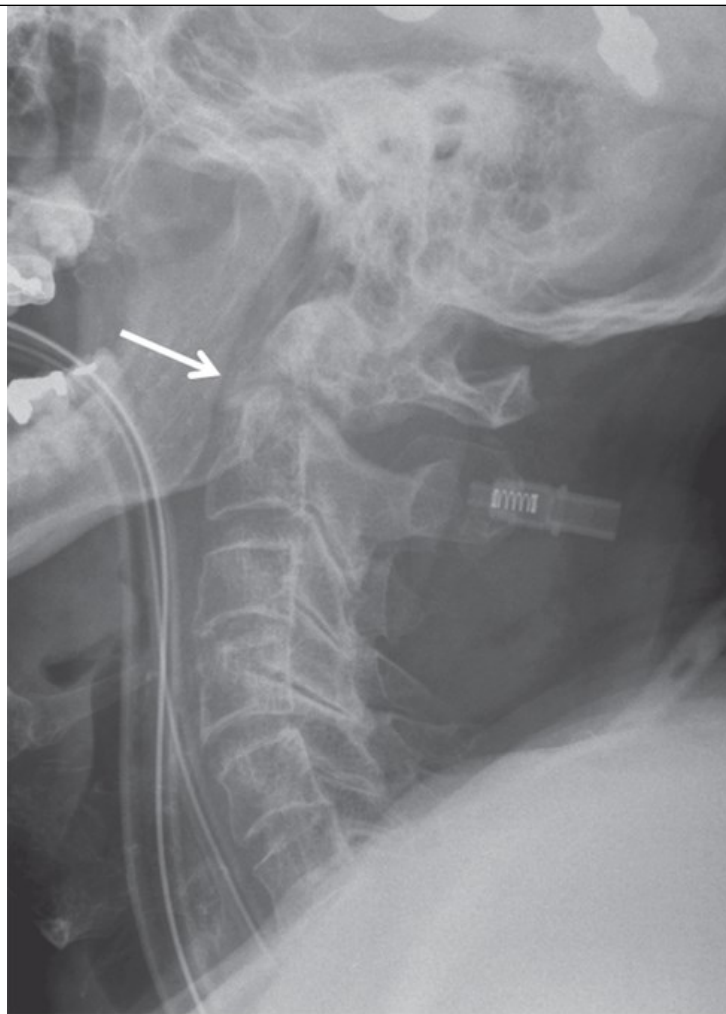
A qualified physician should be in attendance if the examination is performed shortly after injury (hours to days), and the patient needs to be completely alert and able to assume an upright posture and precisely follow commands. An initial lateral radiograph is obtained with the patient upright and with the cervical spine in a neutral position. This image is reviewed by the physician overseeing the examination, and if normal, the patient is asked to actively extend the neck. An additional lateral image in maximum extension is obtained. The patient's cervical spine is then returned to a neutral position. This extension x-ray is evaluated in a manner similar to that taken with the cervical spine in a neutral position. If normal, the examination is repeated with maximum effort at flexion, and an x-ray is obtained. Standards for an adequate examination vary from a range of motion of 30° to 90°. The test is intended to study the capacity of the spine to resist physiologic stresses, however, and the mean normal range of motion in adults is approximately 90°. If the flexion-extension x-rays are abnormal in the acute or subacute setting, MRI is pursued. If the examination does not show an adequate range of motion, the patient's spine is immobilized, and the examination is repeated in 2 weeks if the patient remains symptomatic. It should be noted that approximately one-third of flexion-extension x-rays exhibit suboptimal flexion and/or extension, thus limiting its utility.⁵⁷ As a result, some centers with available resources omit flexion-extension series and move straight to MRI.

Computed Tomography of the Cervical Spine

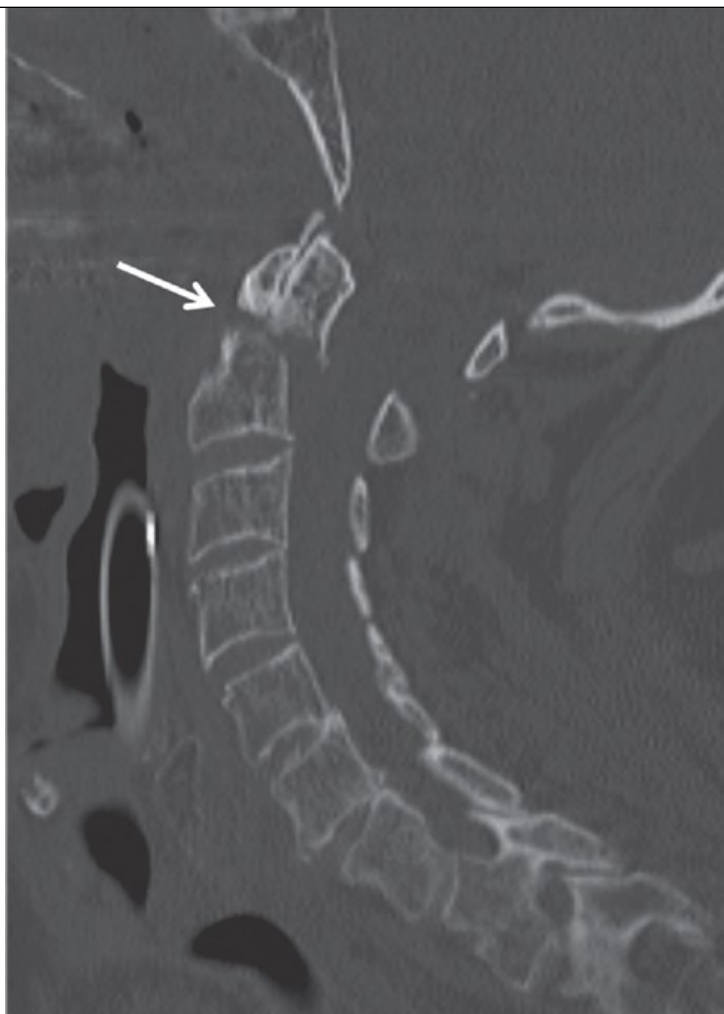
Blackmore et al⁵⁸ developed a clinical prediction rule to determine preimaging risk of fracture in select patients about to undergo a helical CT to survey the cervical spine for fracture and soft tissue injuries (Figs. 19-11 and 19-12). For the application of this rule, it is assumed that the patient will already be undergoing CT of the cranium. Any one of three mechanisms of injury or any one of three clinical findings puts the patient at a pretest risk of greater than 5% of harboring an injury in the cervical spine. High-risk mechanisms of injury include a high-speed motor vehicle crash greater than 35 mph (or greater than 50 km/h), combined impact, motor vehicle crash with a death at the scene, or a fall from a height of greater than 10 ft or greater than 3 m. Clinical parameters suggesting an increased risk for injury to the cervical spine that are associated with a high-risk mechanism include a significant closed injury to the brain (or intracranial hemorrhage shown on head CT), acute neurologic deficits referable to the cervical spine (acute myelopathy or radiculopathy), or either pelvic fracture or multiple extremity fractures. Hanson et al⁵⁹ validated the clinical prediction rule prospectively and showed its application by separating victims of blunt trauma into a high-risk group (12% prevalence of acute cervical spine injury) and a low-risk group (0.2% prevalence of cervical spine injury). No validated clinical decision rules exist for infants (<1 year old) and younger children (<9 years old). In general, patients with greater severities of injury (Injury Severity Score >25) have an elevated risk of injury to the cervical spine. For patients age 9 years or younger, conventional x-rays will depict essentially all clinically important fractures and dislocations. CT is generally not indicated in younger children and infants to screen the cervical spine or to search for other occult injuries causing neurologic deficits.⁶⁰ CT should be reserved as a staging/treatment planning procedure among patients with a known bony abnormality.

FIGURE 19-11

Upper cervical spine injuries. (A, B) Elderly patient status post fall. Lateral cervical spine image (A) demonstrates a fracture at the base of the odontoid process (arrow) compatible with a type II odontoid fracture. Sagittal (B) reformation nicely demonstrates the odontoid base fracture, which is displaced posteriorly with respect to the C2 body proper. (C, D) Another patient with a type III odontoid fracture. Sagittal (C) and coronal (D) reformations demonstrate a fracture of the base of the odontoid (arrows), which extends into the C2 body. (E–G) Another patient with a Jefferson burst fracture of C1 after falling while waterskiing. Lateral radiograph (E) of the upper cervical spine demonstrates prevertebral soft tissue swelling (asterisk) at the skull base and a fracture of the C1 posterior ring (arrow). Open mouth radiograph (F) demonstrates asymmetry of the lateral dental interval (black lines) and a white band (black arrow) due to abnormal overlap of the C1 ring and the lateral mass of C2. Axial computed tomography (CT) image (G) demonstrates fractures of the anterior (arrow) and posterior (arrowhead) arches of C1 compatible with a Jefferson fracture. (H, I) Traumatic spondylolysis (Hangman fracture) following a high-speed motor vehicle collision. (H) Lateral cervical spine radiograph demonstrates bony defects (arrow) in the C2 pars. (I) Corresponding axial CT image demonstrates bilateral C2 pars fractures (white arrows).

**A**

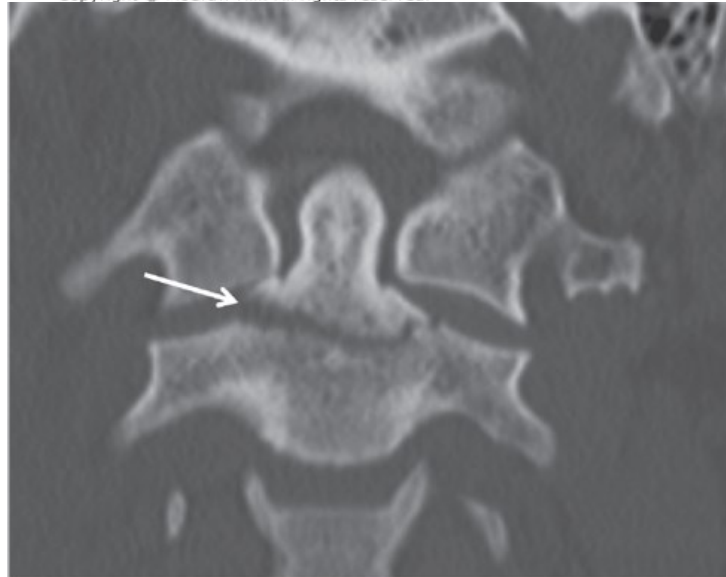
Source: David V. Feliciano, Kenneth L. Mattox,
Ernest E. Moore: Trauma, Ninth Edition
Copyright © McGraw Hill. All rights reserved.

**B**

Source: David V. Feliciano, Kenneth L. Mattox,
Ernest E. Moore: Trauma, Ninth Edition
Copyright © McGraw Hill. All rights reserved.

**C**

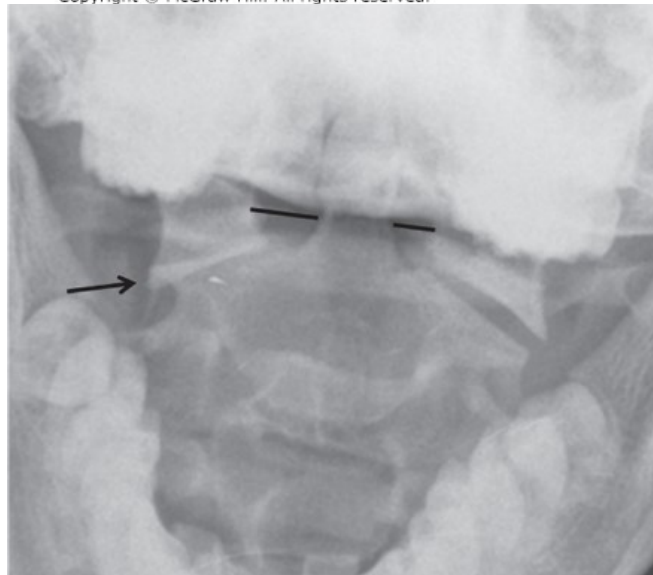
Source: David V. Feliciano, Kenneth L. Mattox,
Ernest E. Moore: Trauma, Ninth Edition
Copyright © McGraw Hill. All rights reserved.

**D**

Source: David V. Feliciano, Kenneth L. Mattox,
Ernest E. Moore: Trauma, Ninth Edition
Copyright © McGraw Hill. All rights reserved.

**E**

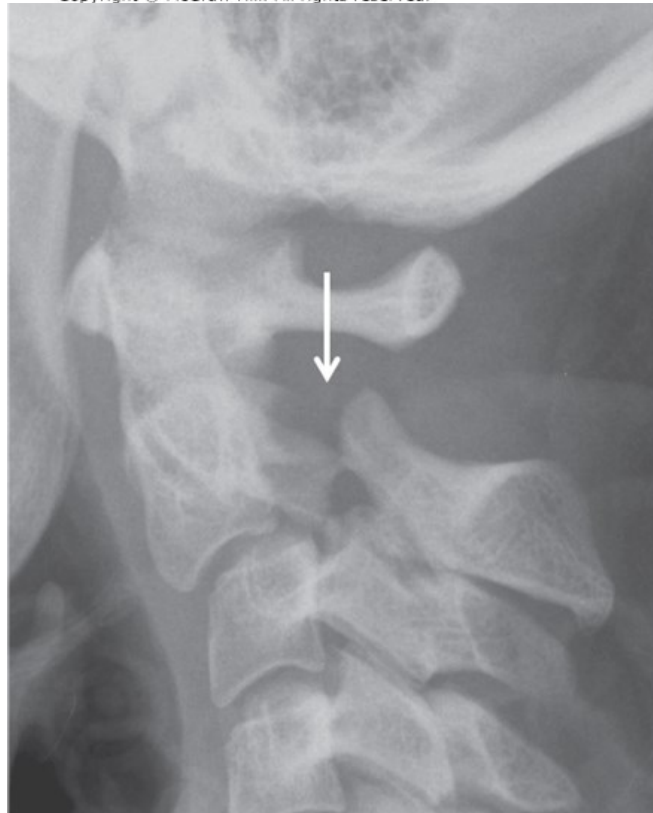
Source: David V. Feliciano, Kenneth L. Mattox,
Ernest E. Moore: Trauma, Ninth Edition
Copyright © McGraw Hill. All rights reserved.

**F**

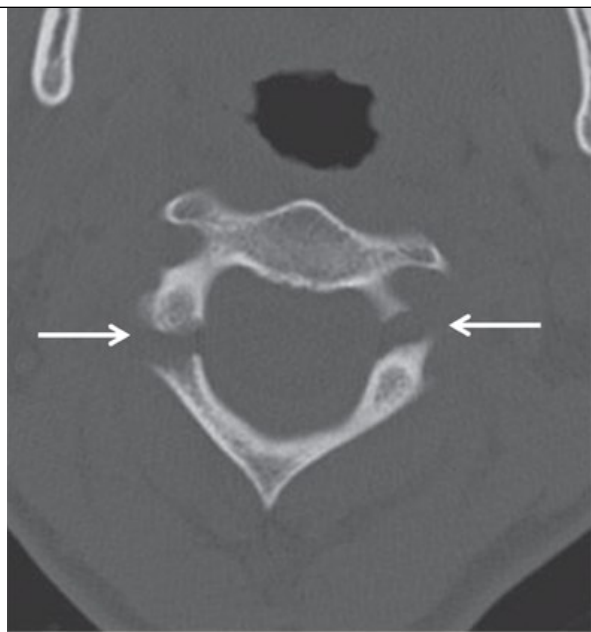
Source: David V. Feliciano, Kenneth L. Mattox,
Ernest E. Moore: Trauma, Ninth Edition
Copyright © McGraw Hill. All rights reserved.

**G**

Source: David V. Feliciano, Kenneth L. Mattox,
Ernest E. Moore: Trauma, Ninth Edition
Copyright © McGraw Hill. All rights reserved.

**H**

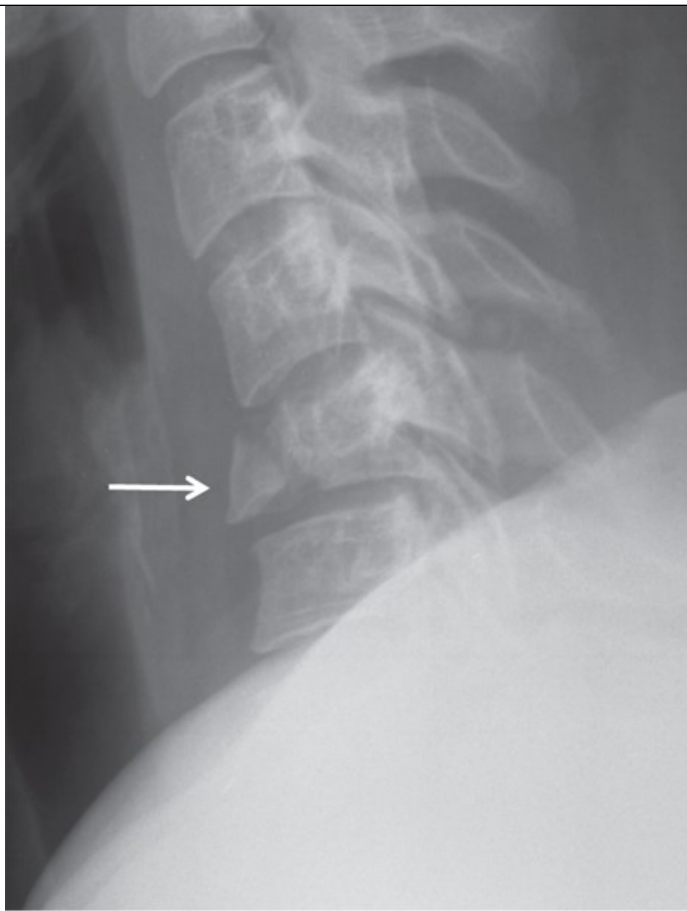
Source: David V. Feliciano, Kenneth L. Mattox,
Ernest E. Moore: Trauma, Ninth Edition
Copyright © McGraw Hill. All rights reserved.



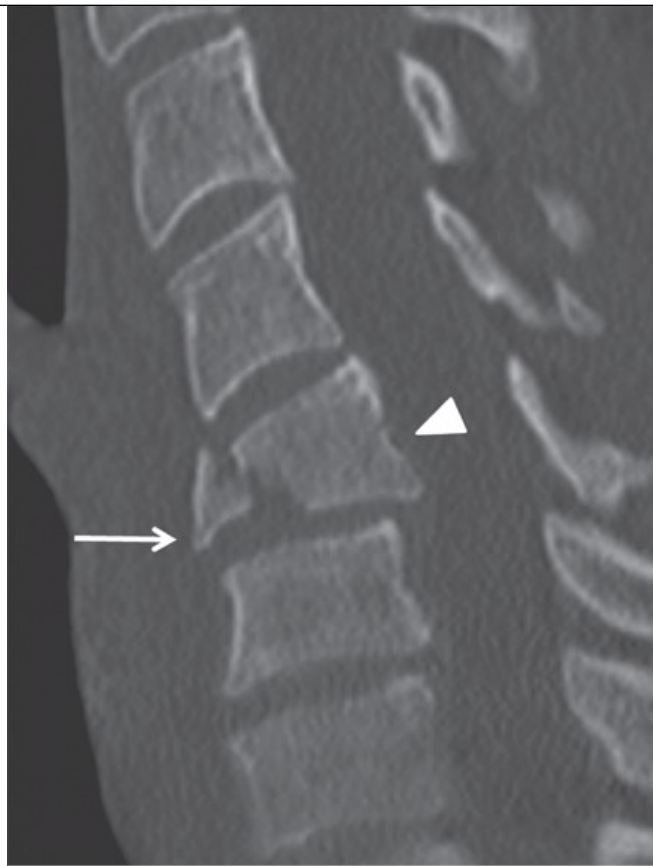
Source: David V. Feliciano, Kenneth L. Mattox,
Ernest E. Moore: Trauma, Ninth Edition
Copyright © McGraw Hill. All rights reserved.

FIGURE 19-12

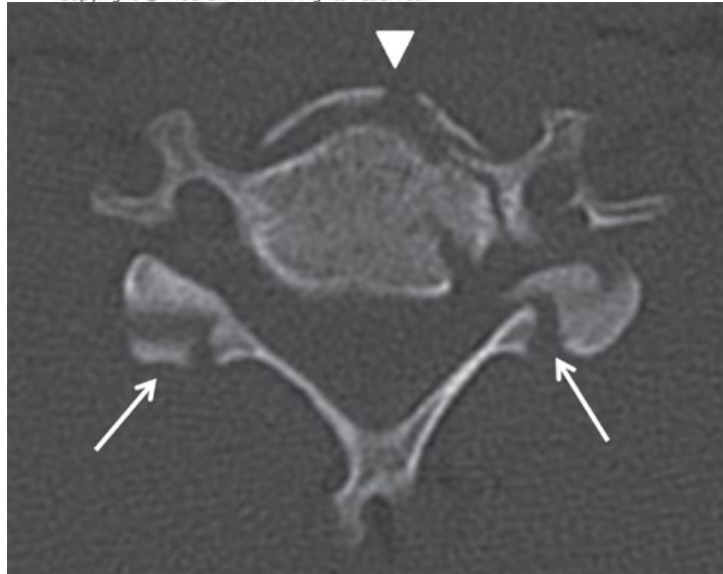
Mid and lower cervical spine fractures. (A–C) Cervical burst fracture. (A) Lateral cervical spine radiograph demonstrating the characteristic, triangular-shaped flexion “teardrop” fracture fragment (arrow) following a hyperflexion and axial load injury. (B) Midline sagittal computed tomography (CT) image of the same patient redemonstrates the teardrop fracture (arrow) and better illustrates retropulsion of bone into the spinal canal (arrowhead). (C) Axial CT image demonstrates a highly disorganized fracture, typical of this type of burst fracture. Bilateral lamina fractures (arrows) and comminuted vertebral body fracture (arrowhead) are better visualized on CT. (D–G) A 45-year-old male with neck pain and cerebellar symptoms following a fall from a mechanical bull. (D) Midline sagittal CT image view using bone windows demonstrates malalignment of C4 with respect to C5 (arrow) with corresponding widening of the interspinous distance (arrowhead). (E) Parasagittal CT image (bone windows) at the level of the facet joints reveals a C5 articular facet fracture (arrow). (F) Coronal oblique CT angiography image viewed using soft tissue windows demonstrates marked focal narrowing of the vertebral artery (black arrow) at the level of the facet fracture. (G) Axial diffusion-weighted magnetic resonance image demonstrates restricted diffusion (arrow) in the left cerebellar hemisphere compatible with acute cerebellar infarction.

**A**

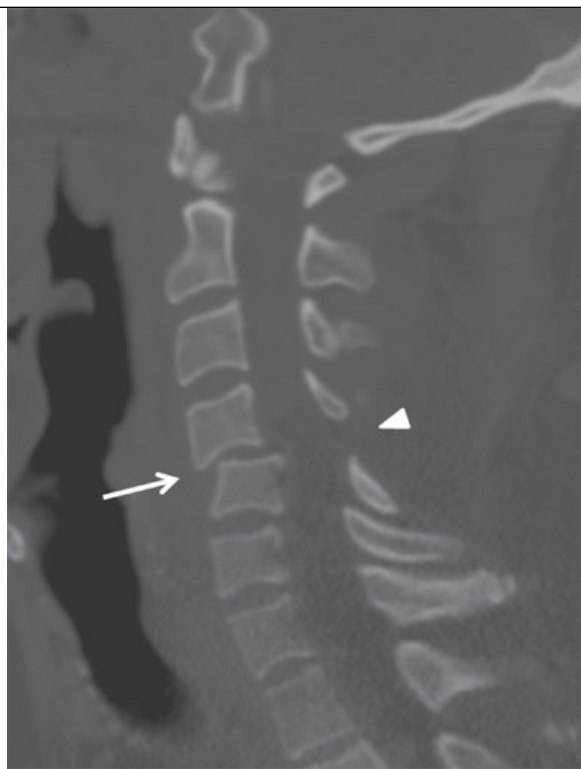
Source: David V. Feliciano, Kenneth L. Mattox,
Ernest E. Moore: Trauma, Ninth Edition
Copyright © McGraw Hill. All rights reserved.

**B**

Source: David V. Feliciano, Kenneth L. Mattox,
Ernest E. Moore: Trauma, Ninth Edition
Copyright © McGraw Hill. All rights reserved.

**C**

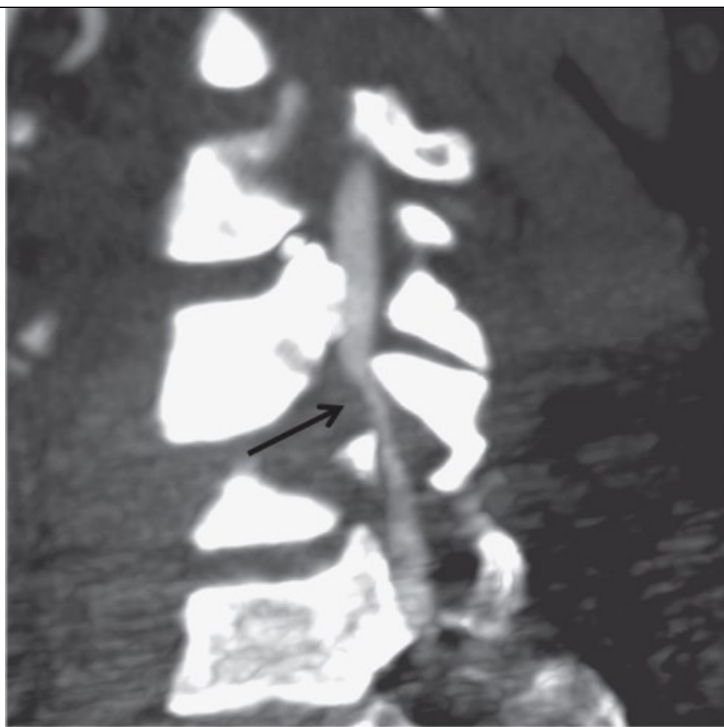
Source: David V. Feliciano, Kenneth L. Mattox,
Ernest E. Moore: Trauma, Ninth Edition
Copyright © McGraw Hill. All rights reserved.

**D**

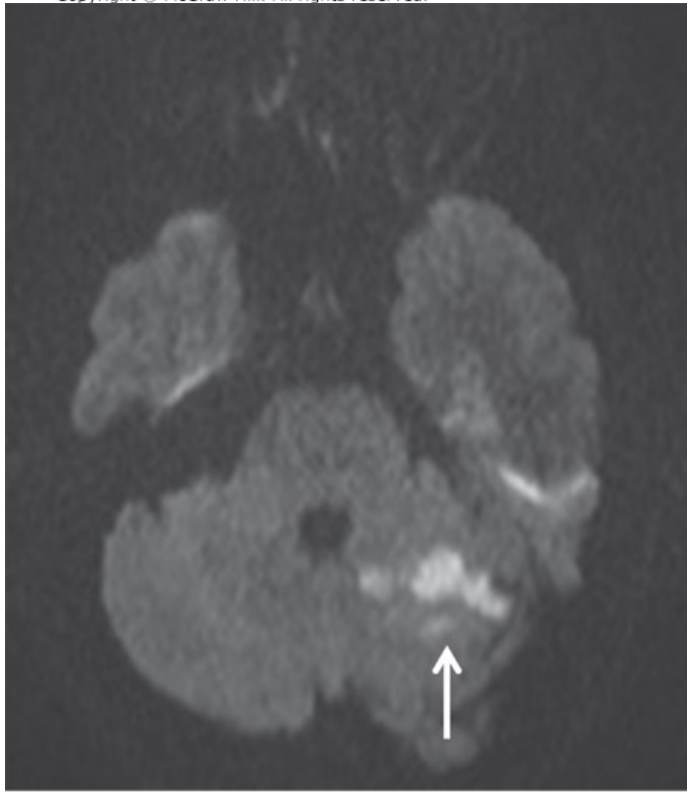
Source: David V. Feliciano, Kenneth L. Mattox,
Ernest E. Moore: Trauma, Ninth Edition
Copyright © McGraw Hill. All rights reserved.

**E**

Source: David V. Feliciano, Kenneth L. Mattox,
Ernest E. Moore: Trauma, Ninth Edition
Copyright © McGraw Hill. All rights reserved.

**F**

Source: David V. Feliciano, Kenneth L. Mattox,
Ernest E. Moore: Trauma, Ninth Edition
Copyright © McGraw Hill. All rights reserved.

**G**

Source: David V. Feliciano, Kenneth L. Mattox,
Ernest E. Moore: Trauma, Ninth Edition
Copyright © McGraw Hill. All rights reserved.

Modern helical MDCT scanners allow for high-resolution imaging of the cervical spine, with the quality of sagittal and coronal images equating to that

of the axial images. Axial slices of the cervical spine are obtained at 1.0- to 3.0-mm slice thickness from the skull base through the upper thoracic spine (T2-T4 vertebral body level). Coronal and sagittal reformations are typically 1.0- to 3.0-mm-thick images and reconstructed using bone and soft tissue algorithms. Generally, the information gathered from these reformations is sufficient and makes plain x-rays unnecessary. PACS workstations can facilitate the rapid review of these large image sets, and the use of cross-referencing tools assists with identification of specific vertebral levels.

Careful review of the entire cervical spine in all three planes is necessary for comprehensive evaluation. Some of the more common fracture patterns (eg, type II fractures of the base of the odontoid process or horizontally oriented fractures of the spinous process) have “in plane” axial fracture lines and thus may be difficult to identify when reviewing the axial images alone. The coronal reformations may be viewed using the same approach as standard AP x-rays, whereas viewing of the sagittal reformations can be performed with guidelines used for the lateral cervical spine. Nonetheless, careful attention to axial images is necessary to detect fractures involving the craniocervical junction, transverse processes (which increase the likelihood of a vertebral artery injury), margins of vertebral bodies, pedicles, lateral mass, or lamina and spinous processes.

The sensitivity and specificity of cervical spine CT for acute bony injuries are routinely in excess of 95%. Although CT does not directly show soft tissue injuries to the spine, focal kyphosis, focal lordosis, and widening of the disk space can be used as with conventional x-rays to suggest associated injuries to soft tissue. Occasionally, acute disk herniations can be identified on axial or sagittal soft tissue images. Some authors feel that clinically important injuries to soft tissue causing biomechanical instability are almost always evident on technically adequate CTs of the cervical spine (especially on the sagittal and parasagittal reformations).⁶¹

Computed Tomography of the Thoracolumbar Spine

A low threshold should be maintained for the use of CT to further evaluate vertebral body deformities identified on conventional x-rays. In addition, patients with high-risk mechanisms and impressive signs or symptoms without abnormal x-rays should undergo a thoracolumbar CT to detect occult minimal burst fractures or Chance or flexion-distraction-type injuries. Dedicated radiographs of the thoracolumbar spine can be omitted if a CT of the chest and/or abdomen is obtained. The CT raw data of the chest and/or abdomen can be used to generate dedicated coned down images of the thoracolumbar spine, reconstructed in axial, sagittal, and coronal planes using a bone algorithm, without the need to reimagine the patient. Limited imaging of specific vertebral body levels based on radiographic findings is being replaced by more comprehensive spinal imaging.

Typically, 2.0- to 3.0-mm-thick axial slices are acquired and are reconstructed using both bone and soft tissue algorithms. Imaging of the entire thoracic or lumbar spine is advised as it allows more accurate determination of the location of injury. Sagittal reformations are made in both algorithms and viewed at bone and soft tissue windows, respectively. Careful attention to the paraspinal structures, such as the ribs, mediastinum, and retroperitoneum, is strongly recommended if a flexion-distraction or Chance fracture is detected on dedicated thoracolumbar CT imaging. This diagnostic pitfall is becoming less of a factor due to the increased use of contrast-enhanced whole-body CT imaging in trauma.

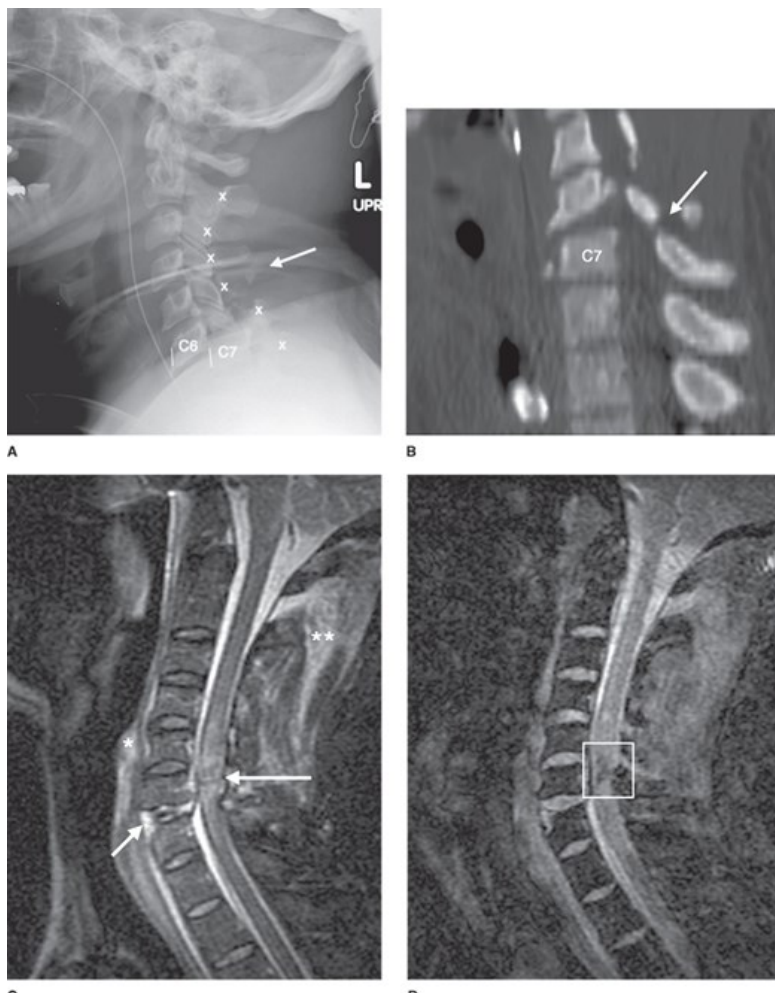
Magnetic Resonance Imaging of the Spine

The principle indications for MRI are to characterize soft tissue injuries and potential spinal cord injuries in patients with associated fractures and/or malalignment of vertebrae (Fig. 19-13). An MRI is indicated in individuals who have no conventional x-rays or CT abnormality but who have an acute myelopathy or radiculopathy (spinal cord injury without radiographic abnormality [SCIWORA]). The use of MRI is frequently controversial in the setting of dislocation of bilateral or unilateral facets. Some advocate initial reduction followed by MRI, but this is a practice that varies from institution to institution. In general, urgent MRI is appropriate when there is an evolving neurologic deficit or neurologic deficits without explanation.

FIGURE 19-13

Multimodality correlations: cervical spine. A patient with C6-C7 fracture dislocation underwent preretraction lateral conventional radiograph (A), postreduction sagittal reformation (B) from axial computed tomography (CT), and magnetic resonance imaging (MRI) of the spine and cord (C) and (D). (A) White Xs mark laminar points, and connecting them shows disruption of spinolaminar line at C6-C7. Arrow points to fractures of inferior articular process of C6. Sagittal CT reformation (B) shows improved alignment of vertebral bodies but persistent encroachment of neural canal from bony fragments from body and posterior elements (arrow). (C, D) Sagittal MRI performed using short tau inversion recovery (STIR) and gradient recalled echo (GRE) sequences following reduction of C6-C7 fracture dislocation. Single asterisk shows precervical edema, and double asterisk shows edema in posterior spinal musculature. Long white arrow shows a region of cord swelling with heterogeneous signal, suggesting cord transection at C6 level. Short arrow shows abnormal signal within C6-C7 disk space. GRE sequences (D) show decreased signal at C6 level within the center of the cord that is

compatible with hemorrhage (white square), which portends poorer neurologic prognosis than edema alone.



Source: David V. Feliciano, Kenneth L. Mattox,
Ernest E. Moore: Trauma, Ninth Edition
Copyright © McGraw Hill. All rights reserved.

Edema of the spinal cord has a much better prognosis than cord hemorrhage. MRI is helpful in making this distinction, as well as detecting epidural hematomas that may require decompression. Evaluations of the disk spaces, ligaments of the spinal column and facet joints, and the craniocervical junction are best made with MRI.

Spine MRI imaging protocols in trauma vary among institutions, but sagittal and axial T1-weighted and fluid-sensitive sequences (eg, T2-weighted short tau inversion recovery [STIR]) are standard. Gradient echo (GRE) sequences are useful in detecting magnetic susceptibility artifact due to blood products. When assessing the transverse atlantal ligament, images should be obtained in the axial plane parallel to Ranawat's line (a line from the anteriormost portion of the anterior tubercle of C1 to the most posterior aspect of the posterior arch of C1).

MRIs have been used to "clear" the cervical spine in obtunded or unexamable patients with otherwise normal imaging (CT or high-quality conventional radiographs).^{62,63} The absence of abnormal high signal intensity in ligaments and disks effectively excludes biomechanically significant injuries; however, an abnormal signal does not necessarily confirm instability.

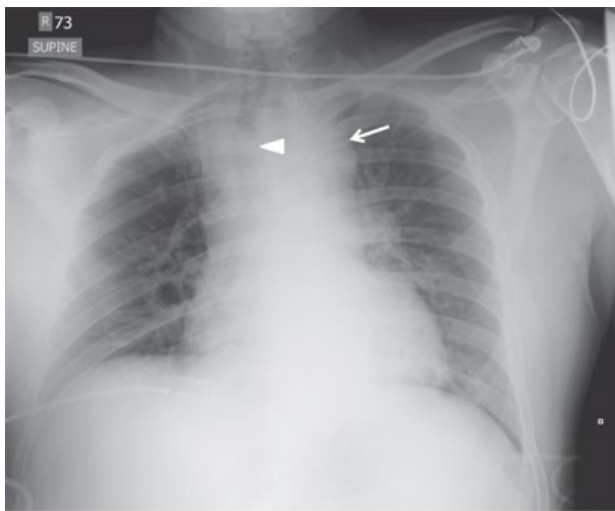
Computed Tomography of the Chest

Chest CT has high sensitivity, specificity, and negative predictive value in the setting of trauma and can provide significant information about the lungs, pleural cavities, thoracic vasculature, and chest wall.⁶⁴ Chest CT is generally performed to evaluate adult victims of high-energy blunt trauma (especially those with chest pain, deformity, or hypoxia), with particular attention to the mediastinal structures (Figs. 19-14, 19-15, 19-16, 19-17, 19-18). Children presenting with hypotension, elevated respiratory rate, abnormal physical examination, depressed consciousness, and femur fractures after

blunt trauma are at a substantially increased risk for an intrathoracic injury.⁶⁵

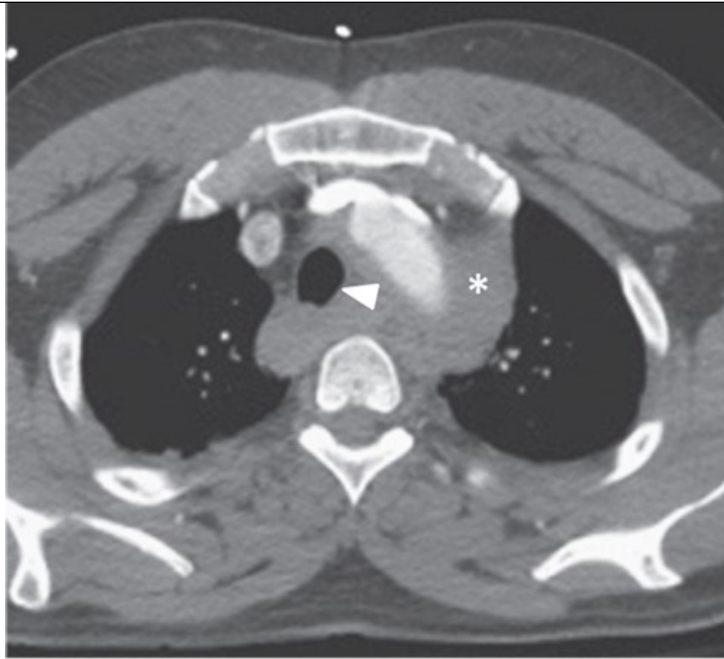
FIGURE 19-14

Blunt traumatic rupture of the thoracic aorta. (A) Anteroposterior supine chest radiograph demonstrates a bulbous aortic arch contour (arrow) and rightward deviation of the trachea (arrowhead), concerning for a mediastinal hematoma. (B) Axial computed tomography angiography (CTA) of the upper mediastinum demonstrates a superior mediastinal hematoma (asterisk) and rightward tracheal deviation (arrowhead). (C, D) Axial and sagittal CTA of the mid thorax demonstrates intimal flaps and abnormal outpouching of contrast along the anterior surface of the proximal descending thoracic aorta due to a traumatic pseudoaneurysm (arrows). There is adjacent mediastinal hematoma (asterisk). (E) Catheter aortography adds little information in this instance. Focal outpouching of the proximal descending thoracic aorta due to a traumatic pseudoaneurysm (arrows) is again identified.

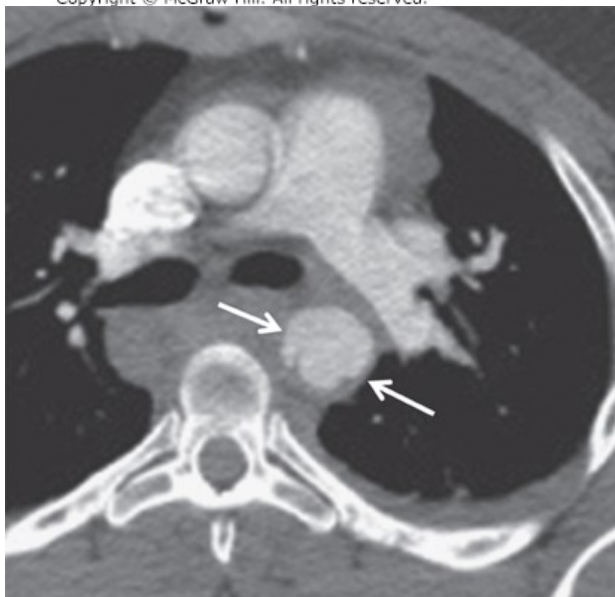


A

Source: David V. Feliciano, Kenneth L. Mattox,
Ernest E. Moore: Trauma, Ninth Edition
Copyright © McGraw Hill. All rights reserved.

**B**

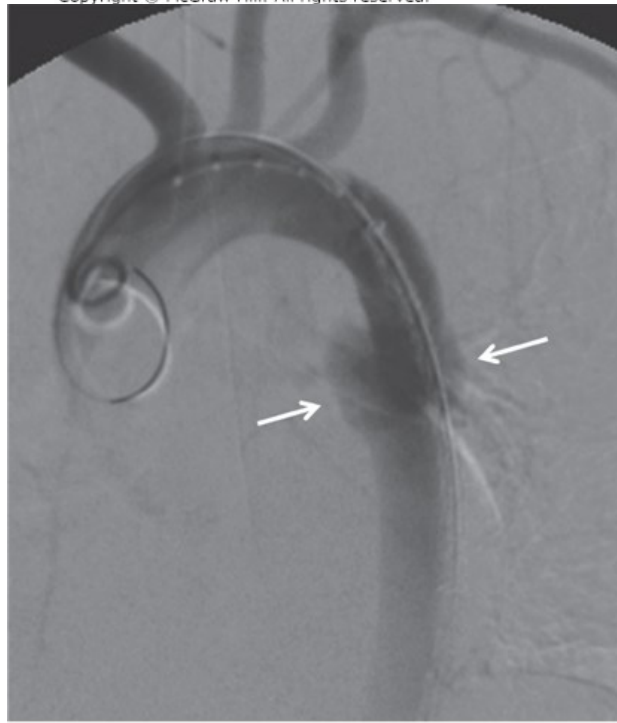
Source: David V. Feliciano, Kenneth L. Mattox,
Ernest E. Moore: Trauma, Ninth Edition
Copyright © McGraw Hill. All rights reserved.

**C**

Source: David V. Feliciano, Kenneth L. Mattox,
Ernest E. Moore: Trauma, Ninth Edition
Copyright © McGraw Hill. All rights reserved.

**D**

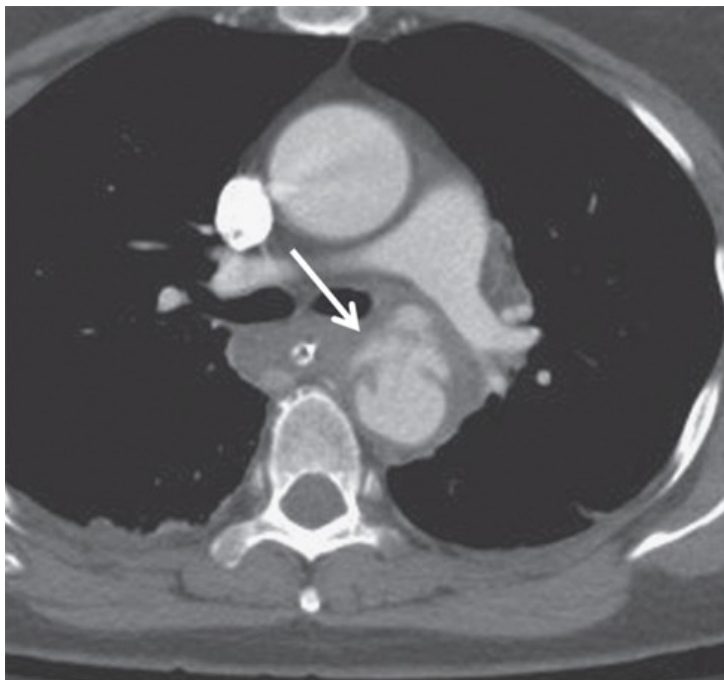
Source: David V. Feliciano, Kenneth L. Mattox,
Ernest E. Moore: Trauma, Ninth Edition
Copyright © McGraw Hill. All rights reserved.

**E**

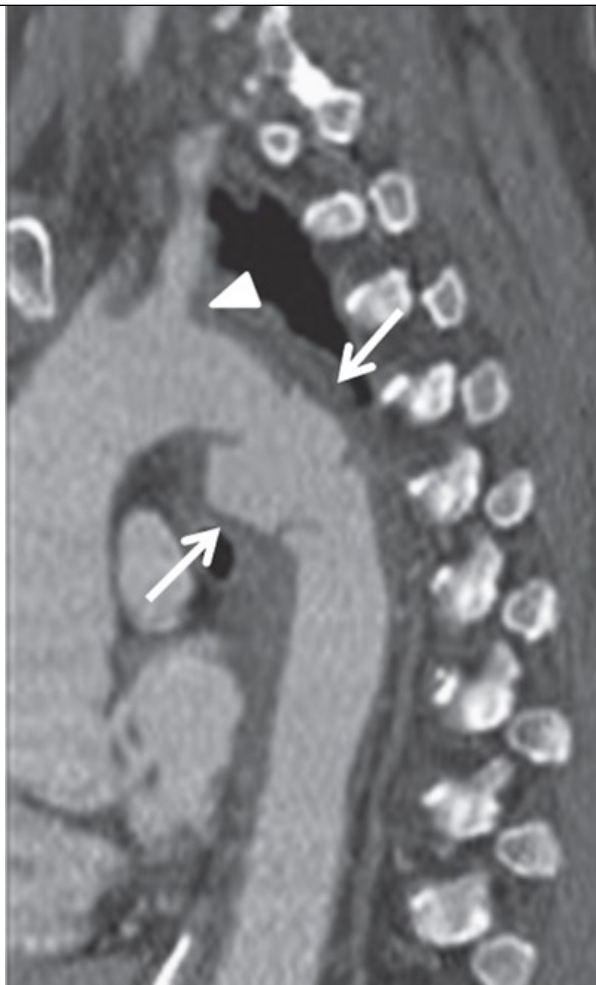
Source: David V. Feliciano, Kenneth L. Mattox,
Ernest E. Moore: Trauma, Ninth Edition
Copyright © McGraw Hill. All rights reserved.

FIGURE 19-15

Acute thoracic aortic injury following blunt chest trauma. Axial (A) and sagittal (B) chest computed tomography angiography shows a transection of the proximal descending thoracic aorta (arrows) just distal to the origin of the left subclavian artery (arrow head). (C) Catheter angiogram of the thoracic aorta showing the aortic injury (arrow), which was successfully treated with an endovascular stent graft (D).

**A**

Source: David V. Feliciano, Kenneth L. Mattox,
Ernest E. Moore: Trauma, Ninth Edition
Copyright © McGraw Hill. All rights reserved.

**B**

Source: David V. Feliciano, Kenneth L. Mattox,
Ernest E. Moore: Trauma, Ninth Edition
Copyright © McGraw Hill. All rights reserved.

**C**

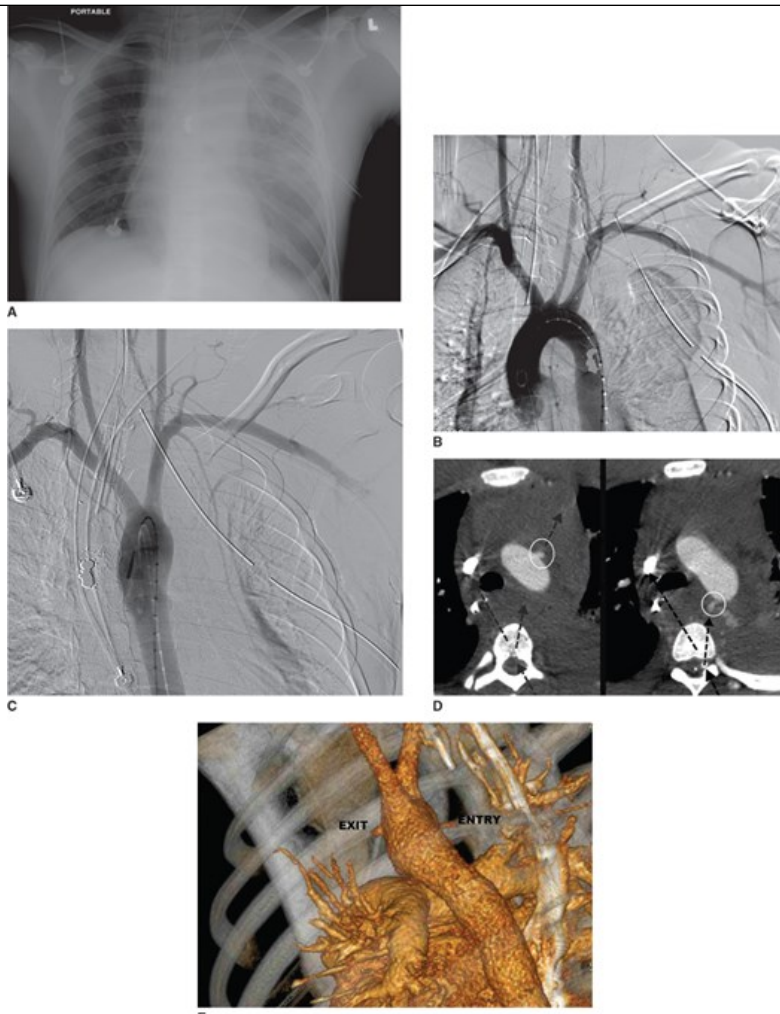
Source: David V. Feliciano, Kenneth L. Mattox,
Ernest E. Moore: Trauma, Ninth Edition
Copyright © McGraw Hill. All rights reserved.

**D**

Source: David V. Feliciano, Kenneth L. Mattox,
Ernest E. Moore: Trauma, Ninth Edition
Copyright © McGraw Hill. All rights reserved.

FIGURE 19-16

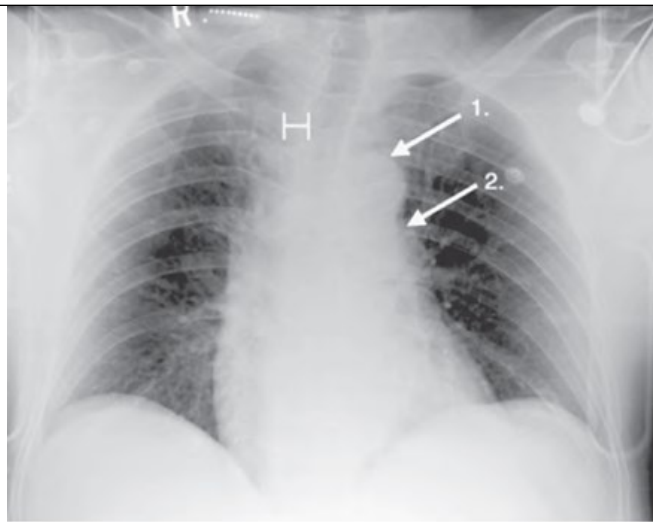
Gunshot injury of the aortic arch not detected on catheter aortography. A 24-year-old male sustained a gunshot wound of the back with mediastinal traverse. He was hemodynamically stable but paraplegic. (A) Portable chest radiography showed hemothorax and a very wide indistinct mediastinum with a bullet in the mediastinum. (B, C) Right and left anteroposterior catheter aortograms did not show any evidence of an injury. (D) However, suspicion of an aortic injury persisted. Therefore, a computed tomography arteriogram was performed. This shows that the bullet had traversed the spine and fragmented into parts that went to the right and the left (dashed arrows). The left fragments penetrated the posterior arch and exited the anterior arch of the aorta (arrows). (E) Surface-rendered reformations clearly show the path of the bullet.



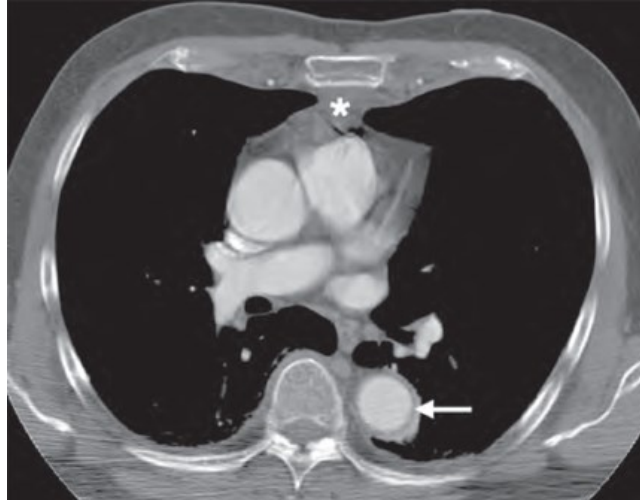
Source: David V. Feliciano, Kenneth L. Mattox,
Ernest E. Moore: Trauma, Ninth Edition
Copyright © McGraw Hill. All rights reserved.

FIGURE 19-17

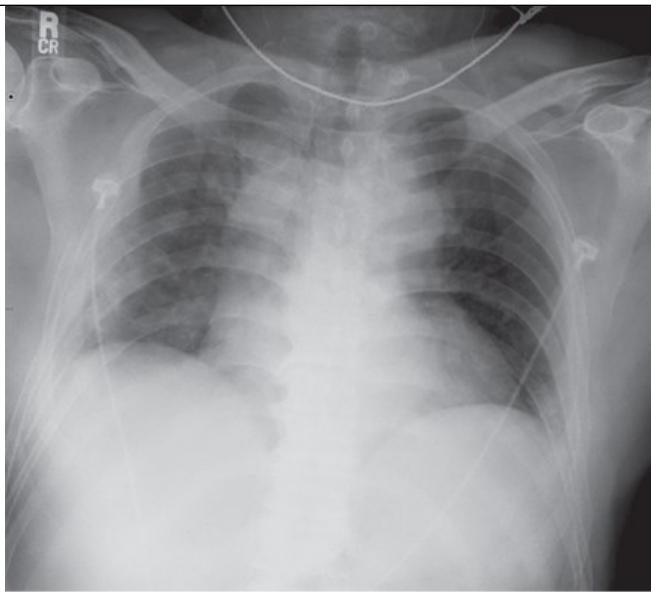
Mediastinal hematoma caused by nonaortic injury. (A) Anteroposterior (AP) chest radiograph performed on 19-year-old unrestrained driver in head-on motor vehicle crash shows multiple injuries, including T6 and left shoulder fractures. Widening of right paratracheal stripe (H), obscuration of aortic arch (black arrow), and abnormal right paraspinal line (white arrows) suggest mediastinal hematoma. In absence of osteophytes, right paratracheal stripes are not typically seen in young adults, and their presence locally should direct search for underlying pathology. Left paraspinal line is typically seen due to descending aorta and should not be seen as continuous line between the lower chest and the apex of lung. Continuous left paraspinal line from apex to diaphragm is pathognomonic for mediastinal collection, such as hematoma in setting of trauma. (B) Same patient as in A; axial computed tomography (CT) following intravenous contrast shows extensive posterior mediastinal hematoma (asterisks). (C–E) This is a 56-year-old male involved in a motor vehicle collision. (C) AP supine chest radiograph demonstrates a widened mediastinum with abnormal and ill-defined aortic contours, concerning for a mediastinal hematoma. (D) Axial postcontrast CT through the upper mediastinum demonstrates retrosternal hematoma (arrow) with a clean fat plane between the hematoma and aorta (asterisk) and no periaortic hemorrhage. (E) Axial postcontrast CT through the mid chest demonstrates a fracture of the sternal body (arrowhead) as a source of the mediastinal hematoma (arrow). The aorta was not injured.

**A**

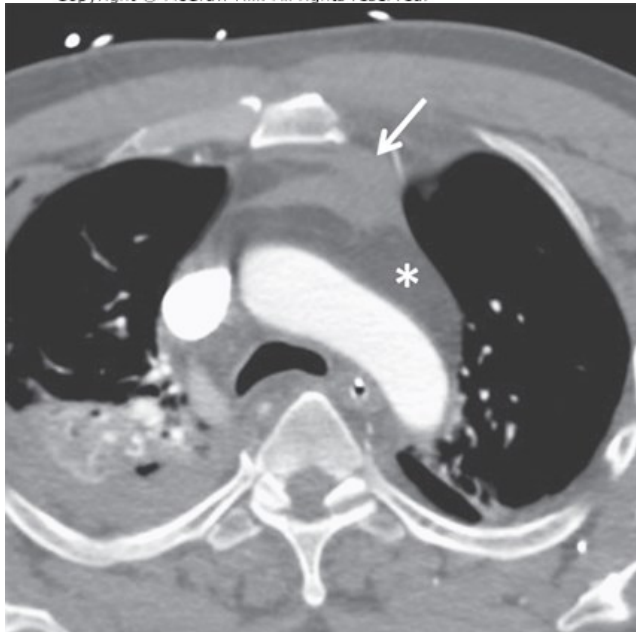
Source: David V. Feliciano, Kenneth L. Mattox,
Ernest E. Moore: Trauma, Ninth Edition
Copyright © McGraw Hill. All rights reserved.

**B**

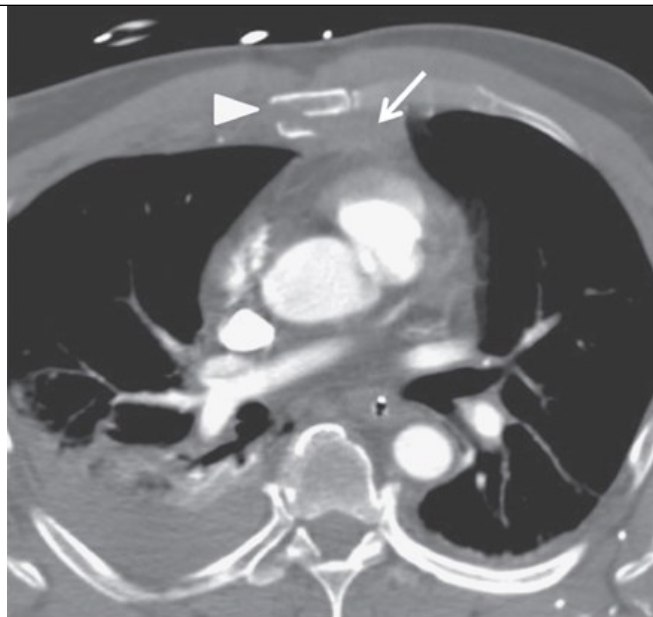
Source: David V. Feliciano, Kenneth L. Mattox,
Ernest E. Moore: Trauma, Ninth Edition
Copyright © McGraw Hill. All rights reserved.

**C**

Source: David V. Feliciano, Kenneth L. Mattox,
Ernest E. Moore: Trauma, Ninth Edition
Copyright © McGraw Hill. All rights reserved.

**D**

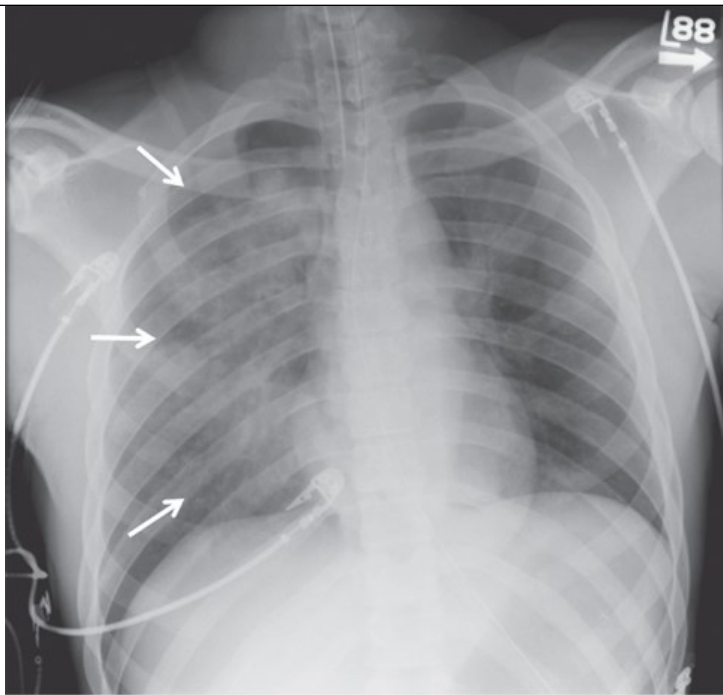
Source: David V. Feliciano, Kenneth L. Mattox,
Ernest E. Moore: Trauma, Ninth Edition
Copyright © McGraw Hill. All rights reserved.

**E**

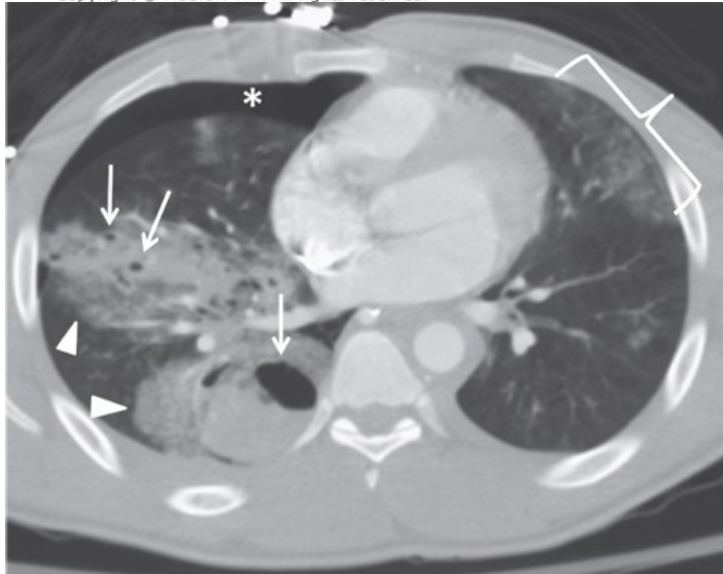
Source: David V. Feliciano, Kenneth L. Mattox, Ernest E. Moore: Trauma, Ninth Edition
Copyright © McGraw Hill. All rights reserved.

FIGURE 19-18

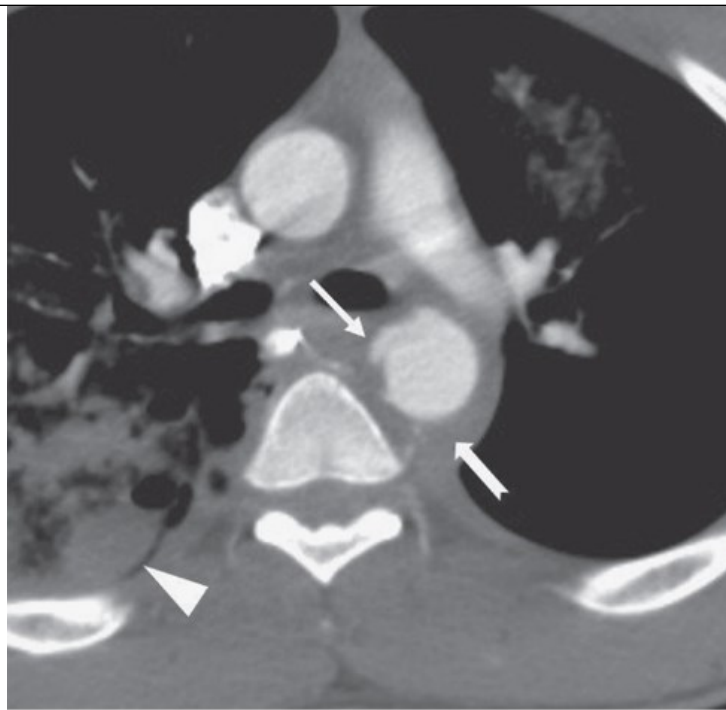
Pulmonary contusions and lacerations due to blunt-force injury. (A) Anteroposterior (AP) supine chest radiograph of a patient involved in a T-bone motor vehicle collision shows extensive right perihilar distribution airspace opacities (arrows). The left lung is clear. (B) Axial postcontrast computed tomography (CT) image reveals a right pneumothorax (asterisk, which was radiographically occult) and multiple pulmonary parenchymal lacerations (arrows) of various sizes, the larger of which demonstrates a layering blood fluid level. Ground glass opacities surrounding these lacerations are due to pulmonary contusions (arrowheads). There are patchy peripheral ground glass opacities in the left upper lobe compatible with pulmonary contusions (bracket), which are better appreciated on CT. Pulmonary contusions are typically present by the time the patient presents to the hospital and may evolve for 48 to 72 hours. Progression thereafter should be considered a complication, such as pneumonia or adult respiratory distress syndrome. Typically, pulmonary contusions resolve within 1 week. This example nicely illustrates that a supine chest radiograph often underestimates the severity of a chest injury. (C) Axial CT through the upper chest shows an aortic injury (arrow) and pulmonary contusions/lacerations (triangle) not as well seen on this soft tissue image.

**A**

Source: David V. Feliciano, Kenneth L. Mattox,
Ernest E. Moore: Trauma, Ninth Edition
Copyright © McGraw Hill. All rights reserved.

**B**

Source: David V. Feliciano, Kenneth L. Mattox,
Ernest E. Moore: Trauma, Ninth Edition
Copyright © McGraw Hill. All rights reserved.

**C**

Source: David V. Feliciano, Kenneth L. Mattox, Ernest E. Moore: Trauma, Ninth Edition
Copyright © McGraw Hill. All rights reserved.

Chest CT is performed with intravenous contrast, preferably with the patient's arms abducted above the head, from the thoracic inlet to the mid abdomen to include the entire thoracic cavity. Continuing the scan through the abdomen and pelvis can be easily performed. Images are acquired during the systemic arterial phase to maximize aortic enhancement and are reconstructed in the axial, sagittal, and coronal planes at 2.0- to 4.0-mm slice thickness. MPRs are used to evaluate not only the thoracic aorta and mediastinum, but also the thoracic spine (see earlier discussion). Tailored MPRs, such as sagittal oblique ("candy cane" view of the aorta), may be helpful in visualization of an aortic injury. Noncontrast chest imaging has limited utility in the setting of trauma, although mediastinal blood, hemopneumothoraces, and fractures to the spine and ribs may be detected on noncontrast imaging. In patients unable to receive contrast due to a known severe allergy, noncontrast CT can be effective in detecting a mediastinal hematoma and guiding the patient to evaluations such as transesophageal echocardiography and MRA. In patients with renal insufficiency, the risk of contrast-induced nephropathy or worsening renal function should be weighed against the risk of missing a major thoracic injury.

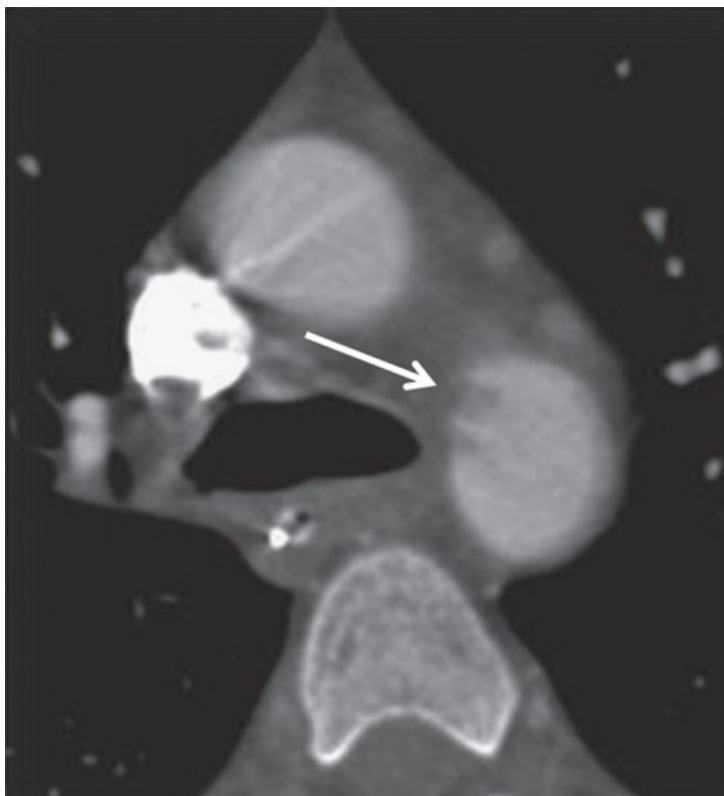
Chest CT is believed to be most cost-effective when patients: (1) are already undergoing another CT examination (eg, CT of the head, abdomen, and pelvis); (2) are at risk for injury to the thoracic aorta because of high-energy mechanism, associated injuries, or age (>50 years old); or (3) have a previously abnormal chest radiograph. A clinical decision rule was proposed by Blackmore et al,⁶⁶ in which individuals with two or more of the following are at high risk for aortic injury: age greater than 50, unrestrained occupant in motor vehicle crash, hypotension, thoracic injury (rib fracture, pneumothorax, pulmonary contusion, or laceration), abdominopelvic injury (fracture of lumbar spine or pelvic ring, injury requiring laparotomy), fractures of appendicular skeleton, or injury to the brain.

The role of MDCT in the diagnosis of acute traumatic aortic injury has undergone significant evolution over the past 25 years, with sensitivity and negative predictive value of contrast-enhanced chest CT routinely in excess of 98% for modern scanners. In fact, patients who have direct signs of a thoracic aortic injury on MDCT no longer require catheter angiography confirmation, as was often the case in the past, and a normal thoracic aorta on chest CTA reliably excludes a traumatic aortic injury.⁶⁷ CT imaging features of a traumatic aortic injury can be divided into direct and indirect findings. Direct findings of traumatic aortic injuries include pseudoaneurysms, intimal flaps, pseudocoarctation (due to subadventitial dissection), and active bleeding. A mediastinal hematoma, however, is an indirect finding and can be present in the absence of an aortic injury. To suggest an aortic injury, a mediastinal hematoma should be contiguous with the aortic wall and should not be separated from the aorta by a rim of fat (Fig. 19-17D). Determination of whether or not a mediastinal hematoma has obliterated juxta-aortic fat can be difficult in thin patients or in patients with extensive soft tissue edema. Complex atheromatous disease can make interpretation of the examination difficult, particularly for subtler injuries. An emerging form of an acute aortic injury, called the "minimal" or "minor" aortic injury, is an injury pattern thought to be secondary to advancing imaging

technology (Fig. 19-19).^{68,69}

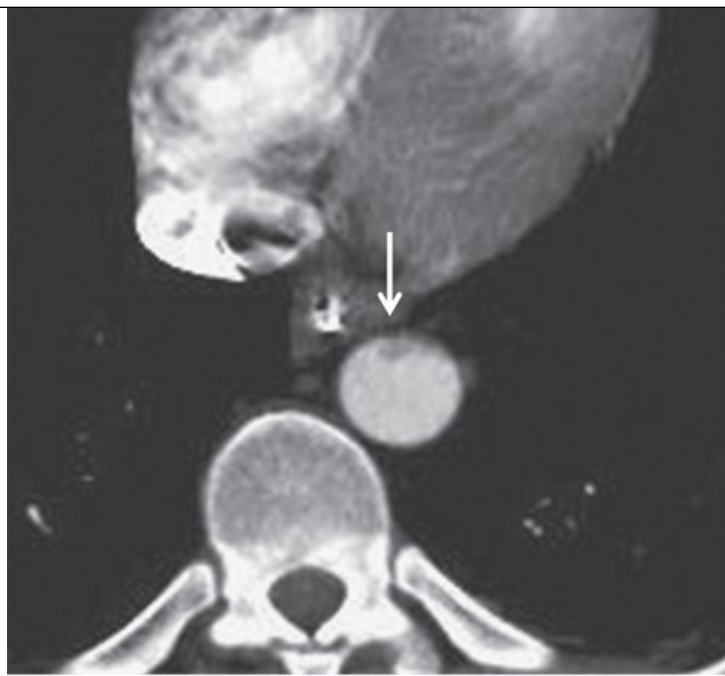
FIGURE 19-19

Minimal aortic injuries following blunt thoracic trauma. (A–B) Axial postcontrast images from two different patients each demonstrates intimal injuries with focal intraluminal thrombi (arrows) involving the aortic arch (A) and mid descending thoracic aorta (B). There is trace adjacent periaortic hemorrhage in A and no periaortic hemorrhage in B. (C) Sagittal postcontrast computed tomography (CT) of another patient with multiple intimal injuries throughout the descending thoracic aorta (arrows) compatible with multifocal minimal aortic injuries. There is no periaortic hemorrhage. (D, E) A 42-year-old female with a minimal aortic injury of the mid descending thoracic aorta. Admission axial postcontrast image (D) demonstrates a focal intimal injury and thrombus of the mid descending thoracic aorta (arrow). (E) One-week follow-up chest CT reveals resolution of intimal injury and thrombus.

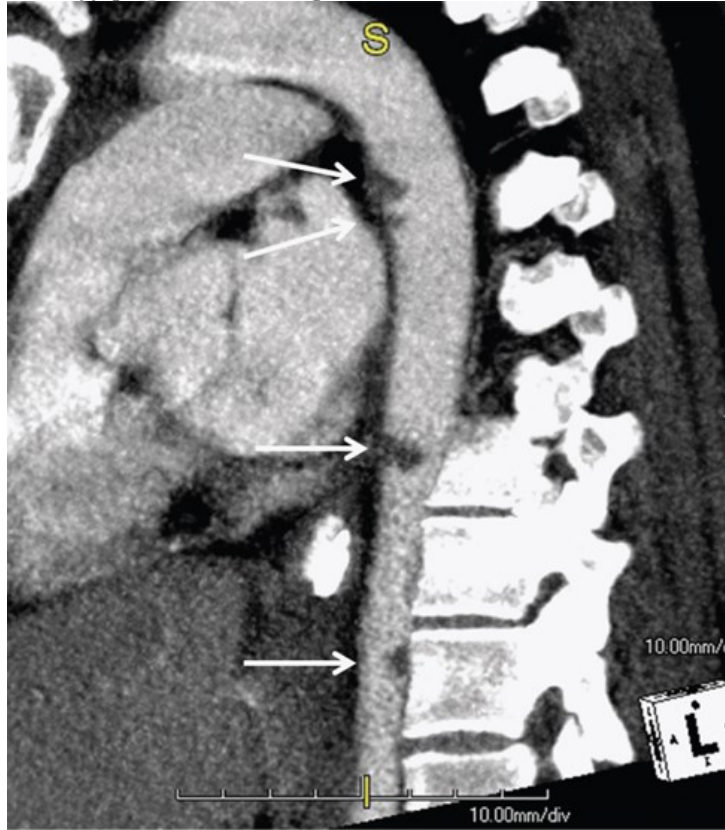


A

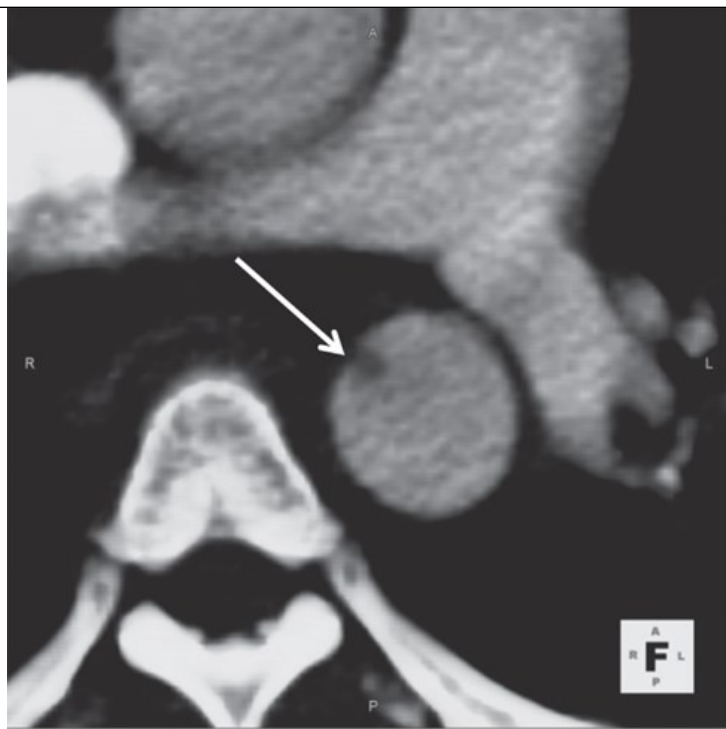
Source: David V. Feliciano, Kenneth L. Mattox,
Ernest E. Moore: Trauma, Ninth Edition
Copyright © McGraw Hill. All rights reserved.

**B**

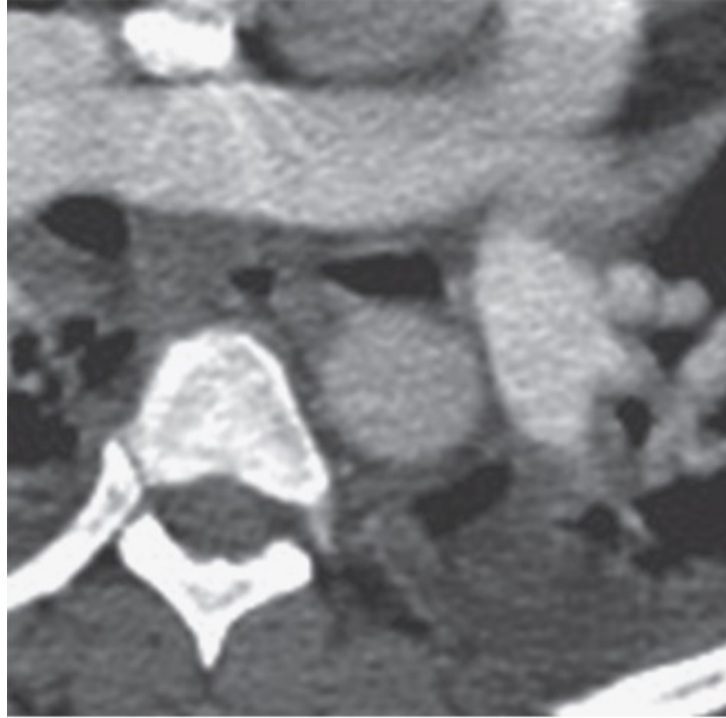
Source: David V. Feliciano, Kenneth L. Mattox,
Ernest E. Moore: Trauma, Ninth Edition
Copyright © McGraw Hill. All rights reserved.

**C**

Source: David V. Feliciano, Kenneth L. Mattox,
Ernest E. Moore: Trauma, Ninth Edition
Copyright © McGraw Hill. All rights reserved.

**D**

Source: David V. Feliciano, Kenneth L. Mattox, Ernest E. Moore: Trauma, Ninth Edition
Copyright © McGraw Hill. All rights reserved.

**E**

Source: David V. Feliciano, Kenneth L. Mattox, Ernest E. Moore: Trauma, Ninth Edition
Copyright © McGraw Hill. All rights reserved.

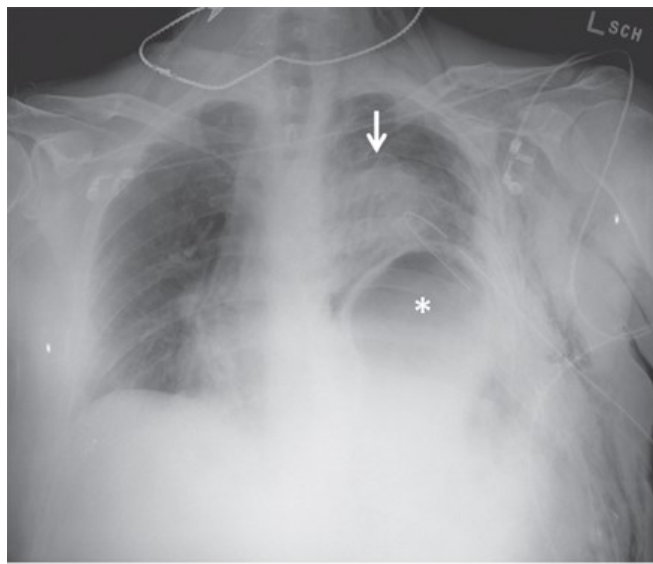
There is significant debate regarding what lesion is defined as a "minimal" aortic injury. More specifically, they may include an intimal injury with thrombus, intimal flap less than 1 cm in length, and pseudoaneurysm less than 1 cm in diameter. There is often very little or no mediastinal hemorrhage with this type of injury.^{68,69} There are no universally accepted imaging follow-up recommendations for patients with minimal aortic

injuries, although serial short interval follow-up to resolution has been advocated.⁶⁹ Finally, aortic pulsation artifact (particularly involving the aortic root and ascending aorta) and beam hardening artifact due to dense contrast in adjacent venous structures may make interpretation difficult. Further evaluation with catheter angiography can be performed in equivocal or suboptimal examinations but is of low diagnostic value in the setting of a high-quality diagnostic chest CT angiogram. Multiplanar and 3D reformations of the injured thoracic aorta are particularly helpful for planning treatment. It is important to delineate the anatomy of interest to the trauma surgeon, such as the distance from the most proximal point of injury to the origin of the left subclavian artery or any anomalous branches. These capabilities have significantly altered the role of catheter angiography from its traditional role of diagnosis, staging, and pretreatment planning, to one more often used for resolving diagnostic conundrums raised by CT or transesophageal echocardiography or as part of treatment using an endovascular stent graft.

CT is the most sensitive diagnostic method for detection of acute blood in the pericardium.⁷⁰ It is also among the most sensitive methods for detection of injuries to the chest wall, pleural cavities, and lungs.⁶⁴ Older CT technology exhibited relatively low sensitivity for the detection of injuries to the hemidiaphragm (sensitivity of 65%–70%) but has vastly improved with helical MDCT technology, now with sensitivities of 71% to 90% and specificities of 98% to 100%.⁷¹ For suspected diaphragmatic injuries, especially herniations through a diaphragmatic tear, coronal and sagittal multiplanar reformations are useful because they better display characteristic findings (Fig. 19-20). Direct CT signs of diaphragmatic rupture include focal diaphragmatic defect, the “dangling” diaphragm sign (from a free-floating diaphragm flap), and herniation of abdominal contents through a diaphragmatic defect. A normal contour of the diaphragm and no pleural collections or adjacent airspace disease effectively exclude diaphragmatic injury.

FIGURE 19-20

A 60-year-old-male with a left diaphragm rupture following a high-speed motor vehicle collision. (A) Portable chest film on admission demonstrates superior displacement of the stomach (asterisk). There is a left upper lobe opacity (arrow) due to pulmonary contusion. (B) Axial computed tomography (CT) image through the lower chest demonstrates the stomach (asterisk) above the diaphragm next to the heart. There is herniation of abdominal fat and colon (arrow) into the left thoracic cavity. Notice that the stomach and abdominal fat are displaced posteriorly and are layering dependently against the posterior chest wall, referred to as the “dependent viscera sign,” a specific sign of a diaphragm rupture. (C) Coronal CT image demonstrates the stomach (asterisk) herniated into the left thoracic cavity. There is a nasogastric tube in place (arrow).

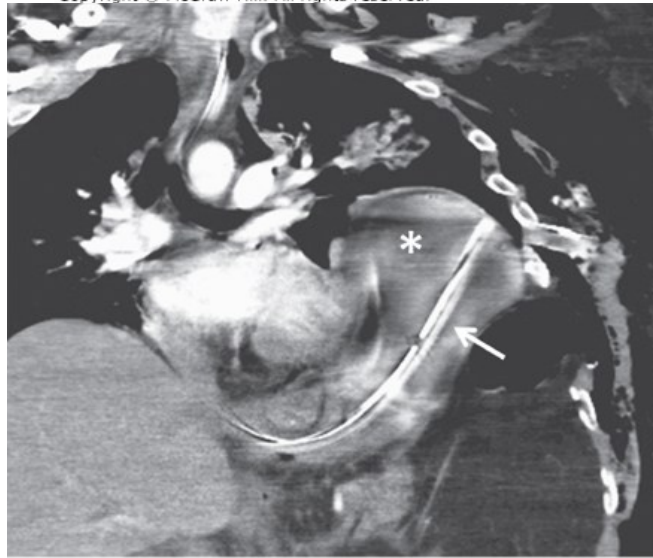


A

Source: David V. Feliciano, Kenneth L. Mattox, Ernest E. Moore: Trauma, Ninth Edition
Copyright © McGraw Hill. All rights reserved.

**B**

Source: David V. Feliciano, Kenneth L. Mattox,
Ernest E. Moore: Trauma, Ninth Edition
Copyright © McGraw Hill. All rights reserved.

**C**

Source: David V. Feliciano, Kenneth L. Mattox,
Ernest E. Moore: Trauma, Ninth Edition
Copyright © McGraw Hill. All rights reserved.

CT is helpful for diagnosing injuries to the tracheobronchial tree and has a sensitivity of 85% for tracheal rupture.³⁰ Nearly all patients with tracheobronchial injuries exhibit a massive pneumomediastinum or soft tissue emphysema (Fig. 19-7A and B; Fig. 19-9D and E).

Computed Tomography of Abdomen and Pelvis

Abdominopelvic CT is one of many adjunctive tests to assist the trauma surgeon in the evaluation of hemodynamically stable patients with suspected occult intra-abdominal injuries or to aid in more definitive characterization of injuries previously detected by other diagnostic tests (eg, DPL or FAST; Figs. 19-21, 19-22, 19-23, 19-24, 19-25, 19-26, 19-27). Usual indications include abdominal signs (eg, lap belt sign) or symptoms (eg, pain and tenderness) following high-energy blunt trauma. The combination of pleuritic chest pain at the left costal margin and left lower rib fractures is an independent predictor of splenic injury and warrants diagnostic evaluation.⁷² Abdominopelvic CT is extremely helpful in guiding management and has been shown to significantly decrease the number of negative or nontherapeutic laparotomies. There has been a recent increase in the utilization of “triple-contrast” abdominopelvic CT in the setting of penetrating trauma, in the absence of indications for immediate laparotomy (eg, peritonitis or hemodynamic instability).⁷³ This is particularly true for back and flank penetrating wounds.

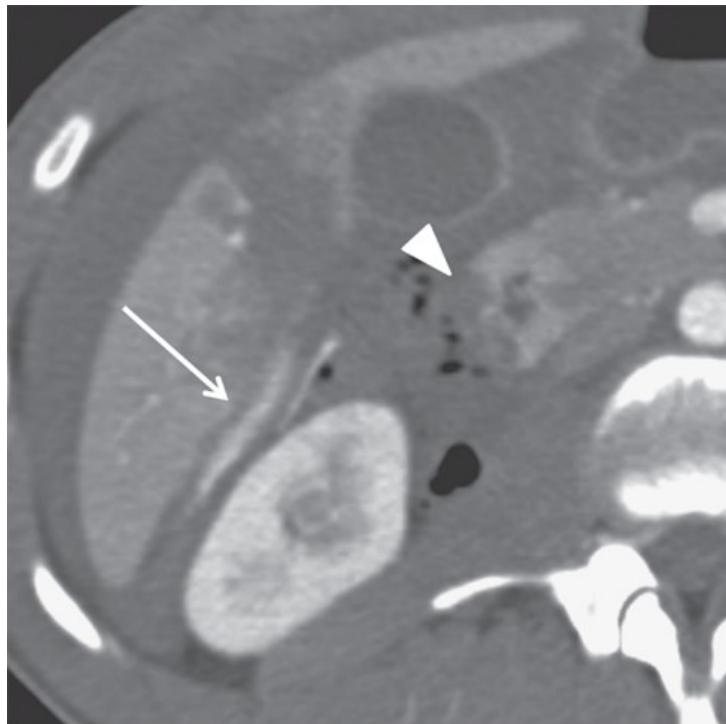
FIGURE 19-21

Downloaded 2024-6-9 5:19 A Your IP is 132.174.254.157

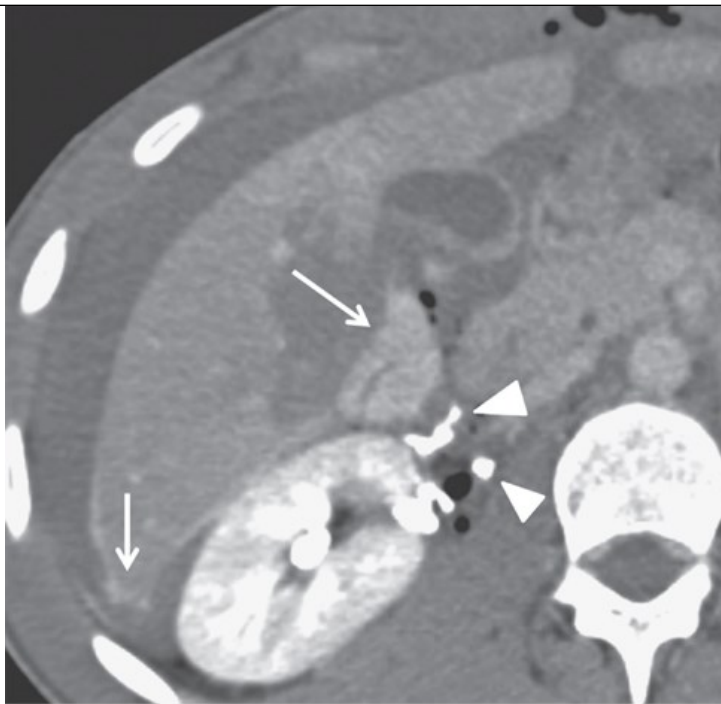
Chapter 19: Diagnostic and Interventional Radiology, Scott D. Steenburg

©2024 McGraw Hill. All Rights Reserved. [Terms of Use](#) • [Privacy Policy](#) • [Notice](#) • [Accessibility](#)

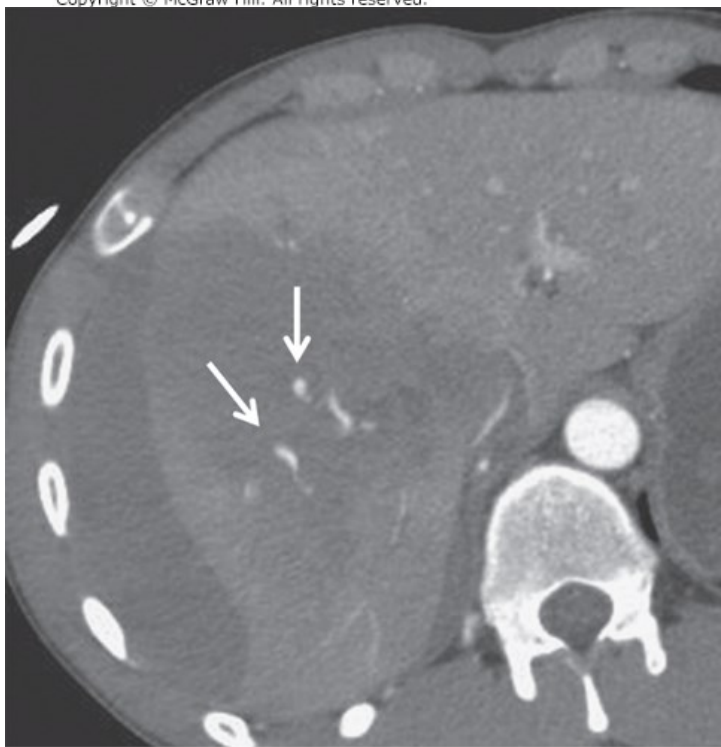
Examples of contrast extravasation in the abdomen. (A, B) Laceration of the right hepatic lobe following a gunshot wound. There is active contrast extravasation seen on arterial phase (A, arrow), which enlarges on 5-minute delayed phase (B, arrows) compatible with active bleeding. There is retroperitoneal gas due to a full-thickness duodenal injury (A, arrowhead). Five-minute delayed scan (B) also reveals extravasated urinary contrast from a renal pelvis laceration (B, arrowhead). (C-E) Active bleeding from a large liver laceration. Axial arterial phase (C), axial portal venous (PV) phase (D), and coronal maximum-intensity projection PV phase. (E) Image demonstrates active bleeding (arrows), which enlarges on the PV phase, accumulating in a large subcapsular hematoma (arrowhead). (F) Bowel contrast leak. A 23-year-old male following a left flank gunshot wound demonstrates leakage of a large amount of rectally administered contrast (arrows) from a full-thickness colon injury. Bubbles of extraluminal gas are seen in the left retroperitoneum (arrowheads). (G) Active contrast extravasation (arrow) from small bowel mesenteric root in a 28-year-old male following a motor vehicle collision. A large amount of free fluid and hemoperitoneum (asterisk) are also present. Active bleeding from the mesentery and an associated small bowel perforation were identified at surgery.

**A**

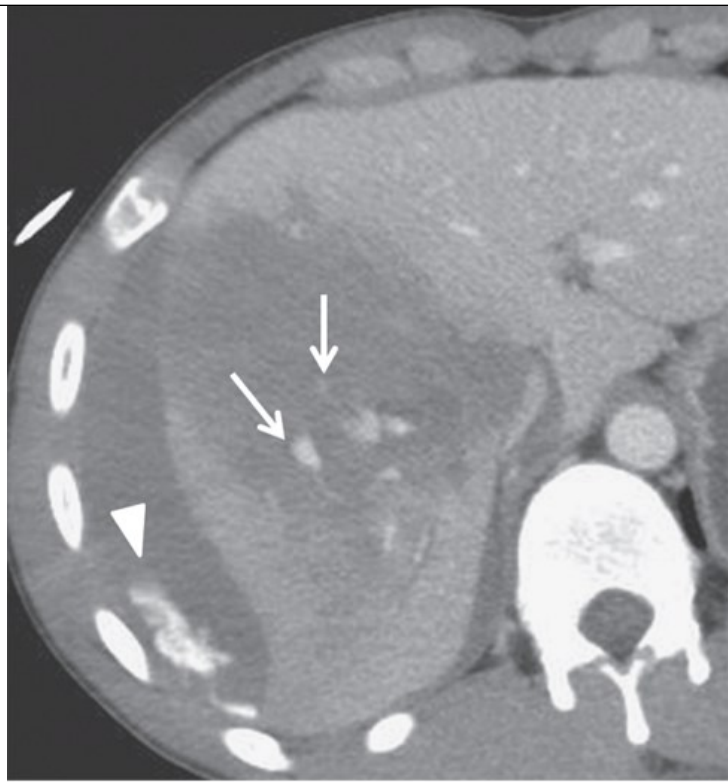
Source: David V. Feliciano, Kenneth L. Mattox,
Ernest E. Moore: Trauma, Ninth Edition
Copyright © McGraw Hill. All rights reserved.

**B**

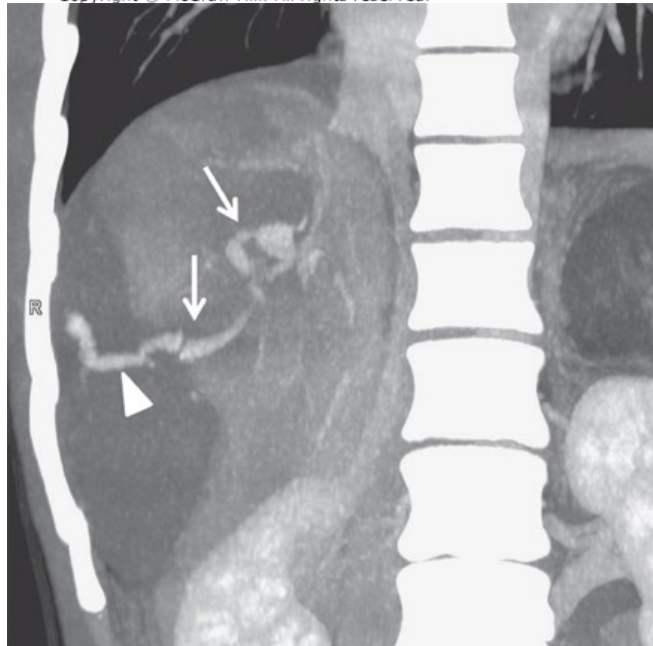
Source: David V. Feliciano, Kenneth L. Mattox,
Ernest E. Moore: Trauma, Ninth Edition
Copyright © McGraw Hill. All rights reserved.

**C**

Source: David V. Feliciano, Kenneth L. Mattox,
Ernest E. Moore: Trauma, Ninth Edition
Copyright © McGraw Hill. All rights reserved.

**D**

Source: David V. Feliciano, Kenneth L. Mattox,
Ernest E. Moore: Trauma, Ninth Edition
Copyright © McGraw Hill. All rights reserved.

**E**

Source: David V. Feliciano, Kenneth L. Mattox,
Ernest E. Moore: Trauma, Ninth Edition
Copyright © McGraw Hill. All rights reserved.

**F**

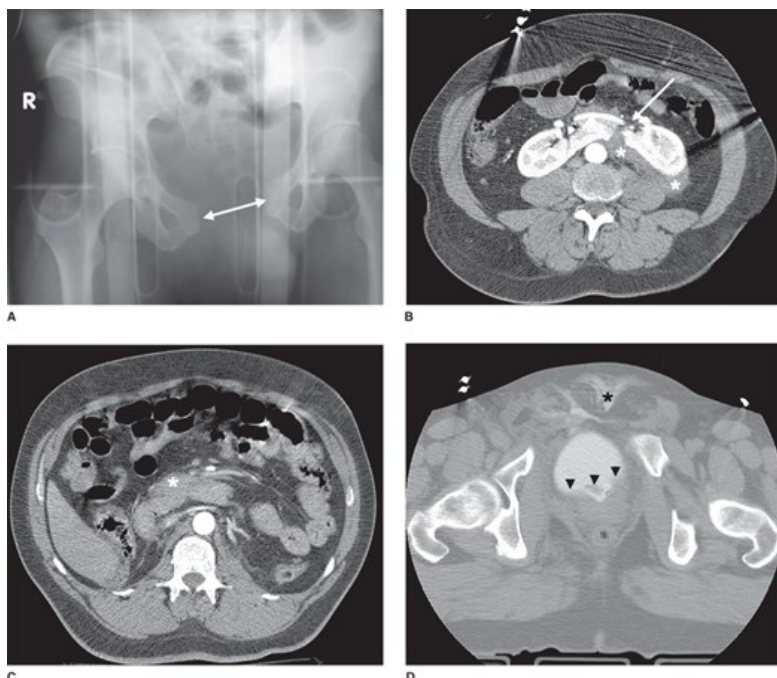
Source: David V. Feliciano, Kenneth L. Mattox,
Ernest E. Moore: Trauma, Ninth Edition
Copyright © McGraw Hill. All rights reserved.

**G**

Source: David V. Feliciano, Kenneth L. Mattox,
Ernest E. Moore: Trauma, Ninth Edition
Copyright © McGraw Hill. All rights reserved.

FIGURE 19-22

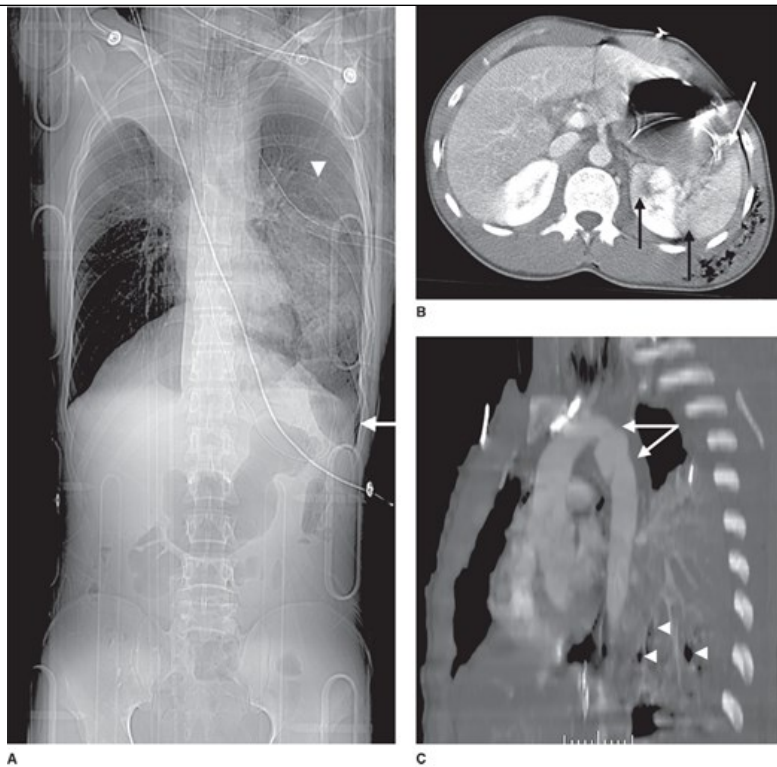
Patterns of injury: “the central package.” This 54-year-old male motorcyclist sustained multiple injuries, including laceration of horseshoe kidney, duodenal contusion, bladder rupture, and anteroposterior (AP) compression fracture of pelvic ring. (A) AP radiograph of pelvis. Greater than 2.5-cm diastasis of pubic symphysis is compatible with disruption of sacrospinous, sacrotuberous, and anterior capsular ligaments of sacroiliac joints. Appearance supports AP compression mechanism and is associated with increased risk for intra-abdominal, intrathoracic, and head injuries. (B) Axial computed tomography (CT) of abdomen at L3-L4 level in the arterial phase. White arrow shows median fracture of horseshoe kidney with posterior perinephric hematoma (asterisks). This is an arterial phase image because there is dense opacification of aorta directly posterior to neck of horseshoe kidney without opacification of the inferior vena cava immediately to its right. Arterial phase images best demonstrate active extravasation and pseudoaneurysms. (C) Axial CT at level of third portion of duodenum shows paroduodenal hematoma (asterisk), suggestive of duodenal injury. (D) Axial CT at level of right acetabulum shows widening of symphysis and extraperitoneal bladder laceration as contrast in anterior abdominal wall (asterisk). Posterior wall of bladder is irregular with double densities within urine contrast compatible with hematoma (arrowheads).



Source: David V. Feliciano, Kenneth L. Mattox,
Eugene E. Moore: Trauma, Ninth Edition.
Copyright © McGraw Hill. All rights reserved.

FIGURE 19-23

Patterns of injury: “the left package.” This 22-year-old male driver was injured in a side-impact crash with substantial intrusion to driver’s side of car. Multiple injuries were sustained. (A) Anteroposterior (AP) scanogram from computed tomography (CT) of chest, abdomen, and pelvis shows extensive opacity of left mid and lower lung fields compatible with contusion, a deep sulcus (arrow) at left costophrenic angle compatible with left pneumothorax, and multiple left-sided rib fractures (arrowhead). Patient is intubated, and there is right upper lobe collapse. (B) Axial CT of upper abdomen during parenchymal phase shows injury of the anterior portion of left kidney (medial arrow) and splenic laceration with sentinel clot (black and white arrows, respectively). Although rib fractures are not shown on current image, subcutaneous emphysema in left chest wall and distal extent of small pneumothorax are shown. (C) Oblique sagittal reformation from CT aortography shows complex segmental intimal injury to proximal descending aorta in the typical location (arrows) and pseudoaneurysm formation due to acute traumatic aortic injury. Air-fluid levels (arrowheads) are compatible with pulmonary lacerations.

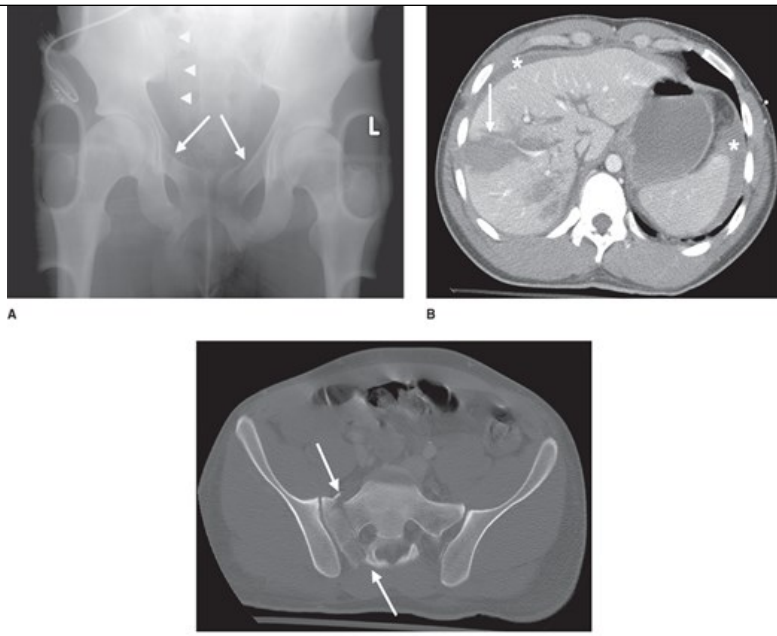


A
Source: David V. Feliciano, Kenneth L. Mattox,
Ernest E. Moore: Trauma, Ninth Edition
Copyright © McGraw Hill. All rights reserved.

C

FIGURE 19-24

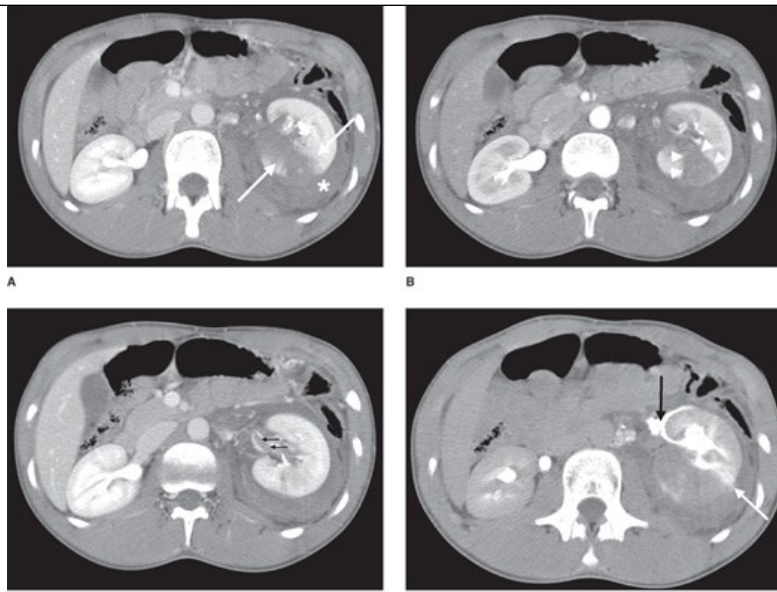
Patterns of injury: “the right package.” This 22-year-old unrestrained passenger was ejected from a car in side-impact high-speed crash. (A) Anteroposterior (AP) view of pelvis shows bilateral iliopubic and ischiopubic ramus fractures (white arrows) and disruption of right sacral arcuate lines (arrowheads); findings are compatible with lateral compression fracture due to right lateral impact. (B) Axial contrast-enhanced abdominal computed tomography (CT) shows free intraperitoneal fluid (asterisks) due to complex collection of liver lacerations (arrow) extending to the intrahepatic inferior vena cava. The relatively uniform enhancement of hepatic parenchyma suggests that the hepatic veins are not occluded. (C) Axial CT through S1, bone windows, shows through-and-through fracture of S1 ala, which traverses S1 neuroforamina (white arrows). Such through-and-through fractures are typically associated with biomechanical instability.



Source: David V. Feliciano, Kenneth L. Mattox,
Ernest E. Moore: Trauma, Ninth Edition
Copyright © McGraw Hill. All rights reserved.

FIGURE 19-25

Grade IV renal laceration. This 14-year-old sustained an injury in a fall from a dirt bicycle while jumping. (A) Contrast-enhanced axial computed tomography (CT) scan, soft tissue windows, performed in parenchymal phase shows perinephric hematoma on left (asterisk) adjacent to laceration that extends into renal hilum (arrows). Right kidney shows normal pyelographic phase. Free intra-abdominal fluid is due to grade III splenic laceration (not shown). (B) Contrast-enhanced axial CT obtained in arterial phase shows wedge-shaped defect in left kidney (arrowheads) compatible with laceration and infarct extending to capsule secondary to segmental arterial occlusion. (C) Contrast-enhanced axial CT at level of kidneys shows thrombus within collecting system (black arrows), perinephric hematoma, and contusion of posterior aspect of kidney, just below laceration seen on image A. Perinephric hematoma surrounds kidney. (D) In such complicated cases, delayed images (10 minutes) are highly valuable in assessing associated urinary leakage. Ten-minute delayed images show a type III extravasation of contrast-enhanced urine from anterior and medial pole of kidney into the perinephric space (black arrow). Striated nephrogram is present posteriorly (white arrow), compatible with contusion adjacent to laceration.



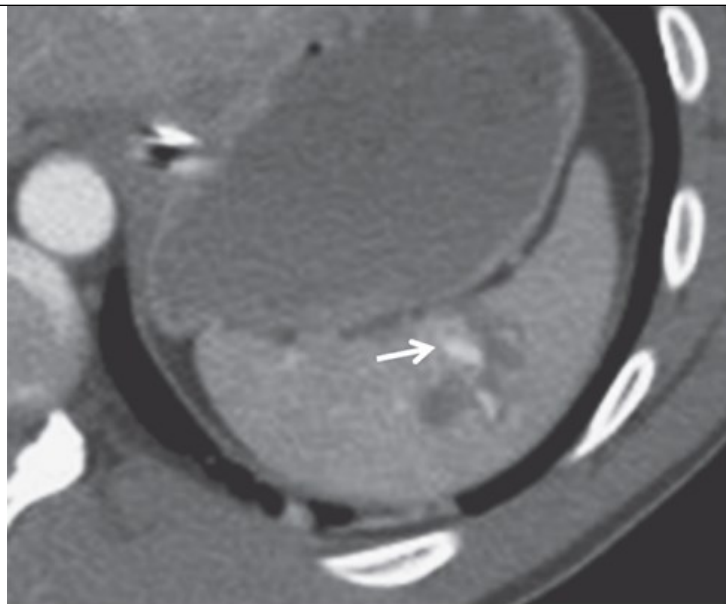
Source: David V. Feliciano, Kenneth L. Mattox,
Ernest E. Moore: Trauma, Ninth Edition
Copyright © McGraw Hill. All rights reserved.

It is estimated that clinical signs and symptoms of intra-abdominal injuries may be misleading in 20% to 50% of patients, that physical examination has a 55% to 65% sensitivity for the detection of internal injuries, and that up to 19% of patients with blunt abdominal trauma have unsuspected injuries.^{9,74,75} This, coupled with a negative predictive value of greater than 97% for abdominopelvic CT, has resulted in overall increased utilization of CT in the setting of blunt abdominal trauma. In addition, abdominopelvic CT is the principle means of both detection and characterization of renal injuries among adults with gross hematuria, children with microscopic hematuria (>50 red blood cells per high-power field), or microscopic hematuria among adults who have had one or more episodes of systolic hypotension.

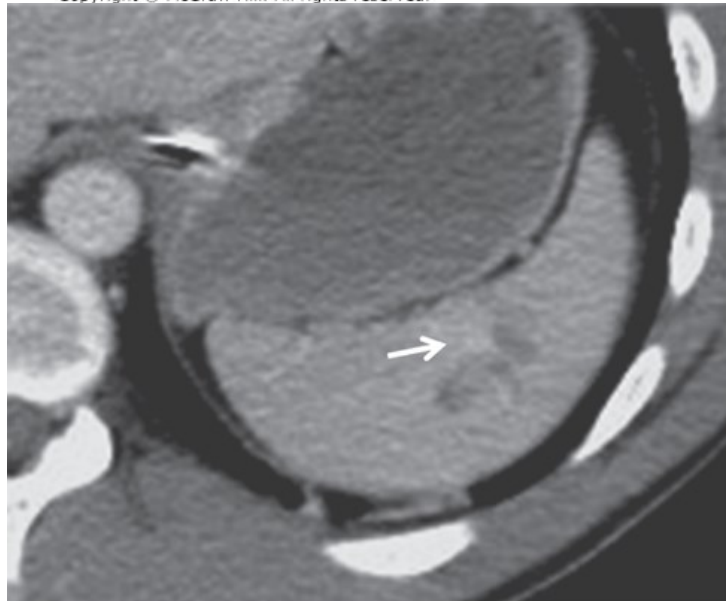
CT of the abdomen and pelvis acquired during the portal venous phase (60- to 75-second scan delay) has been shown to have a high sensitivity, specificity, and negative predictive value for the diagnosis, grading, and exclusion of solid organ injuries. The addition of an arterial phase aids not only in the detection of arterial injuries, but also in the detection of pseudoaneurysms in solid organs, which may not be visible on portal venous phase images (Fig. 19-26).^{76,77}

FIGURE 19-26

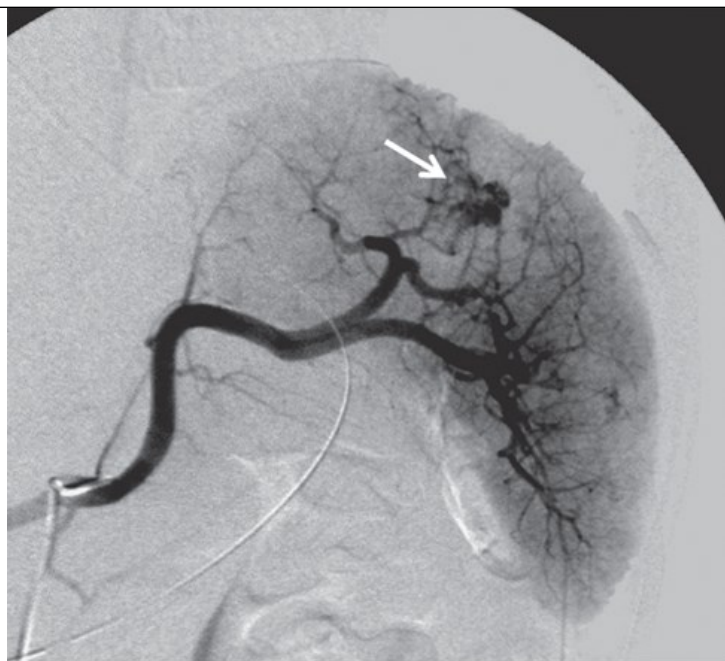
Spleen laceration with associated pseudoaneurysm. Axial postcontrast computed tomography during arterial (A) and portal venous (B) phases demonstrate a laceration of the splenic hilum. There is a focal hyperdensity within the laceration on arterial phase (A, arrow), which becomes isodense to adjacent parenchyma on portal venous phase (B, arrow) consistent with a traumatic pseudoaneurysm. (C) Splenic angiogram confirms the presence of a splenic pseudoaneurysm (arrow).

**A**

Source: David V. Feliciano, Kenneth L. Mattox,
Ernest E. Moore: Trauma, Ninth Edition
Copyright © McGraw Hill. All rights reserved.

**B**

Source: David V. Feliciano, Kenneth L. Mattox,
Ernest E. Moore: Trauma, Ninth Edition
Copyright © McGraw Hill. All rights reserved.

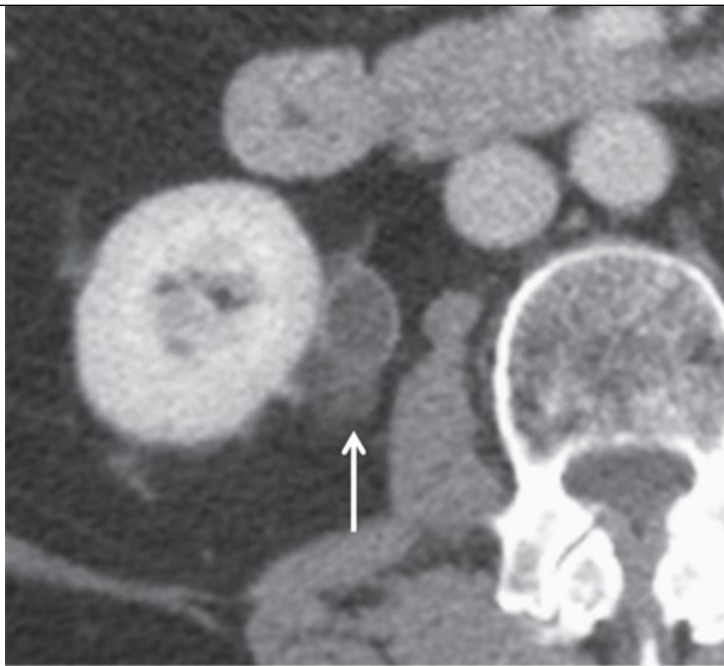
**C**

Source: David V. Feliciano, Kenneth L. Mattox,
Ernest E. Moore: Trauma, Ninth Edition
Copyright © McGraw Hill. All rights reserved.

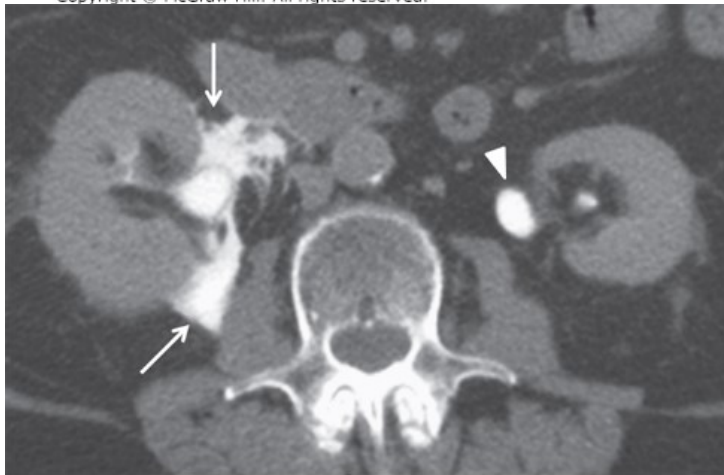
Portal venous or delayed phase imaging can also assist in the detection of active bleeding from the organs or pelvis. CT is accurate in the detection of urinary leaks from the upper genitourinary tract, and delayed excretory phase (>5 minutes) imaging is recommended in the setting of renal lacerations to evaluate for urinary leaks (Fig. 19-25). Isolated fluid around the ureters on initial scanning should raise the possibility of an injury, and 5-minute delayed scanning is indicated (Fig. 19-27).

FIGURE 19-27

Renal pelvis laceration following blunt abdominal trauma. (A) Admission portal venous phase image reveals a small amount of fluid (arrow) surrounding the right renal pelvis. No other injuries or other abnormalities were seen. (B) Delayed excretory phase image reveals a large amount of extravasated urinary contrast (arrows) in the retroperitoneal space compatible with a renal pelvis laceration. The contralateral normal renal pelvis (arrowhead) is included for comparison.

**A**

Source: David V. Feliciano, Kenneth L. Mattox,
Ernest E. Moore: Trauma, Ninth Edition
Copyright © McGraw Hill. All rights reserved.

**B**

Source: David V. Feliciano, Kenneth L. Mattox,
Ernest E. Moore: Trauma, Ninth Edition
Copyright © McGraw Hill. All rights reserved.

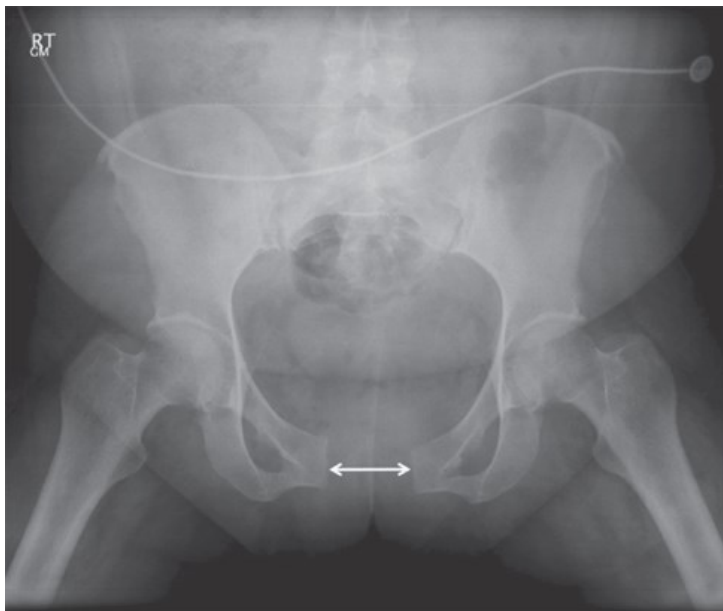
Portal venous or delayed phase scanning through the pelvis is helpful for the detection of pelvic active bleeding. Images of all acquired phases should be reconstructed at 2- to 5-mm slice thickness in the axial, sagittal, and coronal planes.

The arterial-weighted phase images are particularly useful for the detection of brisk arterial bleeding and may detect an intraparenchymal pseudoaneurysm in a solid organ or an arteriovenous fistula, which may otherwise go undetected if portal venous phase imaging alone is acquired (Fig. 19-26). Recent literature suggests that a comprehensive evaluation to assess for the presence of a splenic injury requires both arterial and portal venous phases. The arterial phase performs better for the detection of splenic pseudoaneurysms, and portal venous phase has improved detection for parenchymal lacerations and active bleeding over arterial phase alone.⁷⁶ Extravasation of venous contrast is observed in 5% to 10% of victims of high-energy blunt trauma and may be difficult to differentiate from slow arterial bleeding on CT. The spleen is the most common region of isolated active extravasation of contrast; however, fractures of the pelvic ring are most commonly associated with multiple sites of extravasation.⁷⁸ The amount of hematoma associated with disruptions of the pelvic ring directly correlates with the likelihood of an angiographically demonstrable arterial injury (200 cm^3 , 5% arterial injury; $>500 \text{ cm}^3$, approximately 50% arterial injury).⁷⁹ Nonetheless, otherwise unexplained continued hemodynamic instability in

patients with blunt pelvic fractures warrants angiographic evaluation, even in the absence of a pelvic hematoma or active pelvic bleeding on the initial CT (Fig. 19-28).⁸⁰

FIGURE 19-28

Pelvic ring disruption and active bleeding in a young female following a motorcycle collision. (A) Anteroposterior radiograph demonstrates marked diastasis of the pubic symphysis (double arrow). Axial arterial phase (B) and delayed phase (C) computed tomography images at the level of the widened pubic symphysis reveal active bleeding (B, arrow), which increases in size (C, notched arrow) and diffuses into the existing blood pool. (D) Right posterior oblique pelvic digital subtraction angiogram shows the focus of active bleeding (arrow) next to the right pubic root.



A

Source: David V. Feliciano, Kenneth L. Mattox,
Ernest E. Moore: Trauma, Ninth Edition
Copyright © McGraw Hill. All rights reserved.



B

Source: David V. Feliciano, Kenneth L. Mattox,
Ernest E. Moore: Trauma, Ninth Edition
Copyright © McGraw Hill. All rights reserved.

**C**

Source: David V. Feliciano, Kenneth L. Mattox,
Ernest E. Moore: Trauma, Ninth Edition
Copyright © McGraw Hill. All rights reserved.

**D**

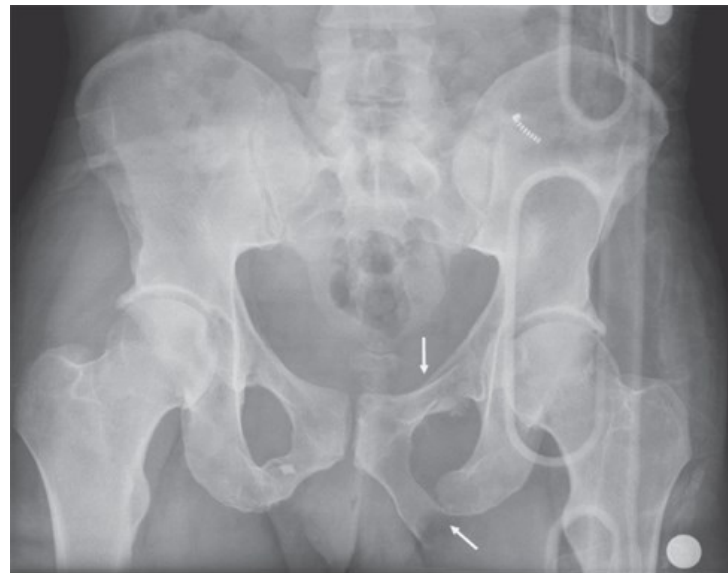
Source: David V. Feliciano, Kenneth L. Mattox,
Ernest E. Moore: Trauma, Ninth Edition
Copyright © McGraw Hill. All rights reserved.

Active bleeding identified on a CT is an independent predictor for the failure of nonoperative management, particularly when bleeding is arising from the spleen, liver, mesentery, or pelvis. Active bleeding from the spleen or liver is a stronger indicator for the need for intervention than the organ injury grade alone (Fig. 19-21). The detection of lacerations that extend to the hepatic veins is of particular importance in the liver, as these have a strong predictive value for failure of nonoperative management when associated with large (>10 cm) hypoperfused regions.⁸¹ Adrenal hemorrhage is relatively common, particularly on the right, and is not of clinical importance unless bilateral. Even then, posttraumatic hypoadrenalinism is rare. It

should be noted that CT grading scales for the solid organs do exist, and although there is significant overlap with the American Association for the Surgery of Trauma (AAST) solid organ grading scales, they are not identical. Thus, open communication with the interpreting radiologist is recommended to avoid any miscommunication. Evaluation of the lower genitourinary tract can be performed with urethrography or cystography (Figs. 19-29 and 19-30). CT cystography typically is performed after the administration of intravenous contrast, as a large amount of leaked extraperitoneal contrast may obscure active arterial extravasation in the pelvis. CT cystography can be easily included in the initial evaluation of the trauma patient after the traditional trauma CT survey and is highly accurate for the diagnosis, exclusion, and comprehensive characterization of bladder injuries.⁸² Passive physiologic filling of the bladder (eg, a 10-minute delay with a clamped Foley catheter) may detect injuries to the bladder but has been shown to be insufficient for the reliable exclusion of all injuries and should not be relied on as the sole examination for suspected bladder trauma (Fig. 19-30).^{82,83}

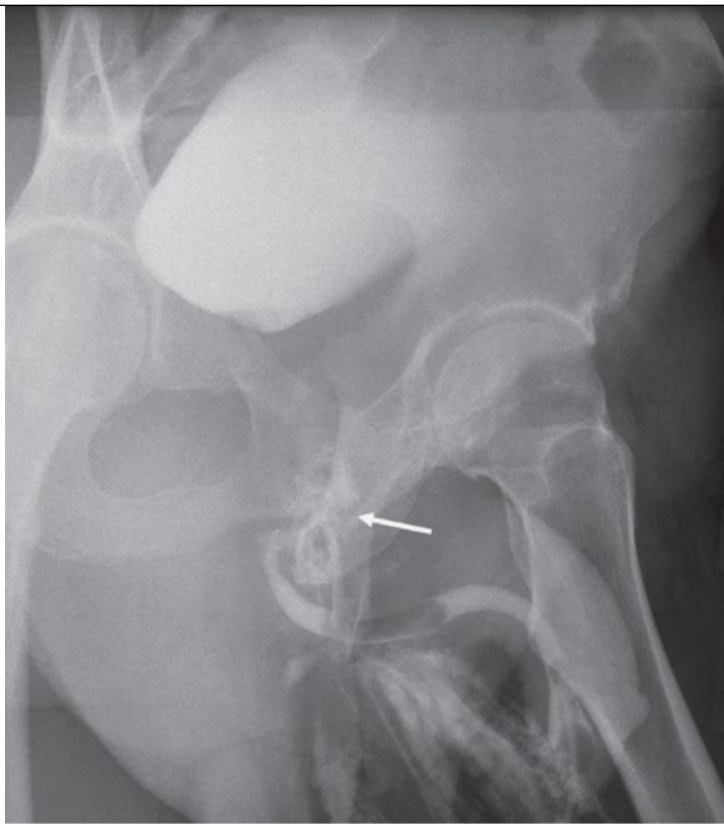
FIGURE 19-29

Urethral injuries. (A, B) Young male status post blunt pelvic trauma. (A) Anteroposterior (AP) pelvic radiograph demonstrates fractures of the left superior and inferior pubic rami (arrows). The patient was unable to void, and there was blood at the penile meatus. (B) Left posterior oblique image from a retrograde urethrogram (RUG) demonstrates leak of contrast from the membranous portion of the urethra (arrow), with contrast extending inferior to the urogenital diaphragm. (C, D) An 11-year-old male with a straddle injury and blood at the meatus. AP (C) and right posterior oblique (RPO) (D) RUG images demonstrate focal contrast outpouching along the right inferior aspect of the bulbous anterior urethra (arrows) indicating a urethral injury. (E, F) A 27-year-old male status post transpelvic gunshot wound. (E) Axial computed tomography image through the lower pelvis shows the bullet trajectory extending through the region of the urethra. The wound tract extends from the left lateral gluteal region (asterisk), through the left ischiopubic ramus (notched arrow), with bullet resting just medial to the right proximal femur (arrow). A Foley catheter (triangle) was able to be passed in the trauma bay without incident. (F) RPO RUG image, performed by inserting a small-bore pediatric feeding tube adjacent to the existing Foley catheter, shows leak of contrast from the prostatic portion of the urethra (notched arrow). The Foley balloon is appropriately positioned in the bladder (arrowhead). Bullet fragment (arrow) is again seen adjacent to the right proximal femur.

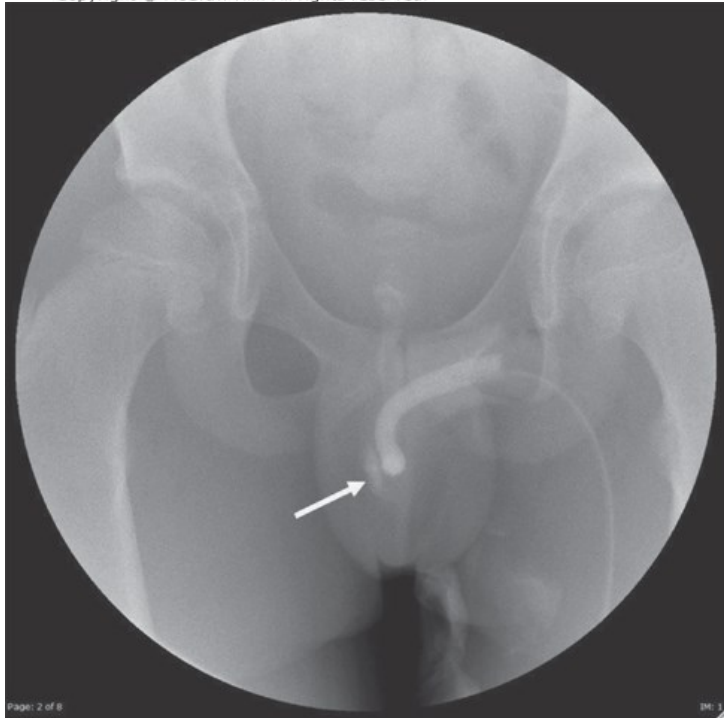


A

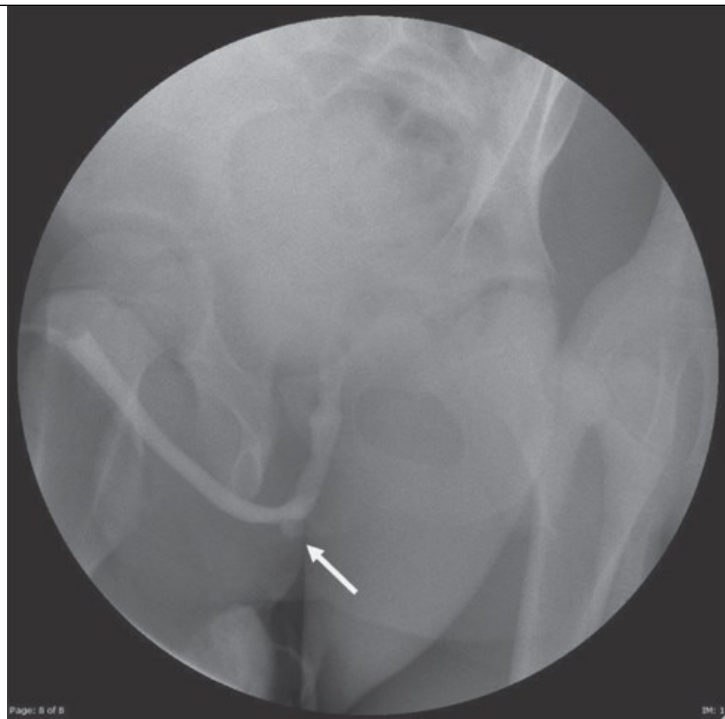
Source: David V. Feliciano, Kenneth L. Mattox,
Ernest E. Moore: Trauma, Ninth Edition
Copyright © McGraw Hill. All rights reserved.

**B**

Source: David V. Feliciano, Kenneth L. Mattox,
Ernest E. Moore: Trauma, Ninth Edition
Copyright © McGraw Hill. All rights reserved.

**C**

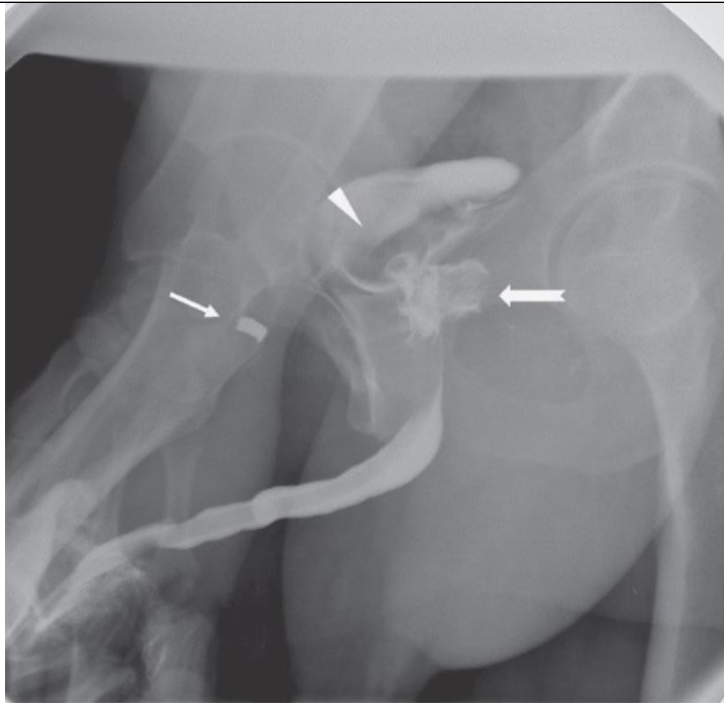
Source: David V. Feliciano, Kenneth L. Mattox,
Ernest E. Moore: Trauma, Ninth Edition
Copyright © McGraw Hill. All rights reserved.

**D**

Source: David V. Feliciano, Kenneth L. Mattox,
Ernest E. Moore: Trauma, Ninth Edition
Copyright © McGraw Hill. All rights reserved.

**E**

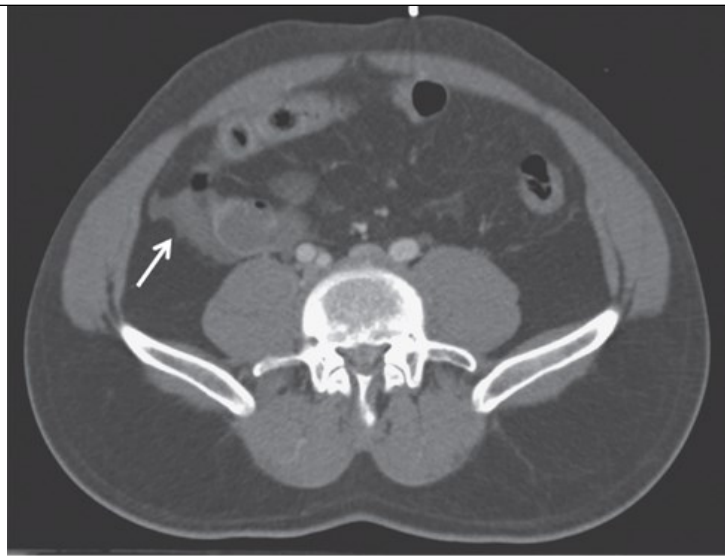
Source: David V. Feliciano, Kenneth L. Mattox,
Ernest E. Moore: Trauma, Ninth Edition
Copyright © McGraw Hill. All rights reserved.

**F**

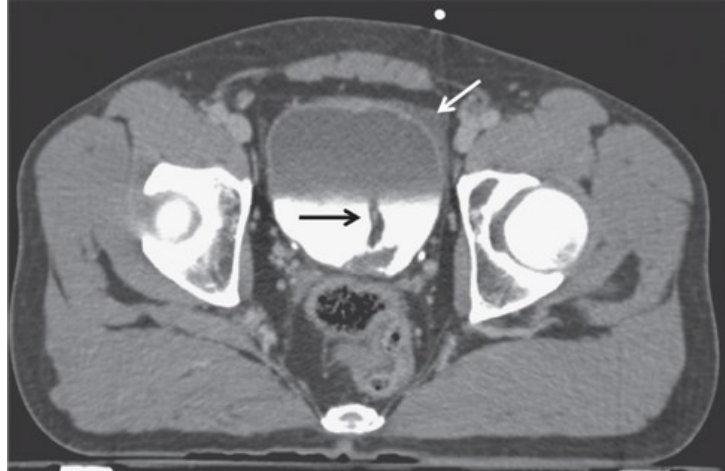
Source: David V. Feliciano, Kenneth L. Mattox, Ernest E. Moore: Trauma, Ninth Edition
Copyright © McGraw Hill. All rights reserved.

FIGURE 19-30

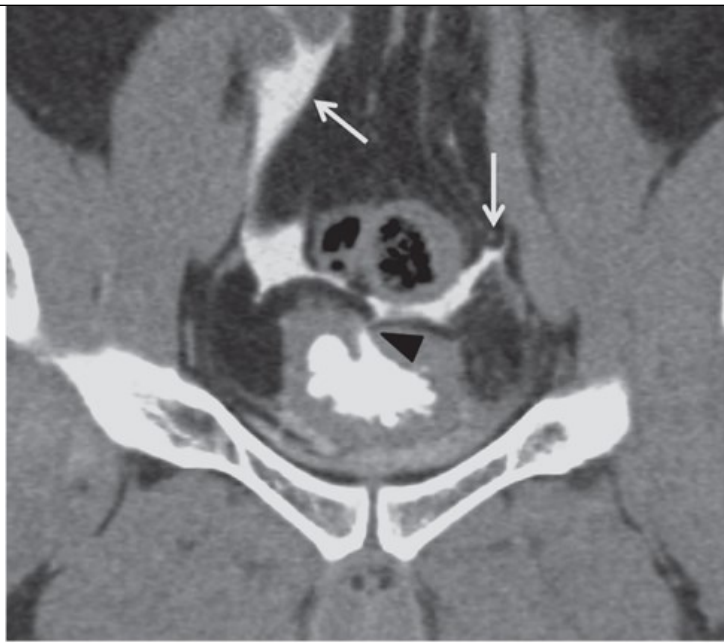
Blunt traumatic bladder rupture. (A–C) Intraperitoneal bladder rupture in a patient following blunt trauma. (A) There is free fluid in the right paracolic gutter (arrow) without other computed tomography (CT) signs of solid organ injury or bowel perforation. (B) Five-minute delayed excretory phase image through the pelvis demonstrates filling defects (black arrow), due to blood clot, in a partially opacified bladder. There is no leak of urinary contrast via passive physiologic filling of the bladder. There is trace free fluid adjacent to the bladder (white arrow). (C) Coronal CT image from a CT cystogram reveals a focal defect in the bladder dome (black arrowhead) and free flow of contrast into the peritoneal cavity (white arrows) consistent with an intraperitoneal bladder injury. (D, E) Extraperitoneal bladder rupture in another patient following blunt trauma. Axial (D) and sagittal (E) CT cystogram images demonstrate a focal defect in the anterior bladder wall (black arrowhead) and leak of urinary contrast into the perivesicular space (asterisk). The leaked contrast is confined to the extraperitoneal space by the peritoneal reflection superiorly (white arrows). (F) Conventional cystogram from another patient with an intraperitoneal bladder injury. Radiograph demonstrates a large amount of intraperitoneal contrast outlining loops of bowel (white arrows). Close inspection of the image demonstrates the bladder catheter balloon (black arrow) outside of the bladder, traversing the bladder wall through a dome injury. Careful inspection of all images, both CT and film, is necessary during the cystogram planning process to ensure proper bladder catheter positioning prior to the initiation of the examination.

**A**

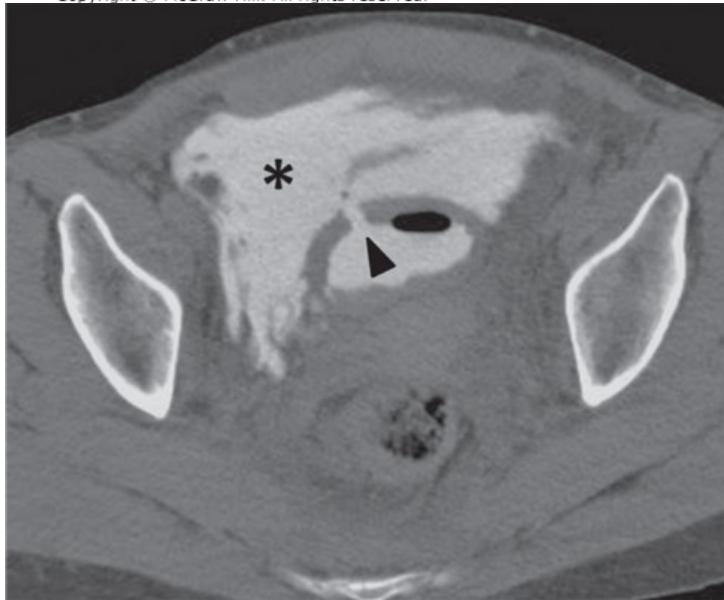
Source: David V. Feliciano, Kenneth L. Mattox,
Ernest E. Moore: Trauma, Ninth Edition
Copyright © McGraw Hill. All rights reserved.

**B**

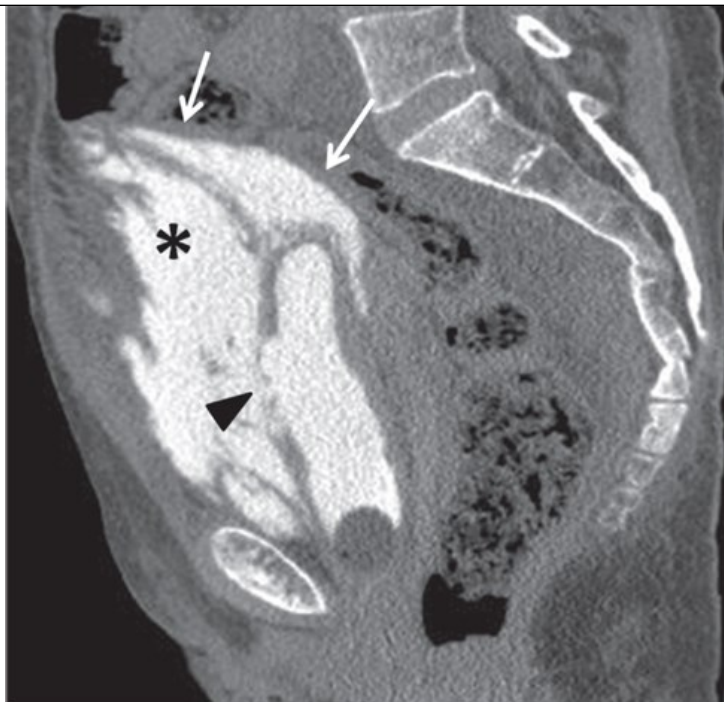
Source: David V. Feliciano, Kenneth L. Mattox,
Ernest E. Moore: Trauma, Ninth Edition
Copyright © McGraw Hill. All rights reserved.

**C**

Source: David V. Feliciano, Kenneth L. Mattox,
Ernest E. Moore: Trauma, Ninth Edition
Copyright © McGraw Hill. All rights reserved.

**D**

Source: David V. Feliciano, Kenneth L. Mattox,
Ernest E. Moore: Trauma, Ninth Edition
Copyright © McGraw Hill. All rights reserved.

**E**

Source: David V. Feliciano, Kenneth L. Mattox,
Ernest E. Moore: Trauma, Ninth Edition
Copyright © McGraw Hill. All rights reserved.

**F**

Source: David V. Feliciano, Kenneth L. Mattox,
Ernest E. Moore: Trauma, Ninth Edition
Copyright © McGraw Hill. All rights reserved.

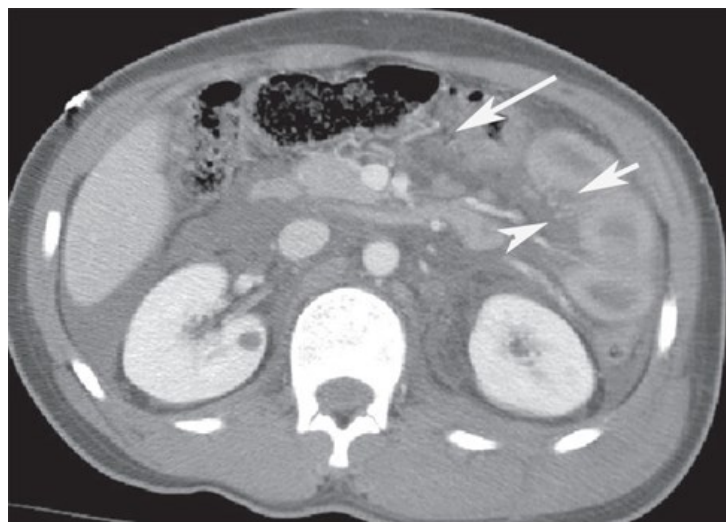
To perform CT cystography, the bladder is first emptied of unopacified urine to diminish the effects of contrast dilution. Scanning through the pelvis is then performed. Administration of dilute water-soluble contrast via low gravity drip can proceed only after the positioning of the Foley catheter within the bladder is confirmed. It is not uncommon for a Foley catheter to be inserted through a laceration of the bladder dome in a patient with an intraperitoneal bladder rupture. The bladder should then be filled with at least 250 to 300 mL of contrast, or until the patient can no longer tolerate the degree of bladder distention or until the contrast stops passively flowing into the bladder. It should be noted that contrast may continue to freely flow in patients with intraperitoneal bladder injuries, and infusing over 350 to 400 mL without scanning is not advised. Scanning through the pelvis with maximum bladder distention is then performed. All scan series are reconstructed in axial, sagittal, and coronal planes at 1- to 3-mm slice thickness.

Review of the images using “bone” windows may make the identification of the source of urinary leak more apparent, depending on the density of the contrast material in the bladder. Postvoid scanning may identify small bladder leaks, but this is rare. Indications for CT cystography include hematuria and fracture of either the pelvic ring or acetabulum or hematuria and free intraperitoneal fluid in the absence of a clearly identifiable source. Cystography is low yield in the absence of hematuria and pelvic fractures.

Injuries to the bowel and mesentery are thought to occur in 1% to 5% of patients with blunt trauma but, when present, are associated with increased morbidity and mortality primarily due to a delayed diagnosis.^{84,85} The physical examination alone lacks sensitivity and specificity, particularly in patients with an unreliable physical examination.⁸⁵ The sensitivity and specificity of CT for bowel injuries are modest, ranging from 69% to 95% and 94% to 100%, respectively.⁸⁵ Specific CT findings of bowel injuries include thickened bowel wall, asymmetric mural enhancement, pneumoperitoneum, leak of oral contrast, focal defect in the bowel wall, and free fluid not explained by other injuries (Fig. 19-31). Unfortunately, the specific signs of a bowel perforation are relatively uncommon and are not sensitive.^{85,86} Active bleeding from the bowel mesentery, as with active bleeding elsewhere in the body, is an indication for intervention and is associated with a high likelihood of injury to the bowel or delayed necrosis of the bowel.⁸⁷ Fluid present in the mesentery or between loops of bowel is very suspicious for a transmural injury to the bowel, even in the presence of injury to a solid organ and even immediately following DPL (Fig. 19-31). One note of caution regarding free intraperitoneal fluid is that women of childbearing age may have small amounts of fluid (± 50 mL) in their pelvis. Recent observations also suggest that a small volume of isolated free fluid in the pelvis in male patients with blunt abdominal trauma, which can be seen in up to 4.9%, is unlikely to be due to a bowel injury.⁸⁸ Patients who have been vigorously resuscitated (especially if they are >24 hours from their injury) may have ascites and interloop fluid present due to a capillary leak syndrome (Fig. 19-32). Acute and subacute hemorrhage typically measures 40 to 70 Hounsfield units (HU), whereas urine, bowel contents, and ascites measure closer to water (eg, 0 +/- 20 HU). If a patient with blunt trauma has free fluid in the peritoneal cavity of uncertain source and lacks signs of peritonitis on physical examination, a repeat short-interval abdominopelvic CT in 4 to 6 hours may be warranted.⁸⁹

FIGURE 19-31

Small bowel perforation: A 14-year-old male, unhelmeted bicycle rider hit by a car sustained a small bowel perforation. Intravenous contrast-enhanced axial computed tomography shows three findings consistent with small bowel (jejunal) injury: (1) diffusely enhancing and thickened jejunum loops within the left side of the abdomen, with a focal hypoenhancing segment compatible with at least partial transmural injury (short arrow); (2) high-density interloop fluid within the mesentery adjacent to abnormal bowel (arrowhead) strongly suggesting transmural bowel laceration; and (3) small amount of pneumoperitoneum (long arrow) collecting within mesentery. Extra-alimentary air almost always correlates with transmural laceration of bowel.



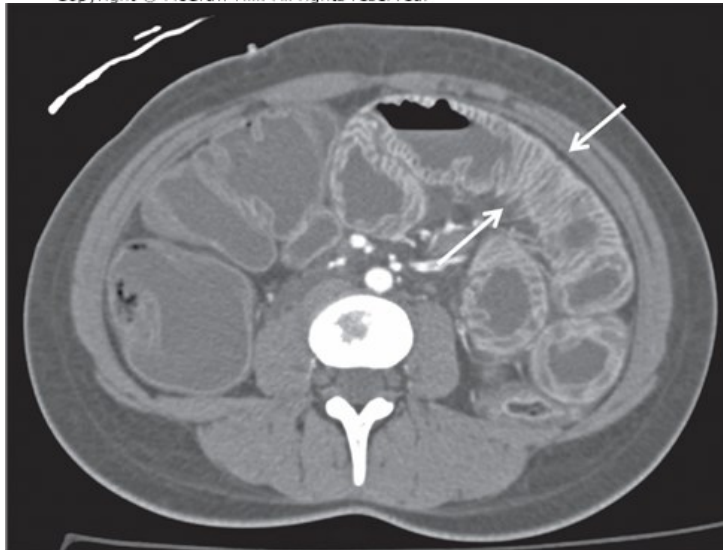
Source: David V. Feliciano, Kenneth L. Mattox,
Ernest E. Moore: Trauma, Ninth Edition
Copyright © McGraw Hill. All rights reserved.

FIGURE 19-32

Hypoperfusion shock complex/shock bowel syndrome. (A) Axial postcontrast computed tomography (CT) demonstrates a thin, slit-like inferior vena cava (arrow) and pancreatic edema (the pseudo-pancreatitis sign) with peripancreatic fluid (arrowheads). (B) Axial postcontrast CT from the same patient also demonstrates dilated bowel with thickened and intensely enhancing bowel wall (arrows). There is also diffuse mesenteric edema. Reduced splanchnic blood flow due to underresuscitation results in capillary leak and prolonged transit time for intravenous contrast. This constellation of findings is consistent with hypoperfusion shock complex/shock bowel syndrome.

**A**

Source: David V. Feliciano, Kenneth L. Mattox,
Ernest E. Moore: Trauma, Ninth Edition
Copyright © McGraw Hill. All rights reserved.

**B**

Source: David V. Feliciano, Kenneth L. Mattox,
Ernest E. Moore: Trauma, Ninth Edition
Copyright © McGraw Hill. All rights reserved.

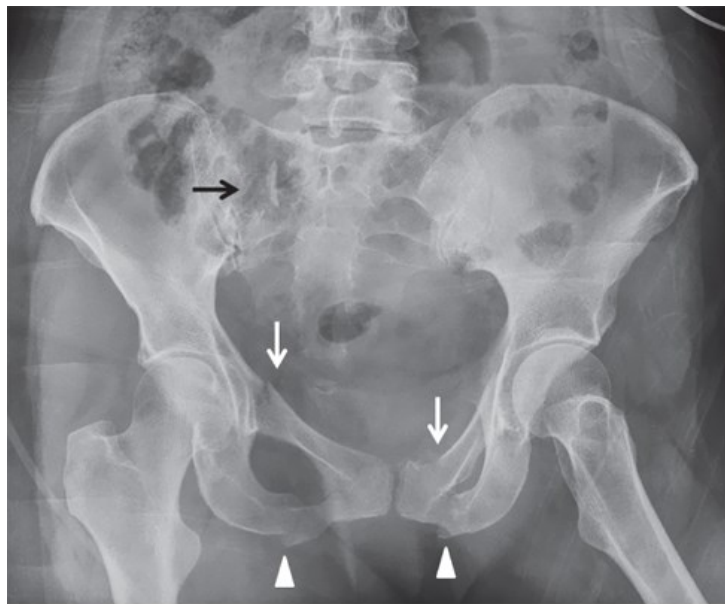
CT performs well in the diagnosis of peritoneal violation and intra-abdominal injuries in the setting of penetrating abdominal trauma.⁷³ The diagnosis of injuries to the bowel following penetrating trauma is aided by the use of the triple-contrast protocol using intravenous, oral, and rectal contrast material. Leakage of enteric contrast is highly specific for bowel injury (Fig. 19-21F). A wound tract that extends to the bowel surface is the most sensitive sign of an associated bowel injury, in the absence of other definitive findings.

Computed Tomography of the Pelvis and Acetabulum

CT is extremely valuable in the evaluation of the pelvic girdle, including the pelvic bones, acetabulum, and sacrum, following both blunt and penetrating trauma. There are several indications for pelvic CT, including the following: (1) to evaluate unstable fractures of the pelvic ring as determined by physical examination or appearances on conventional x-rays; (2) to evaluate for radiographically occult fractures in the setting of high clinical suspicion; (3) to detect entrapped intra-articular debris/bone fragments following hip dislocation; and (4) for preoperative surgical planning (Figs. 19-33, 19-34, 19-35, 19-36, 19-37). Pelvic CT can be performed on its own or be reconstructed from the raw CT data of the abdomen and pelvis performed as a part of a whole-body trauma CT series. Three-dimensional volume-rendered images can be generated from the CT data set, and dedicated evaluation of acetabular fractures can be performed with femoral head subtraction. In fact, some of the most recent CT scanner software packages can generate “virtual pelvis” images from the CT raw data that approximate images of conventional pelvic radiographs (Fig. 19-2D).

FIGURE 19-33

Pelvic ring fracture: lateral compression type. A 54-year-old female passenger involved in a T-bone motor vehicle collision. (A) Anteroposterior (AP) radiograph of pelvis shows disruption of right sacral wing (black arrows), bilateral iliopubic rami (white arrows), and bilateral ischiopubic rami (arrowheads). (B) Axial computed tomography (CT) shows a comminuted fracture of the right sacral ala through the neural arches (arrow). Frequency of injury to sacral nerve roots is greatest when fractures involve medial aspect of the neural canal (Denis zone 3), lowest when lateral to the neuroforamen (Denis zone 1), and intermediate when involving neural foramina (Denis zone 2). (C) Axial CT image at the level of the femoral heads again demonstrates fractures of the superior iliopubic rami (arrows). (D) Axial CT image demonstrates fractures of the bilateral ischiopubic rami (arrowheads). (E) Subsequently performed CT cystogram demonstrates a defect in the anterior bladder wall (black arrow) with leak of contrast into the perivesicular space consistent with an extraperitoneal bladder rupture, an injury often seen in association with midline pelvic ring fractures.

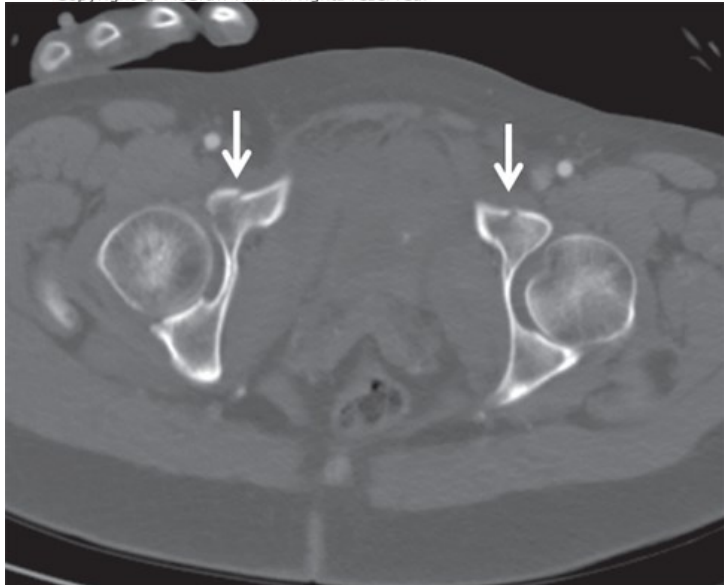


A

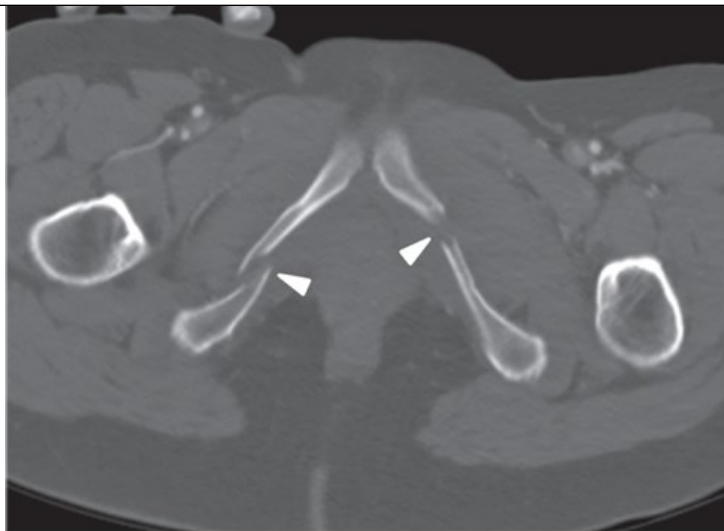
Source: David V. Feliciano, Kenneth L. Mattox, Ernest E. Moore: Trauma, Ninth Edition
Copyright © McGraw Hill. All rights reserved.

**B**

Source: David V. Feliciano, Kenneth L. Mattox,
Ernest E. Moore: Trauma, Ninth Edition
Copyright © McGraw Hill. All rights reserved.

**C**

Source: David V. Feliciano, Kenneth L. Mattox,
Ernest E. Moore: Trauma, Ninth Edition
Copyright © McGraw Hill. All rights reserved.

**D**

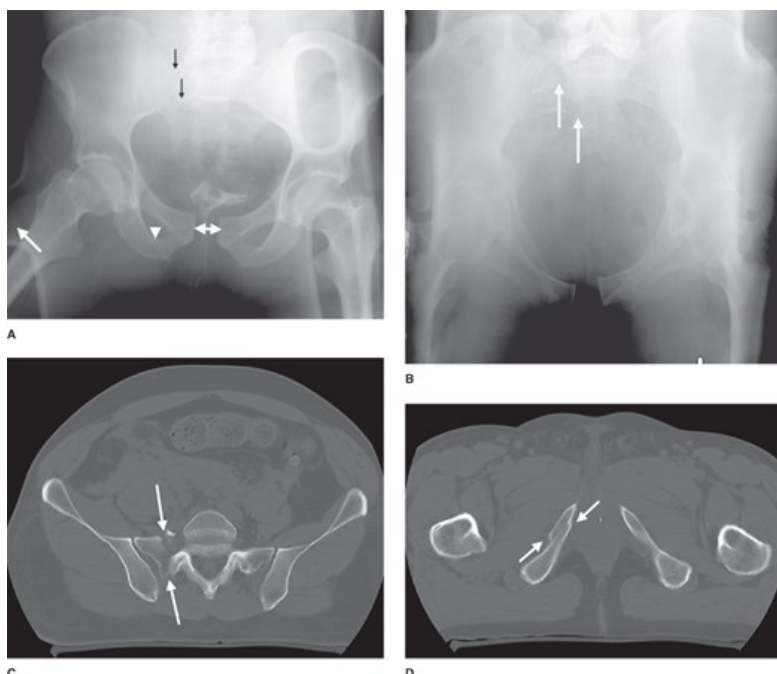
Source: David V. Feliciano, Kenneth L. Mattox, Ernest E. Moore: Trauma, Ninth Edition
Copyright © McGraw Hill. All rights reserved.

**E**

Source: David V. Feliciano, Kenneth L. Mattox, Ernest E. Moore: Trauma, Ninth Edition
Copyright © McGraw Hill. All rights reserved.

FIGURE 19-34

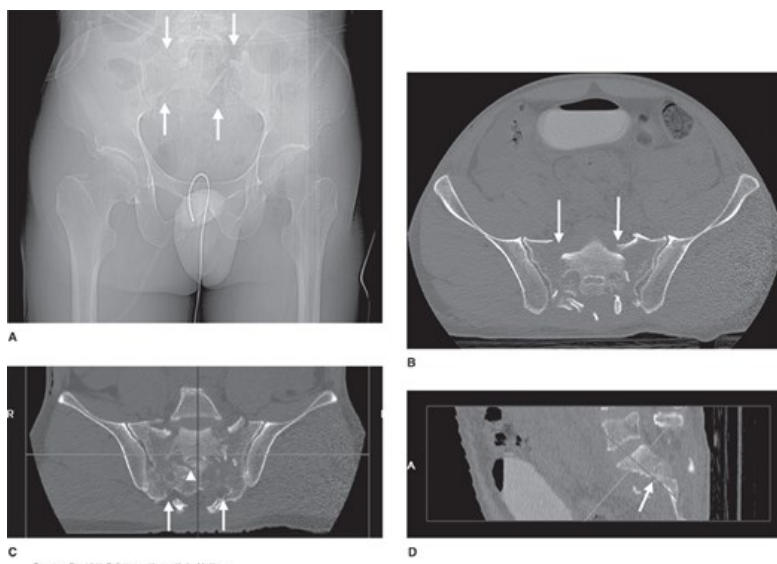
Pelvic ring fracture: anteroposterior (AP) compression type. This 55-year-old male sustained an injury during a 7-m fall onto concrete. (A) AP radiograph of pelvis shows symphyseal diastasis (double-ended arrow); right ischiopubic ramus fracture, which is minimally displaced (arrowhead); and disruption of right sacral arcuate lines (black arrows). Right femur is abducted (white arrow), a finding that is common with fractures of femoral shaft that this patient also sustained. (B) Inlet view of pelvis (obtained with 45° angulation caudally) better shows disruption of arcuate lines (white arrows) and again shows pubic symphyseal diastasis. (C) Axial computed tomography (CT) at the lumbosacral junction shows through-and-through fracture (arrows) of right lateral mass of S1 with 6 mm of lateral and 8 mm of anterior translation. (D) Axial CT image at ischial tuberosities shows oblique sagittal fracture through right ischial pubic ramus (white arrows). Orientation of ischial fractures often reflects mechanism injury (sagittal plane fractures due to AP compression or vertical shear; transverse or axial plane fractures due to lateral compression).



Source: David V. Feliciano, Kenneth L. Mattox,
Ernest E. Moore: Trauma, Ninth Edition
Copyright © McGraw Hill. All rights reserved.

FIGURE 19-35

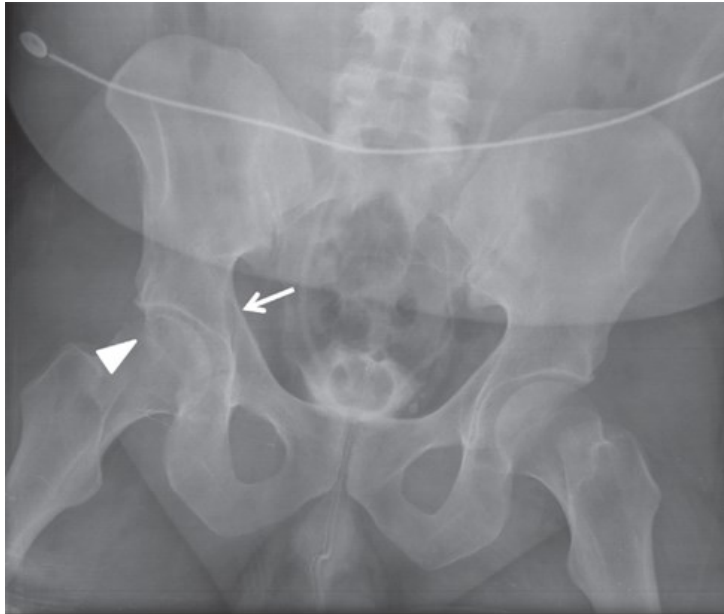
Vertical shear injury with unstable sacral fracture. An H-shaped sacral fracture was sustained in 40-ft fall. This was associated with right calcaneus and T12 compression fractures. (A) Anteroposterior (AP) pelvis computed tomography (CT) scout shows disruption of arcuate lines bilaterally (arrows). Such a finding requires excellent lateral view of sacrum to exclude transverse components of the fracture to create either H- or U-shaped sacral fractures, which are typically biomechanically unstable. This can rarely be obtained. CT better evaluates this area as coronal reformations of thin-section axial CT. (B) Axial CT shows bilateral through-and-through sacral fractures (arrow) that are transforaminal in their course. At this level, no transverse fracture is appreciated. (C) Coronal oblique CT reformation shows bilateral lateral mass fractures (arrow), as well as a portion of transverse fracture (arrowhead). (D) Sagittal CT reformation clearly shows transverse fracture (arrow).



Source: David V. Feliciano, Kenneth L. Mattox,
Ernest E. Moore: Trauma, Ninth Edition
Copyright © McGraw Hill. All rights reserved.

FIGURE 19-36

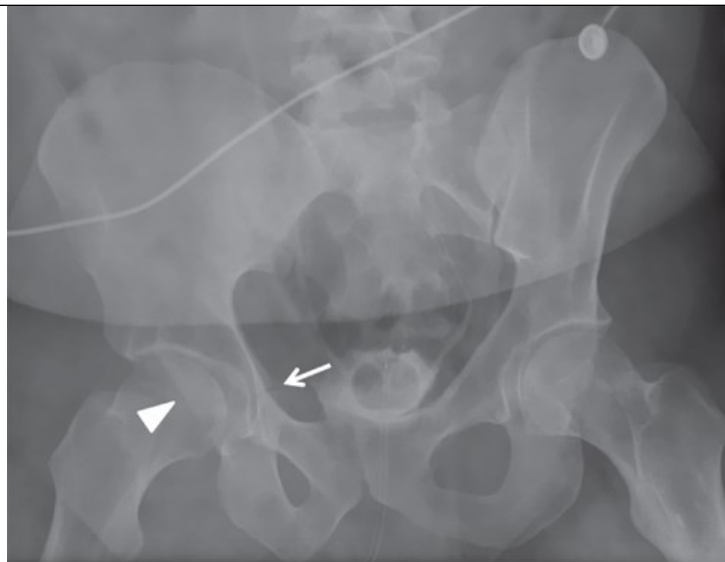
Transverse acetabular fracture with associated posterior wall fracture. (A) Anteroposterior (AP) view of pelvis shows disruption of iliopectineal line adjacent to acetabulum (arrow), with an eyebrow-shaped radiodensity projecting over the femoral head (arrowhead), which is a displaced posterior wall fragment. Bilateral Judet (B, C) oblique radiographs again show transverse fracture (arrow) and a posterior wall fragment (arrowhead). (D) Axial computed tomography (CT) image at the level of the acetabular roof shows a sagittal plane fracture (arrows) characteristic of transverse fractures of acetabulum. The posterior wall fracture fragment is again seen (arrowhead).

**A**

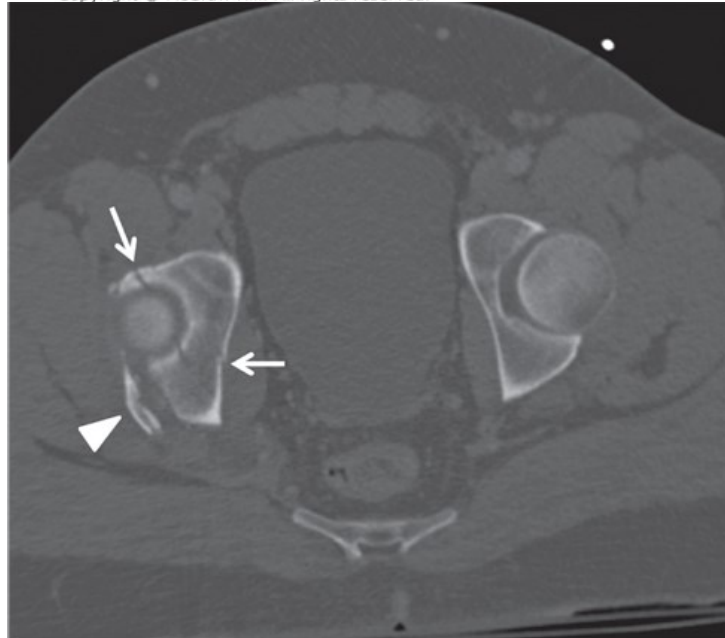
Source: David V. Feliciano, Kenneth L. Mattox,
Ernest E. Moore: Trauma, Ninth Edition
Copyright © McGraw Hill. All rights reserved.

**B**

Source: David V. Feliciano, Kenneth L. Mattox,
Ernest E. Moore: Trauma, Ninth Edition
Copyright © McGraw Hill. All rights reserved.

**C**

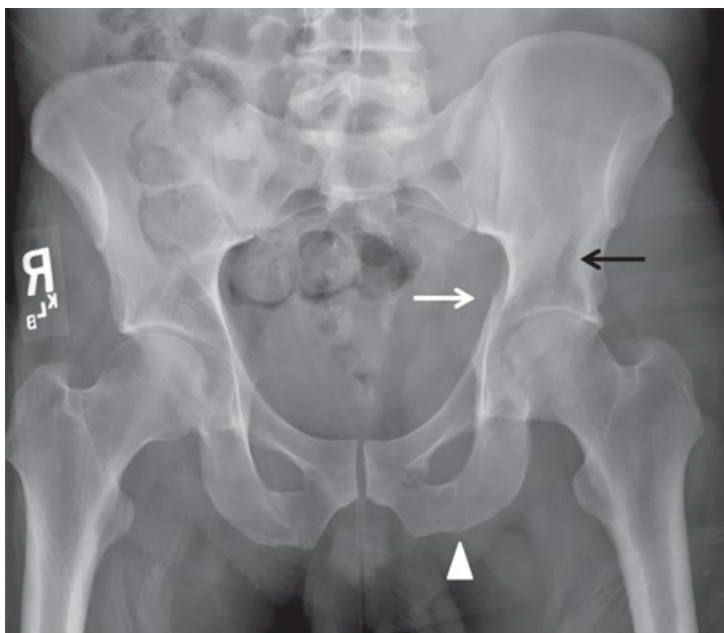
Source: David V. Feliciano, Kenneth L. Mattox,
Ernest E. Moore: Trauma, Ninth Edition
Copyright © McGraw Hill. All rights reserved.

**D**

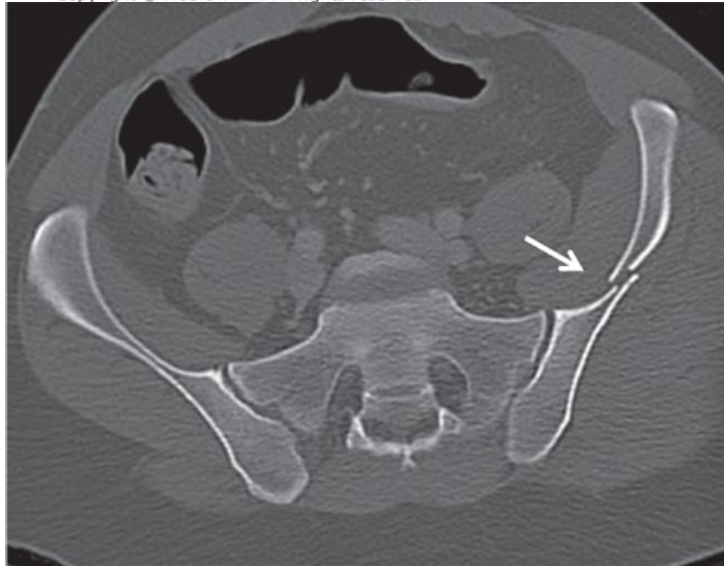
Source: David V. Feliciano, Kenneth L. Mattox,
Ernest E. Moore: Trauma, Ninth Edition
Copyright © McGraw Hill. All rights reserved.

FIGURE 19-37

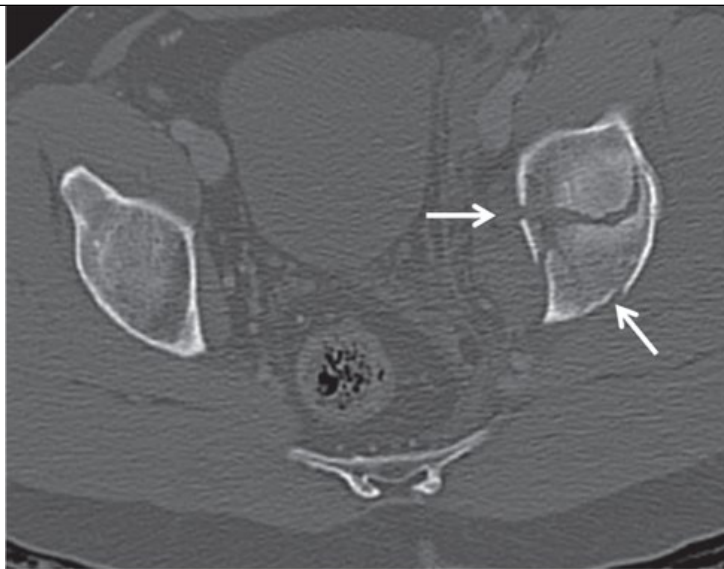
Both-column acetabular fracture. A 34-year-old male with left acetabular fractures following a motor vehicle collision. (A) Anteroposterior (AP) conventional radiograph of pelvis shows disruption of both iliopectineal and ischiopubic lines (arrow) and disruption of left ischiopubic ramus (arrowhead). There is a vertical lucency of the left iliac wing just superior to the acetabulum compatible with a fracture (black arrow). Axial computed tomography of the pelvis viewed using bone windows (B–D) demonstrates a fracture of the left iliac wing (B, arrow), a comminuted fracture of the left acetabulum (C, arrows), and a fracture of the left ischiopubic ramus (D, arrow). These fractures together are characteristic of a both-column acetabular fracture. Three-dimensional surface-rendered image (E) with femoral head subtraction nicely demonstrates the fracture fragments with respect to the acetabular cup.

**A**

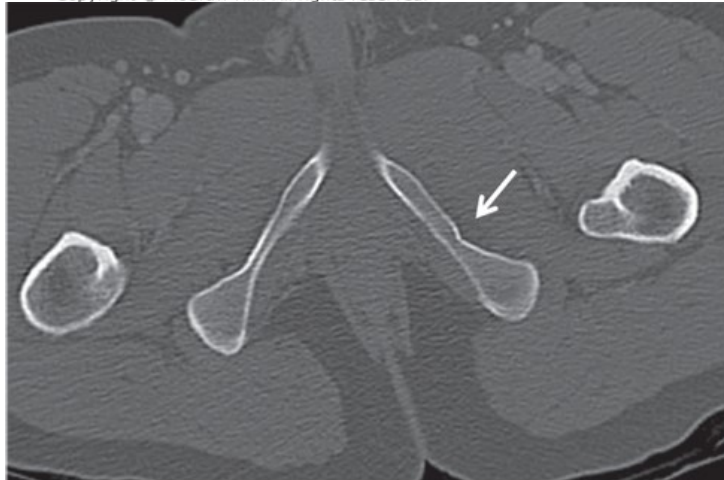
Source: David V. Feliciano, Kenneth L. Mattox,
Ernest E. Moore: Trauma, Ninth Edition
Copyright © McGraw Hill. All rights reserved.

**B**

Source: David V. Feliciano, Kenneth L. Mattox,
Ernest E. Moore: Trauma, Ninth Edition
Copyright © McGraw Hill. All rights reserved.

**C**

Source: David V. Feliciano, Kenneth L. Mattox,
Ernest E. Moore: Trauma, Ninth Edition
Copyright © McGraw Hill. All rights reserved.

**D**

Source: David V. Feliciano, Kenneth L. Mattox,
Ernest E. Moore: Trauma, Ninth Edition
Copyright © McGraw Hill. All rights reserved.

**E**

Source: David V. Feliciano, Kenneth L. Mattox, Ernest E. Moore: Trauma, Ninth Edition
Copyright © McGraw Hill. All rights reserved.

The primary goal of CT evaluation of disruption of the pelvic ring and acetabular fractures is to aid in surgical planning.⁹⁰ CT scans of acetabular fractures are performed for the following: (1) assessment of fracture types; (2) secondary congruence of the hip (eg, are the fracture fragments symmetrically oriented about the intact femoral head?); (3) evidence for marginal impaction (eg, subarticular bone depressed or impacted and not showing secondary congruence); (4) detection of a fracture of the femoral head; and (5) detection of intra-articular debris. There is approximately a 15% concurrent rate for fractures of the pelvic ring and acetabulum, so any fracture of the pelvis or acetabulum should initiate a search for other fractures in the pelvic girdle.

CT of the pelvis and acetabulum typically uses a slice thickness of 1 to 3 mm in the axial plane, and images are reconstructed using a bone algorithm. Sagittal and coronal reformatted images can be helpful in fully characterizing a fracture of the pelvic ring or acetabulum.

A systematic approach should be employed when reviewing pelvic CT images, with special attention paid to the fractures that one would expect to see in the setting of AP compression, lateral compression, and vertical shear force. Correlation with at least an AP pelvic radiograph is recommended to provide an overview of the type of pelvic ring disruption. Fractures of the iliopubic and ischiopubic rami, as well as the sacral wings, are typical of a lateral compression-type injury. The anterior surface of the sacrum is carefully evaluated for “buckle” fractures due to internal rotation of the hemipelvis due to a lateral impact. Fractures of the iliopubic and ischiopubic rami are assessed for their orientation (lateral compression fractures typically show orientation in the axial plane or coronal plane, whereas AP compression and vertical shear fractures will show orientation in the sagittal plane). Diastasis of the pubic symphysis and sacroiliac joints (eg, “open book” pelvis) is typical of an AP-type injury. The normal pubic symphysis should not be more than 1 cm in width in normal subjects, regardless of age. When the pubic symphysis is traumatically wider than 2.5 cm, both sacrospinous and sacrotuberous ligaments are presumed to be injured. In the posterior ilium, it is important to look for avulsion fractures of the posterior superior iliac spine, so-called crescent fractures, as these are strongly associated with biomechanically unstable fractures in the presence of disruption of the anterior pelvic ring. The axial images give good evaluation of the amount of internal or external rotation but underestimate the amount of flexion or extension of a hemipelvis relative to the intact pelvis. Furthermore, evaluation of the amount of pelvic hematoma may be helpful in determining the need for angiography for embolization. Localization of these hematomas is a good predictor of associated pelvic vascular injuries. Indeed, as discussed earlier, a search for active bleeding in the pelvis should be conducted if the patient undergoes the contrast-enhanced trauma CT series.

It should be noted that CT is not a dynamic examination and provides information for a single snapshot in time. As such, the assessment of potential biomechanical instability of the pelvis may be difficult. Certainly, the combination of a crescent fracture from the posterior superior iliac spine and displaced anterior pelvic ring fractures will be unstable under anesthesia. The stability of other patterns, however, is not so predictable, even though CT images provide a great deal of information about the injury pattern. Therefore, conventional x-rays are necessary as guides to intraoperative reduction even for the most experienced pelvic orthopedic surgeon.

If an acetabular fracture is present, the goal is to determine what remains attached to the intact hemipelvis and to describe and characterize the major fracture fragments and their relation to each other and the femoral head. Assessment of the posterior through anterior walls, the ischium for the posterior column, the pubis and symphysis for evaluation of the anterior column, the iliac wing for superior extension, and congruence between the femoral head and acetabular cup allows for a more complete recognition of fracture fragments. There are 10 types of acetabular fractures based on the Judet and Letournel classification scheme. Fortunately, approximately 90% fall into one of five fracture patterns, divided into two groups based on the presence (both-column and T-shaped) or absence (transverse, transverse with posterior wall, and isolated posterior wall) of involvement of the obturator ring.⁹¹

APPENDICULAR SKELETON

Conventional Radiography

Conventional radiography remains the imaging standard for the evaluation of long bones showing obvious deformity, instability, palpable crepitus, pain, and swelling. For perarticular regions, conventional x-rays are indicated for deformity, instability, decreased range of motion, pain, and swelling. The Ottawa ankle and knee clinical prediction rules add considerable precision to specificity.⁹²⁻⁹⁴

For long bones (Fig. 19-38), two orthogonal views are obtained, including an AP view and lateral projection centered at the midshaft. Projections should include both the proximal and distal joints. Joints should be imaged with two orthogonal views at a minimum, with additional optional one or two oblique views, centered at the midportion of the articulation (Figs. 19-38, 19-39, 19-40, 19-42, 19-43).

FIGURE 19-38

Extremity injuries. (A) A 33-year-old man with a Monteggia fracture. Lateral radiograph of the forearm demonstrates a comminuted fracture of the mid ulnar diaphysis (arrow) with associated anterior dislocation of radius at radiocapitellar articulation (triangle). (B-D) A 38-year-old man with elbow pain status post fall. Anteroposterior (AP) (B), lateral (C), and oblique (D) images demonstrate a fracture line through the radial head (arrow). There is elevation of the anterior fat pad (triangle) and posterior fat pad (notched arrow) indicating hemarthrosis. (E-G) A 25-year-old man with knee dislocation after falling 25 ft. AP (E) knee radiograph demonstrates overlap and increased density of the femoral condyles and tibial plateau (arrows). Lateral (F) knee radiograph demonstrates anterior dislocation of the tibia-fibula with respect to the distal femur. Postreduction sagittal computed tomography angiogram image (G) demonstrates popliteal artery transection with active bleeding (arrow).

**A**

Source: David V. Feliciano, Kenneth L. Mattox,
Ernest E. Moore: Trauma, Ninth Edition
Copyright © McGraw Hill. All rights reserved.

**B**

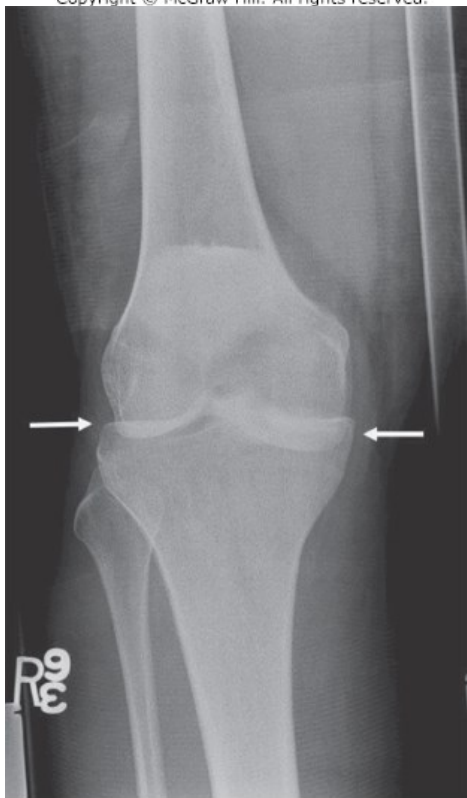
Source: David V. Feliciano, Kenneth L. Mattox,
Ernest E. Moore: Trauma, Ninth Edition
Copyright © McGraw Hill. All rights reserved.

**C**

Source: David V. Feliciano, Kenneth L. Mattox,
Ernest E. Moore: Trauma, Ninth Edition
Copyright © McGraw Hill. All rights reserved.

**D**

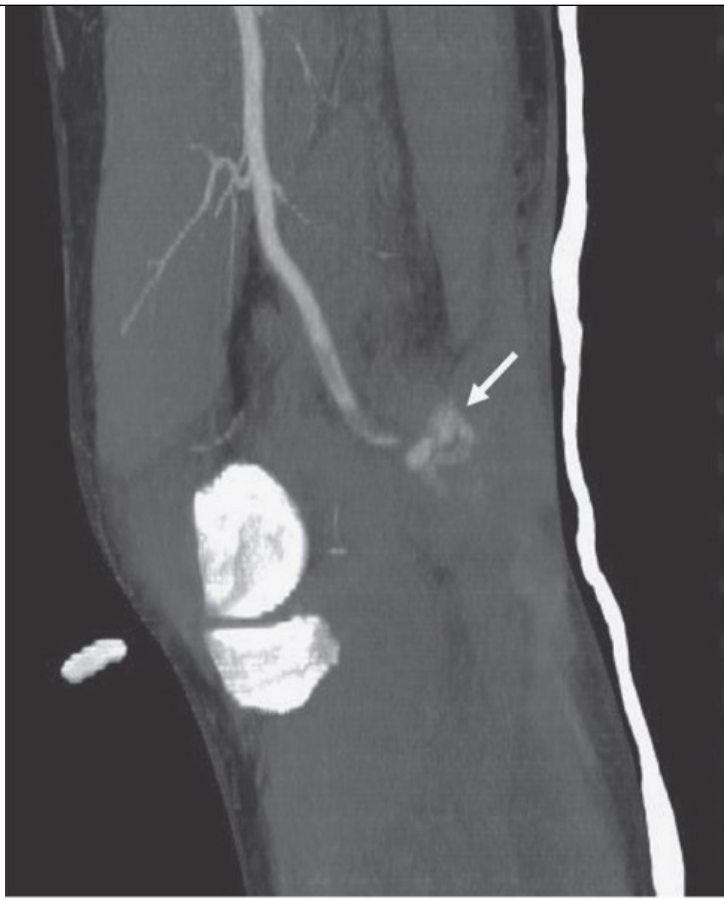
Source: David V. Feliciano, Kenneth L. Mattox,
Ernest E. Moore: Trauma, Ninth Edition
Copyright © McGraw Hill. All rights reserved.

**E**

Source: David V. Feliciano, Kenneth L. Mattox,
Ernest E. Moore: Trauma, Ninth Edition
Copyright © McGraw Hill. All rights reserved.

**F**

Source: David V. Feliciano, Kenneth L. Mattox,
Ernest E. Moore: Trauma, Ninth Edition
Copyright © McGraw Hill. All rights reserved.

**G**

Source: David V. Feliciano, Kenneth L. Mattox, Ernest E. Moore: Trauma, Ninth Edition
Copyright © McGraw Hill. All rights reserved.

FIGURE 19-39

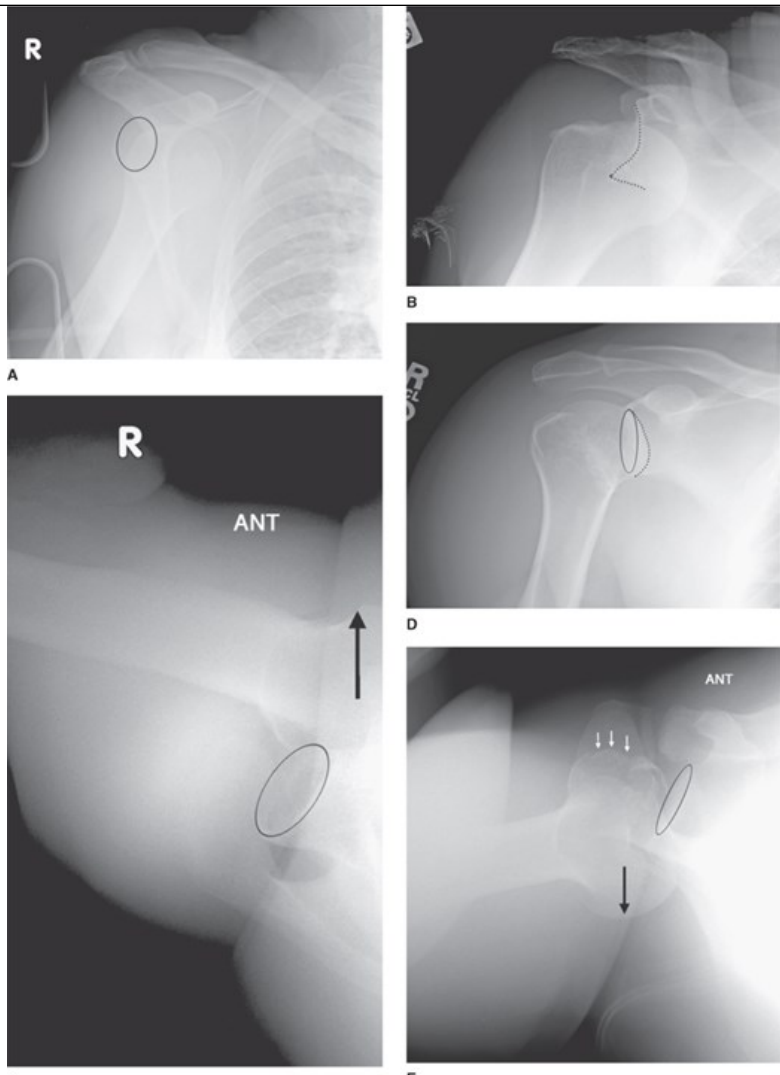
Periarticular fracture: coronoid process fracture of elbow. (A) Anteroposterior (AP) radiograph of left elbow shows displaced coronoid process (arrow). Elsewhere, joint appears congruent. (B) Lateral view of left elbow shows tip of coronoid process fracture (arrow). Coronoid process fractures can be graded by amount of coronoid process involved, such that larger coronoid process fracture fragments are more likely to result in elbow instability. (C) Axial computed tomography (CT) obtained because mismatch between radiographic and clinical findings of instability shows highly comminuted fracture of coronoid process (arrows). Radial head (R) and olecranon process (O) appear normal. (D) Sagittal CT reformation shows nearly all the coronoid process is involved in fracture. Secondary congruence between trochlea and olecranon-coronoid process is fair. (E, F) Three-dimensional surface-rendered CT reformations more graphically demonstrate transverse and distal extent and displacement of coronoid process fracture.



Source: David V. Feliciano, Kenneth L. Mattox,
Ernest E. Moore: Trauma, Ninth Edition
Copyright © McGraw Hill. All rights reserved.

FIGURE 19-40

Periarticular injury: shoulder dislocation. (A–C) Anterior dislocation sustained by a 52-year-old struck by a falling tree on his back. (A) An anteroposterior (AP) radiograph with medial location of humeral head relative to glenoid (circle). (B) Postero-oblique radiograph of humeral head and glenoid (dotted line). Note that amount of overlap of scapula is less on this posterior oblique view than it is on anterior view (A), characteristic of anterior dislocation. (C) An axillary view; shows anterior location of humeral head relative to glenoid (upward pointing arrow and circle, respectively) on axillary lateral view. (D, E) Posterior dislocation sustained in a 42-year-old man who fell during a seizure. Posterior oblique radiograph (D) shows overlap of glenoid (circle) and medial aspect of humeral head (dotted line). (E) An axillary projection that shows the location of the humeral head posterior to glenoid (oval). Posterior margin of the head is denoted by downward pointing black arrow. Three downward pointing white arrows show impaction on anterior margin of humeral head, so-called trough fracture or reverse Hill-Sachs deformity.



C Source: David V. Feliciano, Kenneth L. Mattox,
Ernest E. Moore: Trauma, Ninth Edition
Copyright © McGraw Hill. All rights reserved.

FIGURE 19-41

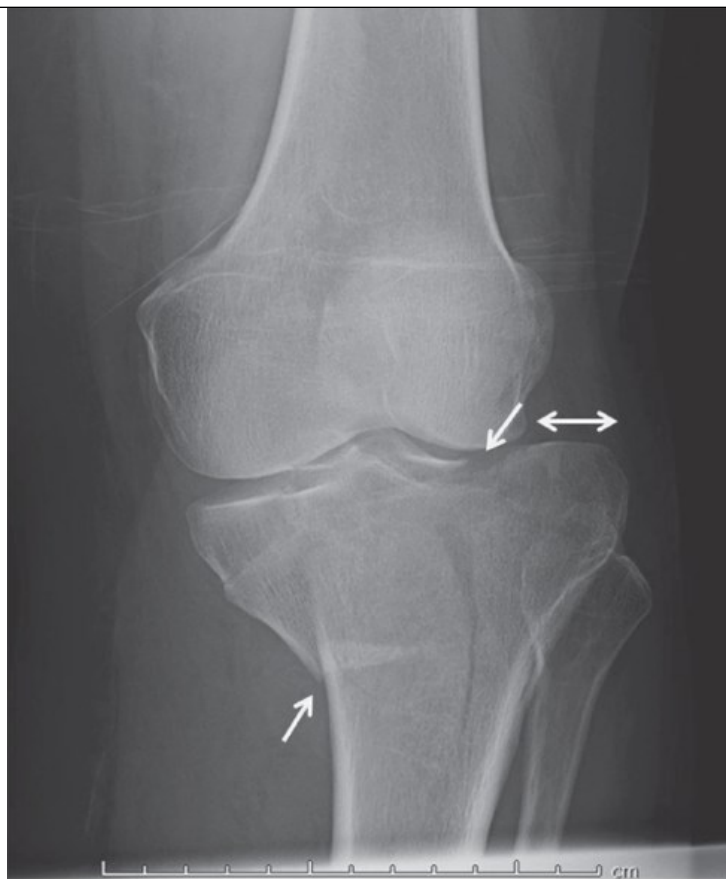
Periarticular fractures: intra-articular intercondylar distal femur fracture. This 20-year-old man was involved in a high-speed motor vehicle crash as a belted driver. (A) Anteroposterior (AP) radiograph of knee shows transverse T-type fracture of distal supracondylar femur, with intra-articular extension into intercondylar notch (arrows). (B) Lateral radiograph of knee shows transverse supracondylar component (arrow), from which femoral condyles have dissociated. In addition, lateral femoral condyle shows coronal plane, comminuted fracture of posterior aspect of condyle (arrowheads). In up to 40% of intra-articular intracondylar fractures caused by high-energy mechanisms, such coronal plane fractures (Hoffa fracture) may be overlooked. (C) Axial computed tomography (CT) shows a sagittal plane fracture extending into midportion of trochlea of the patellofemoral joint and a comminuted coronal plane fracture of posterior aspect of lateral femoral condyle (arrow). (D) Coronal plane reformation from axial CT shows T-type intra-articular fracture with dissociation of medial and lateral femoral condyles (white lines). Asterisk marks developmental variant, nonossifying fibroma. (E) Sagittal reformation from axial CT in central portion of lateral knee joint compartment shows coronal plane fracture of posterior femoral condyle (Hoffa fracture), as marked by arrow. Asterisk notes nonossifying fibroma, a benign developmental variant.



Source: David V. Feliciano, Kenneth L. Mattox,
Ernest E. Moore: Trauma, Ninth Edition
Copyright © McGraw Hill. All rights reserved.

FIGURE 19-42

Periarticular fractures: tibial plateau fracture (Schatzker 4). This is a 57-year-old woman who was hit by a car. (A) Anteroposterior (AP) radiograph of the knee shows a comminuted oblique fracture through the tibial plateau extending into the medial cortex (arrows). There is lateral subluxation (double arrow) of the tibial plateau with respect to the femoral condyles. (B) Cross-table lateral radiograph demonstrates the tibial plateau fracture (arrow) and lipohemarthrosis (triangle). The presence of a fat fluid level in the suprapatellar joint space indicates that the fracture line extends to the tibial plateau surface, thus liberating the fatty elements of the bone marrow into the joint space. Coronal (C) and axial (D) computed tomography (CT) images demonstrate the extent of intra-articular comminution and persistent fracture fragment subluxation despite closed reduction. (E) Three-dimensional surface-rendered CT image nicely demonstrates the fracture lines and relationships between the primary fracture fragments.

**A**

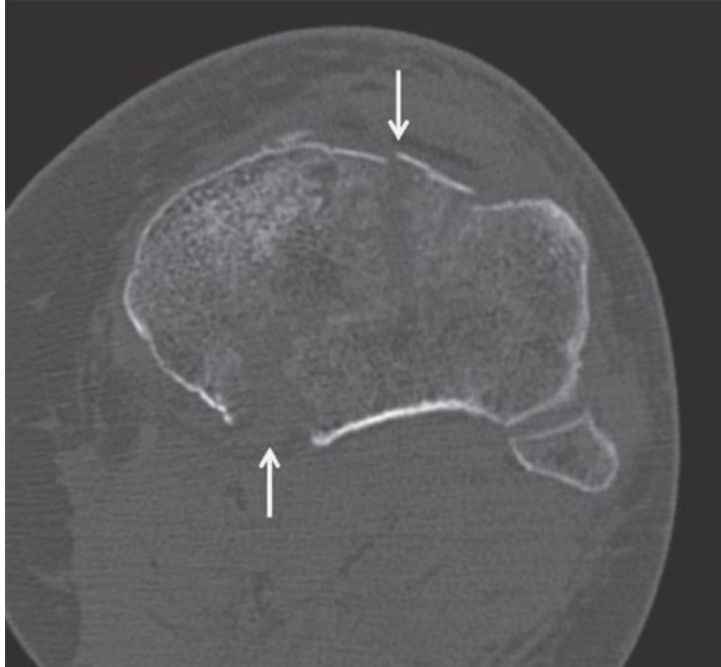
Source: David V. Feliciano, Kenneth L. Mattox,
Ernest E. Moore: Trauma, Ninth Edition
Copyright © McGraw Hill. All rights reserved.

**B**

Source: David V. Feliciano, Kenneth L. Mattox,
Ernest E. Moore: Trauma, Ninth Edition
Copyright © McGraw Hill. All rights reserved.

**C**

Source: David V. Feliciano, Kenneth L. Mattox,
Ernest E. Moore: Trauma, Ninth Edition
Copyright © McGraw Hill. All rights reserved.

**D**

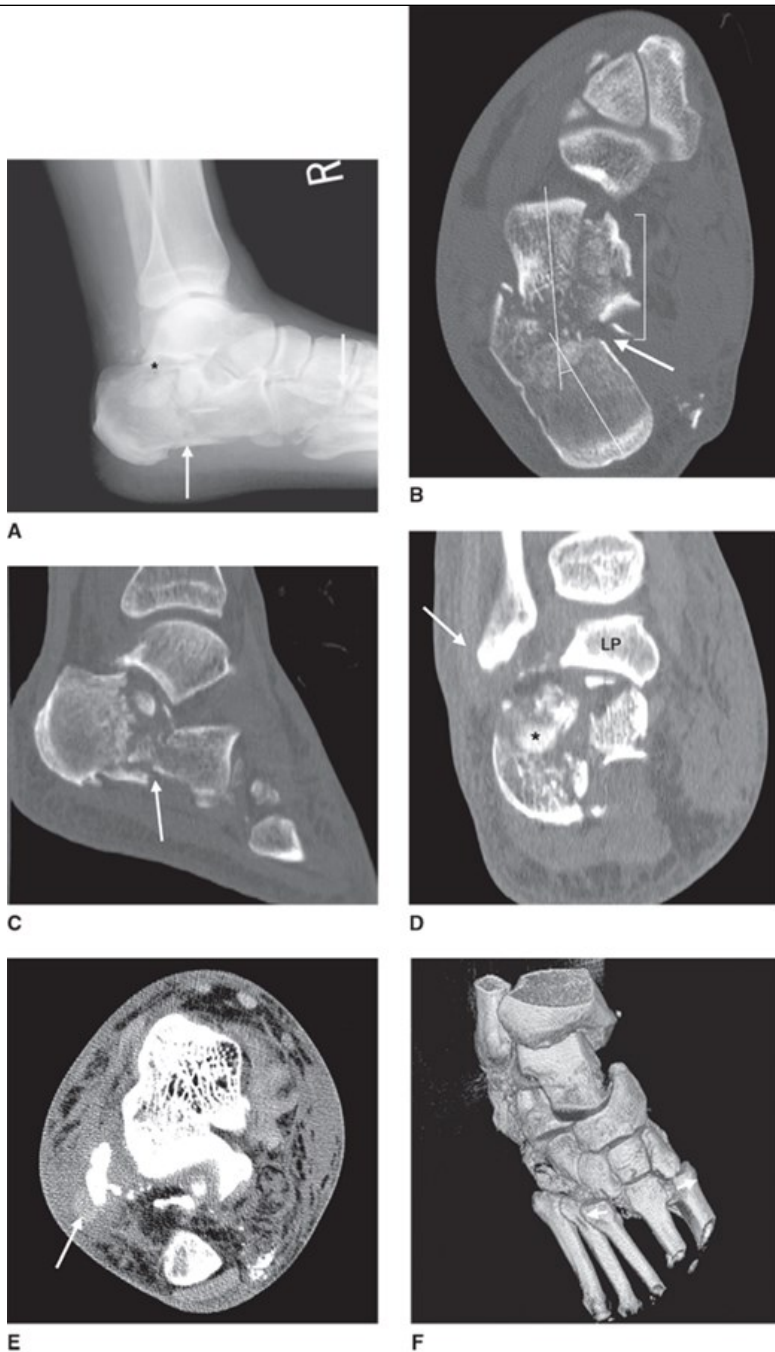
Source: David V. Feliciano, Kenneth L. Mattox,
Ernest E. Moore: Trauma, Ninth Edition
Copyright © McGraw Hill. All rights reserved.

**E**

Source: David V. Feliciano, Kenneth L. Mattox,
Ernest E. Moore: Trauma, Ninth Edition
Copyright © McGraw Hill. All rights reserved.

FIGURE 19-43

Periarticular fractures: calcaneus and Lisfranc fractures of midfoot. This 51-year-old restrained driver in a high-speed motor vehicle crash sustained multiple extremity and torso injuries. (A) Lateral conventional radiograph shows intra-articular fracture of calcaneus (upward pointing arrow denotes primary fracture plane; asterisk shows double density of central lateral fragment of posterior subtalar joint of calcaneus). Downward pointing arrow shows displacement of one of the metatarsal bases with an adjacent cuneiform fracture. (B) Axial computed tomography (CT) image at level of base of sustentaculum tali shows varus deformity through primary fracture (arrow). Secondary fracture plane extends toward anterior process (bracket). It is important to note continuity of cortex of medial wall of anterior process, as it influences distal extent of necessary fixation. (C) Sagittal reformation from axial CT shows primary fracture plane (upward arrow) with centrolateral fragment rotated into its superior extent. (D) Coronal reformation shows comminuted fracture of posterior facet of calcaneus due to bursting of body by lateral process (LP) of the talus. Centrolateral fragment is shown by asterisk. White arrow denotes lateral dislocation of peroneal tendons from peroneal groove in posterior fibula. (E) Axial CT at level of sinus tarsi, soft tissue window, shows lateral and anterior dislocation of peroneal tendons surrounded by hemorrhage and edema (white arrow). (F) Three-dimensional reformation from axial CT, medial oblique projection, shows divergent dislocations of great toe and third to fifth metatarsal bases (arrows).



Source: David V. Feliciano, Kenneth L. Mattox, Ernest E. Moore: Trauma, Ninth Edition
Copyright © McGraw Hill. All rights reserved.

Analysis of the long bone should allow assessment of the direction of the force that created the fracture pattern (eg, twisting injuries result in spiral fractures; bending injuries result in wedge fractures). In general, higher-energy injuries tend to be more comminuted and displaced. If there is a mismatch between the apparent amount of comminution and the reported energy of the injury, osteoporosis or otherwise pathologic bone should be suspected. The degree of displacement and angulation of the predominant fracture fragments, as well as fracture line involvement of an articular surface, must be noted.

Periarticular regions should be evaluated for fracture involvement as well as for partial or complete loss of congruity of the joint. The appearance of a superimposed white line due to overlapping of bones may indicate a dislocation and disruption of expected alignment of adjacent articulating structures (Fig. 19-38E).

Careful attention to soft tissues (eg, focal swelling, obliteration of normal fat pads, joint effusions) is helpful for subtle or otherwise occult fractures (eg, elbow, knee, and wrist). A search for foreign bodies in soft tissue in the setting of an open fracture or soft tissue injury should be performed.

Computed Tomography of Appendicular Joints

CT of appendicular joints, particularly the shoulder, tibial plateau, pilon, midfoot, and calcaneus, is indicated for “displaced” intra-articular fractures (eg, 1–2 mm at the wrist, scapula, or glenoid; 5–10 mm at the tibial plateau) or unstable fracture patterns (Figs. 19-39 and 19-41, 19-42, 19-43). CT is a valuable surgical planning tool and is very helpful in the detection of otherwise occult fractures, particularly of the midfoot.

In most patients, CT should be performed after provisional placement of traction or reduction, if feasible. Use of traction prior to imaging allows ligamentotaxis to indirectly reduce fracture fragments and support indirect assessment of the integrity of soft tissue attachments to major bony fragments. Specifically, bone fragments that do not move or reduce on stretch are presumed to be no longer attached to soft tissue and may require debridement or direct repositioning.

Because acquisition of isotropic image data of modern MDCT scanners allows for reconstruction of images in any conceivable plane, the joint in question no longer needs to be precisely positioned in the CT scanner gantry. Thus, “axial” images of a joint are not necessarily oriented in the axial plane of the body, but instead are oriented in the “axial” plane of the joint. Orthogonal images in both the sagittal and coronal planes are reconstructed from the joint-specific axial plane, usually at 1- to 2-mm slice thickness using a bone algorithm.

Peripheral Vascular Injuries

Vascular injuries in the extremities compose between 40% and 75% of vascular injuries observed in civilian trauma centers, with a majority of these (approximately two-thirds) involving the femoral or popliteal arteries. Approximately three-fourths of peripheral vascular injuries are the result of penetrating trauma, with 70% to 80% secondary to projectiles such as gunshot wounds and shrapnel. Fatal exsanguination, multiorgan failure secondary to hemorrhagic shock, and limb loss are catastrophic consequences of peripheral vascular injuries; thus, rapid identification and appropriate triage are of paramount importance. Vigorous or pulsatile external active hemorrhage, a rapidly expanding hematoma, and loss of distal pulses mandate emergent operative exploration.⁹⁵

The imaging strategy for patients with suspected peripheral vascular injuries depends on a variety of factors that are primarily related to clinical presentation, hospital course, associated injuries, mechanism of injury, and signs of circulatory shock. Imaging modalities available include catheter angiography, CTA, Doppler ultrasound, and MR angiography (MRA).

Doppler ultrasound may be a useful adjunct but is not widely used, primarily because of its decreased sensitivity and accuracy for peripheral vascular injuries when compared to catheter angiography. This, coupled with the operator-dependent nature of the examination and limited visualization of the entire vascular system for a variety of reasons (eg, external fixator devices, overlying split or cast material, and associated soft tissue injuries and gas), makes the utility of Doppler ultrasound for peripheral vascular injuries quite limited.

MRA is useful for the assessment of chronic peripheral vascular disease but is not widely used in the acute setting for the following reasons: (1) it may not be available at all centers at all times of the day; (2) it is technically challenging to effectively manage severely traumatized patients while they are in the magnetic resonance magnet; (3) the presence of metallic foreign bodies may limit patient and operator safety; and (4) even if not ferromagnetic, foreign bodies may still cause extensive artifact, obscuring the adjacent soft tissues. Thus, CT or catheter angiography is the primary imaging choice for patients with extremity injuries and suspected peripheral vascular injuries.

CTA FOR SUSPECTED PERIPHERAL VASCULAR INJURIES

CTA is an extremely useful adjunct for suspected peripheral vascular injuries in patients without indications for immediate surgical exploration. It is readily available, fast, convenient, noninvasive, and reliable. In addition, CTA can be easily integrated into the imaging workup of a traumatized patient, performed either as a stand-alone examination or integrated as part of a whole-body CT for polytrauma. CTA has high sensitivity, specificity, and accuracy when compared to catheter angiography (which remains the reference gold standard). In addition, CT capabilities allow for global evaluation of the adjacent structures and can thus be used to detect and characterize associated nonvascular injuries. The inability to immediately perform interventions on an injured vessel is a major limitation of CTA compared to catheter angiography.

The overall performance of CTA for peripheral vascular injuries compared to catheter angiography is certainly a concern for the trauma surgeon, as there is very little tolerance for missed or mischaracterized vascular injuries. A meta-analysis by Jens et al⁹⁶ pooling data from 11 studies from both the radiology and surgical literature and using a variety of scanner types documented that peripheral CTA for extremity vascular injuries had a sensitivity of 96.2% and specificity of 99.2% compared to catheter angiography. The rate of nondiagnostic CTA examinations was 4.2% in this meta-analysis. Thus, in patients without indications for immediate surgical exploration, CTA is useful to exclude peripheral vascular injuries and to characterize injuries that are present.

The CTA signs of a vascular injury include pseudoaneurysm, active bleeding, occlusion, intimal injury, dissection, and arteriovenous fistula ([Fig. 19-38G](#)). Imaging findings that raise the likelihood of an injury include a perivascular hematoma, a vessel within a projectile wound tract, and projectile fragments within 5 mm of a vessel. The latter two findings should typically prompt further investigation with catheter angiography.

Extremity CTA should be performed using MDCT with thin-section acquisition, peripheral IV access or a power injectable central line, and a high contrast injection rate (4–5 mL/s) and should be acquired during the systemic arterial phase. Images are reconstructed in the true axial plane to the long axis of the extremity at 1- to 3-mm slice thickness, with additional sagittal and coronal images reconstructed with respect to the axial plane. Coronal MIPs (or thick slab images) at 5- to 10-mm slice thickness are extremely valuable in displaying vessels along their long axis using a relatively small number of slices. Thin images should be reviewed as well, because small intimal vascular injuries may not be apparent on MIP images due to volume averaging. Liberal use of a 3D volume viewing station is encouraged, as some vascular injuries may be best displayed on nontraditional planes.

It should be noted that vascular injuries near highly mobile joints, such as the knee, are poorly treated with endovascular techniques. Thus, the decision to image with CTA over catheter angiography must be weighed against patient stability and the need for urgent surgical vascular repair. Despite this, the wide availability of stent grafts has also increased the utilization of angiography as a prelude to nonoperative management of some clinically significant vascular injuries.

CATHETER ANGIOGRAPHY

Catheter angiography (whether based in the radiology suite, operating room, or a hybrid operating theater) remains the reference gold standard for the definitive evaluation of arterial blood vessels for injury, as well as identifying active arterial hemorrhage, pseudoaneurysms, and arteriovenous fistulas. Although CTA is frequently favored for the initial imaging of many traumatic vascular lesions in stable patients, it is limited by the inability to immediately intervene in the event of a positive study. CTA performance is very high, but not yet as accurate as catheter angiography. Catheter angiography is used as a problem-solving tool for equivocal CT examinations and for definitive therapy of some acute vascular conditions.

There are many advantages of catheter angiography. It allows simultaneous detection and treatment of a wide variety of traumatic vascular injuries. It is a very specific method of identifying bleeding at the submillimeter diameter of vessel. It can evaluate many sites of bleeding simultaneously. It has an excellent safety record, especially when using iso-osmolar nonionic contrast agents, coaxial micropuncture access, digital subtraction techniques, coaxial microcatheters, and steerable guidewires.

The disadvantages of catheter angiography are cost, the delay necessary to assemble the interventional radiology team (composed of radiologists, technologists, and nurses), the lack of suitability as a screening test for most traumatic conditions, and the risks of radiation exposure. Technical expertise is limited to predominantly subspecialty-trained interventional radiologists. These disadvantages are magnified when the likelihood of injury is low. Thus, noninvasive vascular techniques such as CTA should be entertained when considering the patient's overall management.

Transcatheter Endovascular Therapies

Endovascular techniques have become a broadly accepted way of controlling traumatic hemorrhage for a variety of reasons. Catheter-based hemostasis allows precise control from a remote site that avoids exacerbation of venous hemorrhage, introduction of pathogens, and hypothermia that may result from open exposure. It is especially valuable for hemorrhage that is remote or hidden from view and requires laborious time-consuming exposures or that is the result of multiple small bleeding sites that are not easily detected or controlled during operative exploration.

Endovascular techniques include embolization, stenting, stent grafting, and temporary balloon occlusion and may be definitive in nature or an adjunct to operative exposure. The methods of embolization include particulate or microcoil embolization of small vessels, proximal and distal control of a bleeding vessel, and coil occlusion to cause selective temporary hypotension of the bleeding zone.

Stenting, which facilitates blood flow beyond an injury, has largely been replaced by covered stent grafts that exclude lacerations, transections, and arteriovenous fistulae while maintaining flow through the conduit. Endografts are made of a variety of porous materials such as expanded polytetrafluoroethylene and are reinforced by a metallic skeleton that apposes the stent graft to the native artery. Reports of midterm patency, while limited at this time, are beginning to show that these are durable options to vascular repairs.

Contraindications to endovascular techniques are highly dependent on skills, teamwork, and hemodynamics; however, there are some injuries that are difficult for rapid surgical control and for which endovascular techniques have a role, even in the unstable patient.

Arch Angiography for Acute Blunt-Force Traumatic Aortic Injury

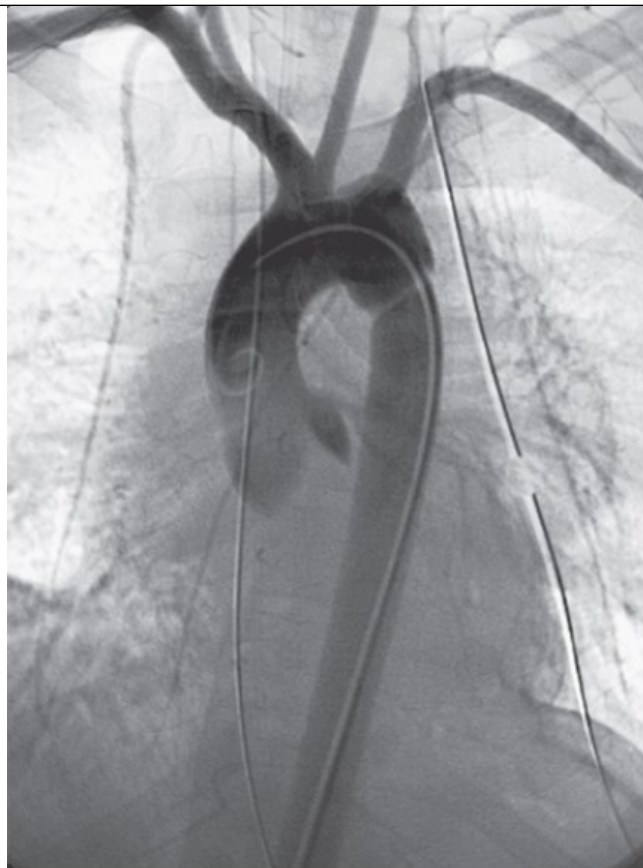
Screening and diagnostic arch angiography for blunt traumatic aortic injuries has largely been replaced by chest CTA, particularly with the widespread availability of MDCT technology.⁶⁷ Arch angiography, however, does have a role in the evaluation of equivocal findings on chest CTA and in potential endovascular stent graft therapy. If patients are going directly to angiography for evaluation of disruptions of the pelvic ring and the mediastinum is not normal on a chest x-ray, catheter arch angiography is the preferred “screening” modality; otherwise, CT is preferred. Modern CTA techniques are quite exquisite in demonstrating aortic injuries as well as providing coronal and sagittal reformations that can illustrate the important relationships and variants necessary for surgeons to create a treatment plan. Among many patients sustaining aortic injury, endovascular stent grafts have been advocated as definitive therapy.

Typically, a 5F pigtail catheter is guided to the ascending aorta via a femoral arterial approach. Patients are positioned and imaged in both 35° right anterior oblique and left anterior oblique projections, using injection rates of approximately 25 to 30 mL/s for a 40- to 60-mL volume (depending on hemodynamic status) and positioning to include the great vessels and diaphragm.

The angiographic appearance is classical. Linear filling defects indicate torn and ruffled intimal lining, with expansion of the lumen (typically at the ligamentum arteriosum) indicating the presence of a pseudoaneurysm (Fig. 19-44). The tear of the aortic wall may be segmental or circumferential and is sometimes associated with distal narrowing of the contrast column (pseudocoarctation). Minimal aortic injuries, as discussed earlier in this chapter, may be very difficult to visualize angiographically, and a “negative” aortogram following a positive chest CTA for a minimal aortic injury does not exclude the diagnosis.

FIGURE 19-44

Traumatic aortic pseudoaneurysm. A 30-year-old man following a high-speed motor vehicle accident. Left anterior oblique digital subtraction arch aortogram shows traumatic aortic pseudoaneurysm extending proximal to the left subclavian artery. Of note, the aortic diameter and the distance from the left subclavian artery are important when considering endovascular therapy.



Source: David V. Feliciano, Kenneth L. Mattox,
Ernest E. Moore: Trauma, Ninth Edition
Copyright © McGraw Hill. All rights reserved.

Associated mediastinal vascular injuries should also be identified. Injuries of the arch arteries may occur instead of, or in association with, an aortic injury. Bleeding from the internal mammary or the intercostal arteries may be easily overlooked without diligence.

Hepatic Angiography for Blunt-Force Lacerations

Visceral catheter angiography is appropriate to evaluate hepatic lacerations (Fig. 19-45), particularly in patients with a labile hemodynamic status or those with active extravasation or vascular abnormalities as seen on a contrast-enhanced CT. Visceral catheter angiography may have a role after a “damage control” operation. Gross hemodynamic instability and profound shock, however, usually mandate urgent celiotomy.

FIGURE 19-45

Liver laceration. (A) Computed tomography of the upper abdomen reveals a grade V liver laceration with pseudoaneurysm of the right hepatic lobe in this 18-year-old man status post high-speed motor vehicle accident. (B) Right hepatic angiogram identified the pseudoaneurysm. Note the size of the feeding vessel in relation to the 5F diagnostic catheter. Selective coil embolization was performed through a microcatheter. When selective catheterization is not possible, the liver is quite tolerant of wide arterial embolization due to the dual blood supply, provided the portal veins are patent.



A



B

Source: David V. Feliciano, Kenneth L. Mattox,
Ernest E. Moore: Trauma, Ninth Edition
Copyright © McGraw Hill. All rights reserved.

On CT, hepatic fracture lines that traverse the hepatic triad result in bleeding more often than those that run parallel to the triad. Contrast extravasation on CT tends to be associated with a positive arteriogram, but the decision to use angiography should primarily be based on clinical status rather than the CT appearance. Lack of enhancement of liver segments on CT is a very important finding, as these regions represent an intraparenchymal hematoma, occlusion of the portal triad, or injury of the hepatic outflow from that segment. It is vital to distinguish nonenhancement from a hematoma, which can be challenging. A large hepatic hematoma pushes the hepatic fragments away from each other and lacks hepatic vessels. If the area of nonenhancement has vessels running through it, it suggests an occlusion of the portal vein and hepatic artery or injury to a hepatic vein. Therefore, CT nonenhancement of the liver is an indication for angiography to confirm such injuries and to control ongoing arterial hemorrhage. As surgical exploration of damaged hepatic veins may be quite difficult, hepatic embolization and observation of a nonbleeding hepatic venous injury can be lifesaving. Hepatic angiography can also be helpful in the management of penetrating liver injuries that are isolated to the liver.

Selective catheterization of both the celiac trunk and the superior mesenteric artery (SMA) is essential due to the high rate of hepatic vascular variants, particularly the aberrant replaced right hepatic artery from the SMA (15%–20%). Imaging should be continued through the late portal venous phase to

evaluate for slowly bleeding vessels. There should be careful inspection for abnormal parenchymal enhancement and intrahepatic portal venous filling, as these are features of hepatic arterial-portal venous fistulae, which can easily be overlooked.⁹⁷

Critical findings include arterial extravasation, spasm and occlusion, or shunting and fistula to portal or hepatic venous structures. Embolization of discretely abnormal vessels can be performed using a number of methods. A diffusely abnormal parenchymal injury with arterial bleeding may be safely embolized with Gelfoam due to the dual blood supply of the liver (hepatic arterial and portal venous). Embolization of hepatic arteries in the absence of portal flow increases the risk of developing an infarction or abscess. Depending on the location of bleeding and on the difficulty with catheterization, particulate embolization is the fastest technique; however, single microcoil embolization is preferred if time and circumstances allow. While formation of a postprocedure abscess is a complication of embolization, outcomes are favorable by integrating percutaneous image-guided drainage into the scheme.

Splenic Angiography for Blunt-Force Lacerations

Patients with splenic injuries diagnosed on CT are candidates for nonoperative management with overall good salvage rates, particularly when combined with splenic angiography and embolization.^{77,98} When CT demonstrates active arterial extravasation or a parenchymal vascular abnormality (eg, an intraparenchymal pseudoaneurysm), one should consider angiography, as these are independent predictors of failure of nonoperative management.⁹⁹ It is thought that there was poor correlation between the CT grading system and outcome of treatment, as many grade IV injuries can be observed, and some grade I injuries become worse, rebleed, and require definitive procedural therapy. However, there is emerging evidence that a CT-based grading scheme, in combination with clinical parameters (eg, Abbreviated Injury Scale score), may be helpful for patient triage.^{100,101} The treatment algorithms for patients with splenic injuries in the absence of active bleeding or other vascular lesions vary greatly by institution. The absence of arteriographic extravasation is a highly reliable predictor of successful nonoperative therapy regardless of injury grade. Identification of active arterial extravasation is the standard indication for endovascular treatment.

Diagnostic angiography of the celiac trunk is followed by selective splenic artery catheterization with a 5F catheter. If splenic artery anatomy permits and a solitary pseudoaneurysm or focus of extravasation is seen, distal coil embolization at the site of injury can be attempted. This is especially true in a patient in whom the extravasation extends beyond the splenic capsule into the peritoneal cavity. One should note that distal superselective embolization is associated with the development of more postprocedure splenic infarctions and abscess, although these complications are uncommon. Finally, most patients have tortuous splenic arteries, and most extravasations are multiple.

Diffuse intrasplenic extravasation is far more common, and superselective occlusion of these multiple sites would be very time consuming and less effective. In addition, the splenic tortuosity that results from medial displacement of the spleen by the perisplenic hematoma often prevents rapid catheterization (Fig. 19-46). In such cases, embolization of the proximal splenic artery by coils or other occlusion devices placed distal to the dorsal pancreatic branch and proximal to the pancreatic magna branches is advocated to reduce the arterial pressure head at the injury site while allowing perfusion through collateral vessels. Such collaterals prevent splenic infarction by maintaining splenic perfusion through connections between the left gastric and the short gastric arteries, between the dorsal pancreatic artery and the greater pancreatic artery branches, between the right and left gastroepiploic vessels, and others.

FIGURE 19-46

Splenic intraparenchymal false aneurysms. Digital subtraction angiogram of the splenic artery reveals multiple focal extravasations in this 56-year-old man status post motor vehicle accident. Selective embolization is not desirable because so many vessels are injured and selective catheterization would be difficult due to splenic artery tortuosity. In such cases, proximal splenic artery coil embolization proximal to the pancreatic magna branch is usually successful in controlling this hemorrhage.



Source: David V. Feliciano, Kenneth L. Mattox,
Ernest E. Moore: Trauma, Ninth Edition
Copyright © McGraw Hill. All rights reserved.

Complications are uncommon when proximal splenic artery embolization is performed. A poorly selected coil size may result in hilar occlusion if the selected coil is too small and migrates distally. Coils that are too large may migrate proximally to occlude the celiac axis or embolize into the aorta. As noted earlier, distal microembolization bypasses the collateral circulation and results in more loss of immune function. It should be noted, however, that splenic blood flow is maintained in most patients via a combination of intact left gastroepiploic and short gastric arteries. This preserves immune function of the spleen, as well as distal flow. Occlusion of the pancreatic branches may result in pancreatic necrosis and pancreatitis, although these complications are rare and can be avoided by careful review of the angiographic images if main splenic artery embolization is considered.

Interventions for Renal Trauma

Many renal injuries are usually well tolerated and do not require angiography, especially when caused by blunt trauma. Initial nonoperative management of blunt renal injuries with an intact pedicle is the current accepted management standard. High-grade injuries that result in massive hemorrhage may necessitate nephrectomy. Angiography for embolization of active bleeding is appropriate for hemodynamically stable patients. Angiography is recommended for patients with CT evidence of a major renal injury and ongoing blood loss or persistent gross hematuria. Peripheral wedge-shaped regions of nonenhancement on CT suggest a segmental or distal renal artery injury, often due to avulsion injury or intimal stretch resulting in distal platelet embolization. Penetrating renal injuries are more aggressively approached by angiography if nonoperative management is undertaken. Large perinephric hematomas, areas of nonenhancement, and active bleeding on CT warrant angiography following penetrating trauma.

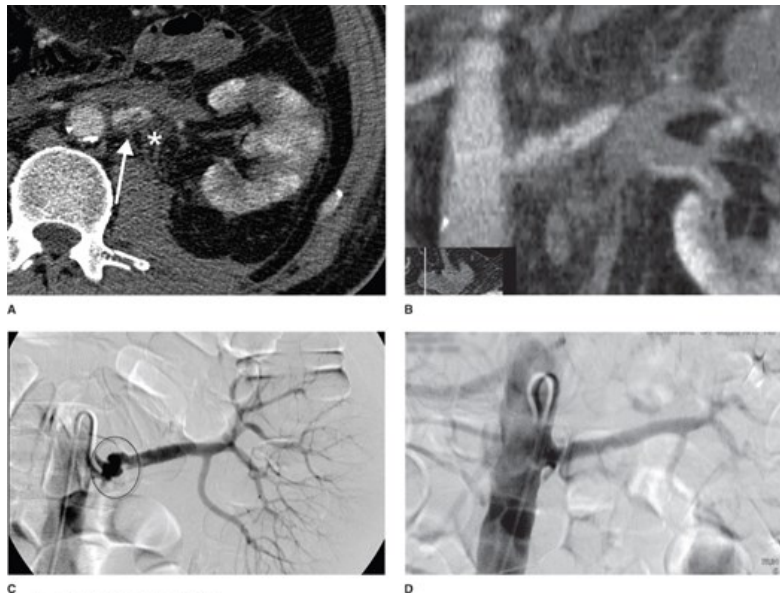
Aortography is helpful to assess injury of the origin of the renal artery, to exclude renal parenchymal injury perfused by accessory renal arteries, and to look for associated bleeding sites. A selective renal arteriogram using a 5F catheter is then performed. Most injuries will require use of a coaxial microcatheter and embolization of small branches. Coils are preferred as they can be carefully placed to prevent infarction of adjacent noninjured renal tissue, but surgical gelatin pledges can be used as well. Because renal branches are end vessels with little collateralization, infarction is likely, and the goal is to reduce these infarctions to a minimum.

The treatment of vascular injury in the renal pedicle continues to be a vexing problem, especially because delays in revascularization usually result in a renal infarction or renovascular hypertension. Partial wall injuries that result in a pseudoaneurysm or segmental infarction often went unrecognized prior to the widespread use of CT. Such injuries are routinely detected before complete arterial thrombosis and renal infarction occur. Therefore, arteriography is indicated when an injury in the renal artery is suspected. When such injuries are detected, treatment options are many, including operative revascularization, antiplatelet therapy and observation, and the application of covered stent grafts. Stent grafts can effectively seal full-

thickness injuries and cover exposed media that results in embolic infarctions. Although long-term follow-up of series of these patients is lacking, the midterm (1–5 years) patency of stent grafts throughout the body remains high (Fig. 19-47).

FIGURE 19-47

Renal artery injury. A 56-year-old man fell from a height of about 10 m. (A) During computed tomography evaluation, inhomogeneous enhancement of the spleen was detected. Central perinephric hemorrhage (asterisk) and irregularity of the renal artery (arrow) were seen. (B) Coronal reformation shows irregularity of the renal artery and thickening of its wall. (C) Aortography shows irregular enlargement of the proximal renal artery near the ostium (circled). Slight extravasation was seen on the later images. (D) Therefore, a stent graft was placed over the area of injury. The vessel wall was then smooth, and no extravasation was seen. Two-year follow-up arteriography showed continued patency and no stenosis.



Source: David V. Feliciano, Kenneth L. Mattox,
Ernest E. Moore: Trauma, Ninth Edition
Copyright © McGraw Hill. All rights reserved.

Angiography for Pelvic Hemorrhage

Pelvic fractures are potentially life-threatening injuries that are caused by high-energy impact trauma and are the third most common lethal injury following motor vehicle crashes. The majority of patients with pelvic fractures do not require massive transfusion as bleeding in most cases is likely to be venous or osseous in nature and often self-limited. Radiologic intervention is not commonly required in patients with routine pelvic fractures. Severe hemorrhage, however, occurs in 3% to 10% of patients, and mortality rates may be as high as 40% in patients with unstable pelvic fractures.¹⁰² Thus, the use of angiography in patients with pelvic fractures is highly dependent on the hemodynamic status, the type of pelvic fracture pattern, the transfusion requirements, and the presence or absence of pelvic hematoma.

BLUNT PELVIC FRACTURES

Blunt pelvic fractures with crushing or shearing tear the small branches of the internal iliac artery that accompany ligaments, muscles, and tendons. Injuries tend to be multiple and bilateral and from several branches. In addition, bony fragments can penetrate or perforate vascular structures. Examples include a fracture of the superior pubic ramus injuring the internal pudendal or obturator artery, a fracture of the iliac wing through the sciatic notch injuring the superior gluteal artery, and disruption of the sacroiliac joints injuring the lateral sacral arteries.

Most of the indications for angiography in blunt pelvic trauma have remained the same for many decades and include the following:

1. Hemodynamic instability in a patient with a pelvic fracture with no or little hemoperitoneum detected by FAST or DPL.
2. Pelvic fracture and transfusion requirement of greater than 4 units in 24 hours or 6 units in 48 hours.

3. Pelvic fracture and a large or expanding hematoma identified during celiotomy.
4. CT evidence of large retroperitoneal hematoma with extravasation of contrast.
5. Need for detection and treatment of other injuries during angiography.

The presence of contrast extravasation on MDCT has been used as an indication for follow-up pelvic angiography. Although it should not delay angiography that is already indicated for pelvic hemorrhage, CT is helpful in localizing the vessels likely to be bleeding not only in the pelvis, but also from the solid organs and thoracic cavity. Correlations of location of the hematoma and site of vascular injury include obturator space and obturator artery, presacral space and lateral sacral artery, space of Retzius and internal pudendal artery, and buttock and gluteal artery.

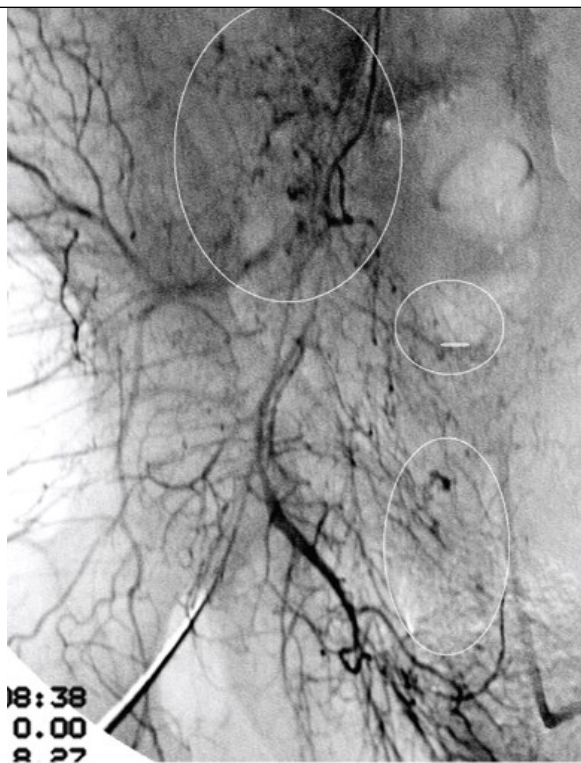
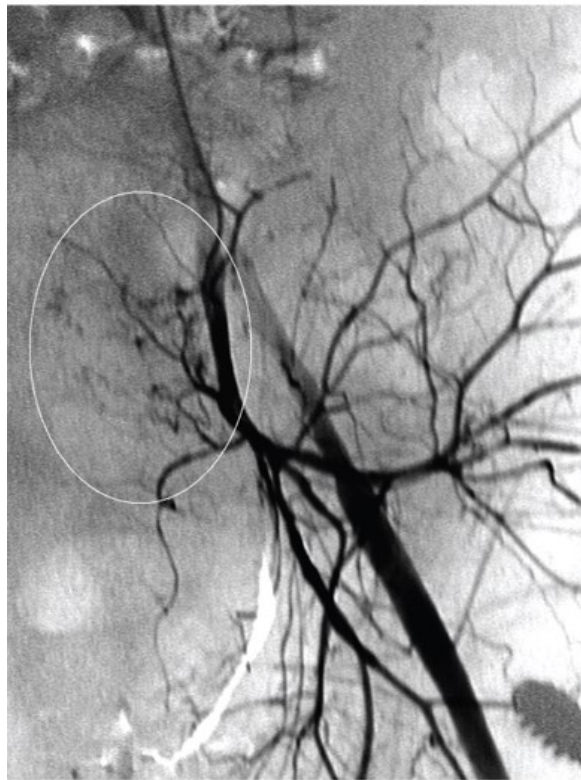
Femoral access is the preferred approach; however, catheterization may be difficult because of hypotension, tachycardia, and difficulty in palpating the vessels as the pelvic hematoma expands. Ultrasound or fluoroscopic guidance is very helpful in these situations. A 5F aortic flush catheter is used for flush abdominopelvic aortography. This is valuable to screen the abdominal viscera and mesentery, to exclude aortoiliac and other retroperitoneal bleeding sources, and as a road map of the pelvic vessels. Selective bilateral internal iliac arteriography is mandatory to exclude bleeding sites since aortography may not identify all bleeding. From one access, both internal iliac arteries are sequentially catheterized and opacified. Then, external iliac arteriography is used to evaluate the external pudendal and external obturator vessels.

It is common to identify multiple areas of extravasation during pelvic angiography. These may be bilateral and may involve multiple vascular beds. Extravasation is often punctate but can be large and coarse, and the size of such extravasations may not correlate with the degree of blood loss. Vascular occlusions due to transection or dissection with subsequent occlusion can be present as well. It can be difficult to differentiate between arterial injury due to thrombosis and vasospasm. Failure to treat these occlusions may result in recurrent hemorrhage when vasospasm resolves. Arteriovenous fistulas can occur but are more common in penetrating trauma.

Because bleeding is usually multifocal and originates from multiple small blood vessels, embolization requires small particulate embolization. Large coil occlusion is as ineffective as surgical ligation of the internal iliac artery because bleeding soon resumes through numerous collateral circuits. Surgical **gelatin** pledges are ideal because they are inexpensive, readily available, and often temporary, lasting only a few weeks and allowing reestablishment of normal blood flow after the tissue has healed ([Fig. 19-48](#)). Permanent particulate emboli, however, are often used because of their ease of use through a microcatheter ([Fig. 19-49](#)). Embolization is technically successful in more than 90% of patients, and hemorrhage control is highly effective. Survival depends on many other factors including associated injuries, the presence of an open fracture, transfusion requirements, and delays to embolization.

FIGURE 19-48

Multiple bleeds from pelvic fractures: 48-year-old male driver in a motor crash sustained pelvic fractures requiring transfusions. (A) Circles surround multiple bleeding sites from the region of the sacroiliac joint; from the pelvic side wall on the right hemipelvis emanate anterior and posterior branches of the right internal iliac artery and in the region (B) multiple points of extravasation were detected (circle). They are emanating from the left lateral sacral artery. Such diffuse hemorrhage is not amenable to superselective embolization because it would be too time consuming. Pledgets of surgical **gelatin**, 2 to 3 mm in size, can occlude these vessels effectively.

**A****B**

Source: David V. Feliciano, Kenneth L. Mattox,
Ernest E. Moore: Trauma, Ninth Edition
Copyright © McGraw Hill. All rights reserved.

FIGURE 19-49

A 26-year-old motorcyclist sustained unstable pelvic fractures during a crash. He developed expanding perineal and scrotal hematomas requiring red cell transfusion. **(A)** Left internal iliac arteriogram reveals a source of bleeding from the left internal pudendal artery (curved arrow). The more medial contrast stain (straight arrow) is a normal finding. It represents the blush of the perineal body and root of the ischiocavernosa muscle that is frequently seen on internal iliac arteriography of males. **(B)** Because this was focal hemorrhage, selective embolization via 2.8F catheter placed coaxially through the 5F catheter was attempted and successfully achieved hemostasis.

**A****B**

Source: David V. Feliciano, Kenneth L. Mattox,
Ernest E. Moore: Trauma, Ninth Edition
Copyright © McGraw Hill. All rights reserved.

PENETRATING PELVIC TRAUMA

Penetrating trauma is an uncommon indication for pelvic angiography, as many patients are hemodynamically unstable or have clear indications for

immediate exploratory celiotomy, often due to injury to a large vessel. Because the extraperitoneal space has been exposed by a penetrating wound, intraperitoneal bleeding is likely, and direct exploration is typically warranted. Occasionally, angiography is valuable when operative control cannot be initially accomplished and damage control has been performed. Angiography and embolization prior to unpacking can aid in decreasing blood loss at a reoperation.

Injuries to large vessels require a very different endovascular strategy than small vessels or end organ vessels. When an injury to a noncritical internal iliac artery or branch has been missed at operation but detected on postoperative angiography, coil occlusion of both the proximal and distal end of the vessel (whenever possible) is the standard treatment.

Catheter Angiography for Peripheral Vascular Injuries

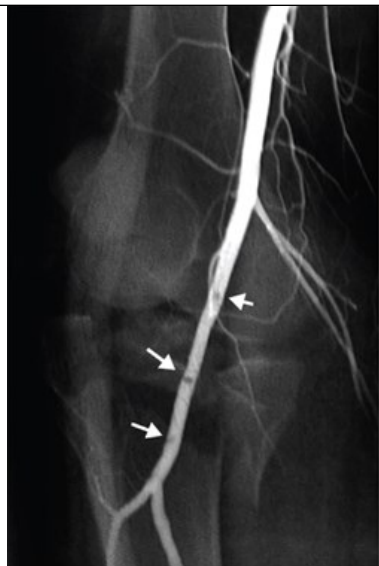
Almost all peripheral vascular injuries can be reached using a 5F catheter from femoral access provided a long enough catheter is available. Angiography should be done in multiple projections with opaque marking of surface wounds demonstrating that the entire course of the wounding agent is within the field of view. Iso-osmolar nonionic contrast medium is the optimal agent for visualization. Multiple images in the arterial, capillary, and venous phases are necessary.

There is a body of literature demonstrating that the combination of physical exam findings and noninvasive tests (eg, ankle-brachial index and Doppler ultrasound) is reliable in the exclusion of significant peripheral vascular injuries for patients with low likelihood of vascular injury. The overall incidence of extremity vascular injuries in the setting of penetrating trauma for asymptomatic patients is relatively low (3%–4%). Thus, screening CTA or angiography for “proximity” injuries is likely to be low yield in the absence of “hard” clinical signs.

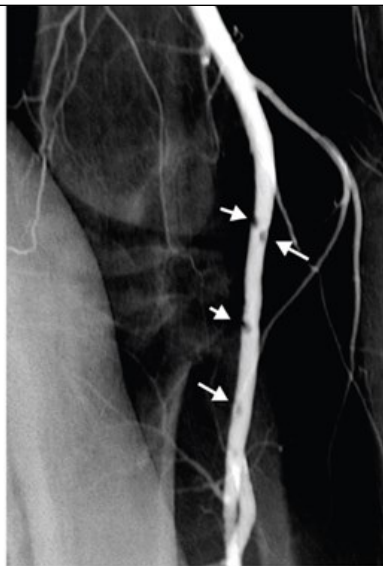
Vascular injuries resulting from fractures and dislocations are uncommon. Clinical evaluation is often difficult because the hematoma from a fracture may be quite large and indistinguishable from one associated with a vascular injury. Crush wounds, angulation deformities, and fracture hematomas may cause a pulse deficit by kinking, entrapping the vessel, or inducing spasm without an intrinsic vascular injury. A laceration into muscle may result in external blood loss without major vascular injury. The natural history of many injuries cannot be predicted by the angiographic appearance alone. Therefore, observation of some injuries is warranted. Equivocal findings such as luminal narrowing can be assessed by repeating angiography, after infusion of an intra-arterial vasodilator, on a subsequent day. Small irregularities and intimal tears that do not restrict flow may be treated by antiplatelet therapy and will generally heal ([Fig. 19-50](#)).

FIGURE 19-50

“Minimal injury” of the popliteal artery. Pedestrian who was struck by a motor vehicle sustained comminuted tibial plateau fracture of the left knee. Pulses were diminished and angiography was sought after incomplete reduction. (A, B) Initial popliteal arteriogram showed numerous filling defects consistent with intimal tears (white arrows). Patient was treated with [aspirin](#). (C, D) Arteriogram 1 week later showed healing of the intimal tears.



A



B



C



D

Source: David V. Feliciano, Kenneth L. Mattox,
Ernest E. Moore: Trauma, Ninth Edition
Copyright © McGraw Hill. All rights reserved.

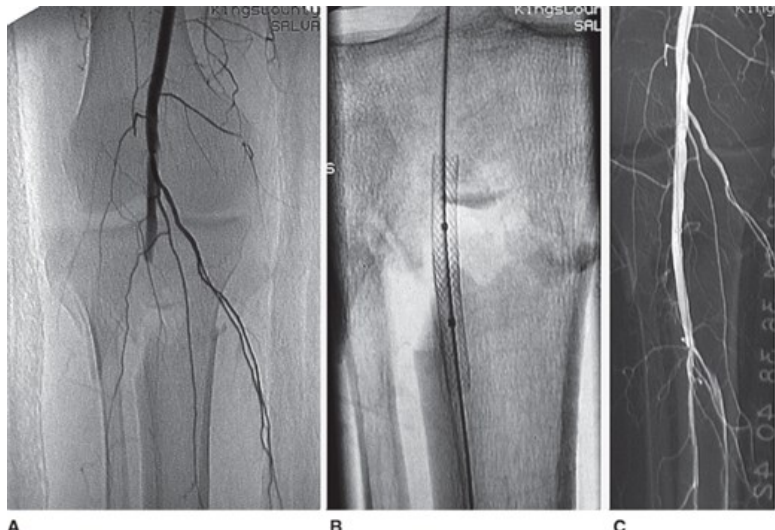
Source: David V. Feliciano, Kenneth L. Mattox,
Ernest E. Moore: Trauma, Ninth Edition
Copyright © McGraw Hill. All rights reserved.

Treatment of angiographically diagnosed vascular injuries is based on the anatomic role of the bleeding vessel; its size, location, and accessibility; the hemodynamic condition of the patient; and the specific type of lesion. Small vessels that are not essential for tissue perfusion can be treated by small-particle embolization, using surgical gelatin pledges or more permanent smaller agents. Permanent agents have no advantage but, in some instances, are more easily administered through microcatheters than surgical gelatin. These agents are delivered by flow direction toward the path of least resistance, which is usually toward the bleeding site. Microcoils can be used for injury to a small vessel provided they can be delivered near enough to the injury site to avoid collateral recruitment that permits continued bleeding. Examples of vessels that can be treated by embolization of small particles include hemorrhage from a pelvic fracture, multifocal hepatic arterial hemorrhage, and injuries to muscular branches such as those of the profunda femoris artery in the lower extremity.

Injury to larger vessels such as those greater than 3 mm in diameter requires two techniques, one for essential vessels and one for expendable vessels. The treatment of essential vessels mandates repair of the bleeding site while allowing continued blood flow. Thus, stent grafts can be deployed to cover the injured segment while allowing antegrade flow (Fig. 19-51).

FIGURE 19-51

Thrombosis of popliteal artery with endovascular repair. A 46-year-old morbidly obese woman sustained comminuted tibial plateau fractures after a fall from curb. Pulses were absent. (A) Popliteal arteriogram shows complete occlusion of the mid-popliteal artery. (B) The catheter was quickly advanced to a location just above the occlusion, and a guidewire was advanced easily into the posterior tibial artery. An expanded polytetrafluoroethylene-reinforced stent graft was deployed between proximal and distal extent of the occlusion. (C) Follow-up popliteal arteriogram showed restoration of direct line flow. The entire procedure took less than 1.5 hours.

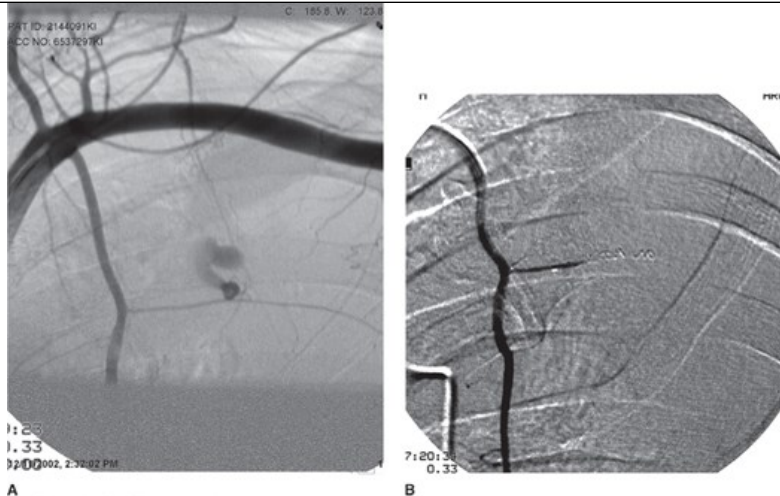


Source: David V. Feliciano, Kenneth L. Mattox, Ernest E. Moore: Trauma, Ninth Edition
Copyright © McGraw Hill. All rights reserved.

Nonessential conduits, such as branches of the profunda femoris artery or the brachial artery, or one of the arteries in the shank, can be safely embolized. Particulate embolization will flow past the injury and penetrate deep into the vascular bed. When conduits are injured, this insult to the vascular bed is unnecessary. Therefore, large-vessel agents are used to occlude the damaged segment of the conduit while the vascular bed is perfused through collaterals (Fig. 19-52).

FIGURE 19-52

Example of vascular isolation by proximal and distal coil occlusion. A 22-year-old man sustained a single stab wound of the upper left chest resulting in a very large hemothorax. (A) Subclavian arteriogram shows that there is active arterial hemorrhage from a lacerated fourth anterior intercostal branch of the left internal mammary artery. (B) Because there was continuity between anterior and posterior intercostals, it was necessary to advance a 2.8F microcatheter across the laceration into the distal segment to deliver a coil distally before withdrawing the catheter and delivering a coil proximally.



A
Source: David V. Feliciano, Kenneth L. Mattox,
Ernest E. Moore: Trauma, Ninth Edition.
Copyright © McGraw Hill. All rights reserved.

Coils in various sizes, some containing threads or fibers to accelerate thrombosis, are the most common devices used to occlude a large vessel. A coil is sized to have a diameter large enough to prevent distal migration, but not too large to end up recoiling into a parent, nontarget vessel.

The technique of arterial isolation attempts to occlude both the proximal and distal vessels around the area of injury by coiling (Fig. 19-52). The goal is to exclude the vascular defect and prevent rebleeding through collateral vessels. This is highly desirable in most circumstances, but mandatory when treating arteriovenous fistulas. The guidewire is carefully maneuvered distal to the injured segment but proximal to any branches, and coils are delivered. The catheter is then withdrawn, and coils are placed in the proximal segment.

REFERENCES

1. American College of Surgeons. *ATLS: Advanced Trauma Life Support for Doctors*. 9th ed. Chicago, IL: American College of Surgeons; 2012.
2. Stengel D, Bauwens K, Sehouli J, et al. Systematic review and meta-analysis of emergency ultrasonography for blunt abdominal trauma. *Br J Surg*. 2001;88:901. [PubMed: 11442520] □
3. Davis DP, Campbell CJ, Poste JC, et al. The association between operator confidence and accuracy of ultrasonography performed by novice emergency physicians. *J Emerg Med*. 2005;29:259. [PubMed: 16183443] □
4. Branney SW, Wolfe RE, Moore EE, et al. Quantitative sensitivity of ultra-sound in detecting free intraperitoneal fluid. *J Trauma*. 1995;39:375. [PubMed: 7674411] □
5. Chiu WC, Cushing BM, Rodriguez A, et al. Abdominal injuries without hemoperitoneum: a potential limitation of focused abdominal sonography for trauma (FAST). *J Trauma*. 1997;42:617; discussion 623. [PubMed: 9137247] □
6. Poletti PA, Wintermark M, Schnyder P, et al. Traumatic injuries: role of imaging in the management of the polytrauma victim (conservative expectation). *Eur Radiol*. 2002;12:969. [PubMed: 11976841] □
7. Ballard RB, Rozycki GS, Knudson MM, et al. The surgeon's use of ultrasound in the acute setting. *Surg Clin North Am*. 1998;78:337. [PubMed: 9602850] □
8. Stengel D, Bauwens K, Sehouli J, et al. Emergency ultrasound-based algorithms for diagnosing blunt abdominal trauma. *Cochrane Database Syst Rev*. 2005;2:CD004446.
9. Salim A, Sangthong B, Martin M, Brown C, Plurad D, Demetriaeds D. Whole body imaging in blunt multisystem trauma patients without obvious signs of injury. *Arch Surg*. 2006;141:468. [PubMed: 16702518] □

-
10. Huber-Wagner S, Lefering R, Qvick LM, et al. Effect of whole body CT during trauma resuscitation on survival: a retrospective, multicentre study. *Lancet.* 2009;373(9763):1455. [PubMed: 19321199] □
11. Becker CD, Poletti PA. The trauma concept: the role of MDCT in the diagnosis and management of visceral injuries. *Eur Radiol.* 2005;15:D105. [PubMed: 16479658] □
12. Fang JF, Wong YC, Lin BC, et al. Usefulness of multidetector computed tomography for the initial assessment of blunt abdominal trauma patients. *World J Surg.* 2006;30:176. [PubMed: 16411014] □
13. Dreizin D, Munera F. Blunt polytrauma: Evaluation with 64-section whole-body CT angiography. *Radiographics.* 2012;32:609. [PubMed: 22582350] □
14. Linsenmaier U, Krotz M, Hauser H, et al. Whole-body computed tomography in polytrauma: techniques and management. *Eur Radiol.* 2002;12:1728. [PubMed: 12111064] □
15. Novelline RA, Rhea JT, Rao PM, et al. Helical CT in emergency radiology. *Radiology.* 1999;213:321. [PubMed: 10551209] □
16. Toyama Y, Kobayashi T, Nishiyama Y, et al. CT for acute stage of closed head injury. *Radiat Med.* 2005;23:309. [PubMed: 16342901] □
17. Parizel PM, Van Goethem JW, Ozsarlar O, et al. New developments in the neuroradiological diagnosis of craniocerebral trauma. *Eur Radiol.* 2005;15:569. [PubMed: 15696294] □
18. Oman JA, Cooper RJ, Holmes JF, et al. Performance of a decision rule to predict need for computed tomography among children with blunt head trauma. *Pediatrics.* 2006;117:e238. [PubMed: 16418311] □
19. Mower WR, Hoffman JR, Herbert M, et al. Developing a decision instrument to guide computed tomographic imaging of blunt head injury patients. *J Trauma.* 2005;59:954. [PubMed: 16374287] □
20. de Lacey G, McCabe M, Constant O, et al. Testing a policy for skull radiography (and admission) following mild head injury. *Br J Radiol.* 1990;63:14. [PubMed: 2306583] □
21. Holmgren EP, Dierks EJ, Assael LA, et al. Facial soft tissue injuries as an aid to ordering a combination head and facial computed tomography in trauma patients. *J Oral Maxillofac Surg.* 2005;63:651. [PubMed: 15883940] □
22. Whitesell RT, Steenburg SD, Lin H, Shen C. Facial fracture in the setting of whole body computed tomography for trauma: incidence and clinical predictors. *AJR.* 2015;205(1):W4. [PubMed: 26102417] □
23. Lambert DM, Mirvis SE, Shanmuganathan K, et al. Computed tomography exclusion of osseous paranasal sinus injury in blunt trauma patients: the "clear sinus" sign. *J Oral Maxillofac Surg.* 1997;55:1207; discussion 1210. [PubMed: 9371108] □
24. Dos Santos DT, Costa e Silva AP, Vannier MW, et al. Validity of multislice computerized tomography for diagnosis of maxillofacial fractures using an independent workstation. *Oral Surg Oral Med Oral Pathol Oral Radiol Endod.* 2004;98:715. [PubMed: 15583546] □
25. Saigal K, Winokur RS, Finden S, et al. Use of three-dimensional computerized tomography reconstruction in complex facial trauma. *Facial Plast Surg.* 2005;21:214. [PubMed: 16307402] □
26. Rake PA, Rake SA, Swift JQ, et al. A single reformatted oblique sagittal view as an adjunct to coronal computed tomography for the evaluation of orbital floor fractures. *J Oral Maxillofac Surg.* 2004;62:456. [PubMed: 15085513] □
27. Ploder O, Klug C, Voracek M, et al. Evaluation of computer-based area and volume measurement from coronal computed tomography scans in isolated blowout fractures of the orbital floor. *J Oral Maxillofac Surg.* 2002;60:1267; discussion 1273. [PubMed: 12420258] □

-
28. Brenner D, Elliston C, Hall E, Berdon W. Estimated risks of radiation-induced fatal cancer from pediatric CT. *AJR Am J Roentgenol.* 2001;176:289. [PubMed: 11159059] □
29. Becker M, Duboe P-D, Platon A, et al. MDCT in the assessment of laryngeal trauma: value of 2D multiplanar and 3D reconstructions. *AJR Am J Roentgenol.* 2013;201:W639. [PubMed: 24059404] □
30. Chen JD, Shanmuganathan K, Mirvis SE, Killeen KL, Dutton RP. Using CT to diagnose tracheal rupture. *AJR Am J Roentgenol.* 2001;176(5):1273. [PubMed: 11312194] □
31. DemetriaDES D, Velmahos GG, Aesnso JA. Cervical pharyngoesophageal and laryngotracheal injuries. *World J Surg.* 2001;25(8):1044. [PubMed: 11571970] □
32. McConnell DB, Trunkey DD. Management of penetrating trauma to the neck. *Adv Surg.* 1994;27:97. [PubMed: 8140981] □
33. LeBlang SD, Nuñez DB Jr. Noninvasive imaging of cervical vascular injuries. *AJR Am J Roentgenol.* 2000;174:1269. [PubMed: 10789775] □
34. Bub LD, Hollingsworth W, Jarvik JG, et al. Screening for blunt cerebrovascular injury: evaluating the accuracy of multidetector computed tomographic angiography. *J Trauma.* 2005;59:691. [PubMed: 16361914] □
35. Sliker CW. Blunt cerebrovascular injuries: imaging with multidetector CT angiography. *Radiographics.* 2008;28(6):1689. [PubMed: 18936030] □
36. Liang T, Tso DK, Chiu RYW, Nicolaou S. Imaging of blunt vascular neck injuries: a review of screening and imaging modalities. *AJR Am J Roentgenol.* 2013;201:884. [PubMed: 24059380] □
37. Sliker CW, Shanmuganathan K, Mirvis SE. Diagnosis of blunt cerebrovascular injuries with 16-MDCT: accuracy of whole-body MDCT compared with neck MDCT angiography. *AJR Am J Roentgenol.* 2008;190(3):790. [PubMed: 18287454] □
38. Biffl WL, Egglon T, Benedetto B, et al. Sixteen-slice computed tomographic angiography is a reliable noninvasive screening test for clinically significant blunt cerebrovascular injuries. *J Trauma.* 2006;60:745; discussion 751. [PubMed: 16612293] □
39. Biffl WL. Diagnosis of blunt cerebrovascular injuries. *Curr Opin Crit Care.* 2003;9:530. [PubMed: 14639074] □
40. Cothren CC, Moore EE, Ray CE Jr, et al. Carotid artery stents for blunt cerebrovascular injury: risks exceed benefits. *Arch Surg.* 2005;140:480; discussion 485. [PubMed: 15897444] □
41. Mutze S, Rademacher G, Matthes G, et al. Blunt cerebrovascular injury in patients with blunt multiple trauma: diagnostic accuracy of duplex Doppler US and early CT angiography. *Radiology.* 2005;237:884. [PubMed: 16251399] □
42. Bromberg WJ, Collier BC, Diebel LN, et al. Blunt cerebrovascular injury practice management guidelines: the Eastern Association for the Surgery of Trauma. *J Trauma.* 2010;68(2):471. [PubMed: 20154559] □
43. Miller PR, Fabian TC, Croce MA, et al. Prospective screening for blunt cerebrovascular injuries: analysis of diagnostic modalities and outcomes. *Ann Surg.* 2002;236:386; discussion 393. [PubMed: 12192325] □
44. Stein DM, Boswell S, Sliker CW, Lui FY, Scalea TM. Blunt cerebrovascular injuries: does treatment always matter? *J Trauma.* 2009;66:132. [PubMed: 19131816] □
45. Inaba K, Brano BC, Menaker J, et al. Evaluation of multidetector computed tomography for penetrating neck injury: a prospective multicenter study. *J Trauma Acute Care Surg.* 2012;72(3):576. [PubMed: 22491539] □
46. Múnera F, Soto JA, Palacio D, et al. Diagnosis of arterial injuries caused by penetrating trauma to the neck: comparison of helical CT angiography

-
- and conventional angiography. *Radiology*. 2000;216(2):356. [PubMed: 10924553] □
47. Múnera F, Soto JA, Palacio DM, et al. Penetrating neck injuries: helical CT angiography for initial evaluation. *Radiology*. 2002;224(2):366. [PubMed: 12147829] □
48. Inaba K, Muñera F, McKenney M, et al. Prospective evaluation of screening multislice helical computed tomographic angiography in the initial evaluation of penetrating neck injuries. *J Trauma*. 2006;61(1):144. [PubMed: 16832262] □
49. Shiroff AM, Gale SC, Martin ND, et al. Penetrating neck trauma: a review of management strategies and discussion of the “no zone” approach. *Am Surg*. 2013;79(1):23. [PubMed: 23317595] □
-
50. Holmes JF, Akkineni R. Computed tomography versus plain radiography to screen for cervical spine injury: a meta-analysis. *J Trauma*. 2005;58(5):902. [PubMed: 15920400] □
51. Stiell IG, Wells GA, Vandemheen KL, et al. The Canadian C-spine rule for radiography in alert and stable trauma patients. *JAMA*. 2001;286:1841. [PubMed: 11597285] □
-
52. Hoffman JR, Wolfson AB, Todd K, et al. Selective cervical spine radiography in blunt trauma: methodology of the National Emergency X-Radiography Utilization Study (NEXUS). *Ann Emerg Med*. 1998;32:461. [PubMed: 9774931] □
53. Holmes JF, Panacek EA, Miller PQ, et al. Prospective evaluation of criteria for obtaining thoracolumbar radiographs in trauma patients. *J Emerg Med*. 2003;24:1. [PubMed: 12554032] □
-
54. Hsu JM, Joseph T, Ellis AM. Thoracolumbar fracture in blunt trauma patients: guidelines for diagnosis and imaging. *Injury*. 2003;34:426. [PubMed: 12767788] □
-
55. Brohi K, Healy M, Fotheringham T, et al. Helical computed tomographic scanning for the evaluation of the cervical spine in the unconscious, intubated trauma patient. *J Trauma*. 2005;58:897. [PubMed: 15920399] □
56. Kuhns L. *Imaging of Spinal Trauma in Children*. Hamilton, Ontario, Canada: BC Decker Inc; 1998.
-
57. Wang JC, Hatch JD, Sandhu HS, Delamarter RB. Cervical flexion and extension radiographs in acutely injured patients. *Clin Orthop Relat Res*. 1999;365:111.
-
58. Blackmore CC, Emerson SS, Mann FA, et al. Cervical spine imaging in patients with trauma: determination of fracture risk to optimize use. *Radiology*. 1999;211:759. [PubMed: 10352603] □
-
59. Hanson JA, Blackmore CC, Mann FA, et al. Cervical spine injury: a clinical decision rule to identify high-risk patients for helical CT screening. *AJR Am J Roentgenol*. 2000;174:713. [PubMed: 10701614] □
-
60. Hernandez JA, Chupik C, Swischuk LE. Cervical spine trauma in children under 5 years: productivity of CT. *Emerg Radiol*. 2004;10:176. [PubMed: 15290484] □
-
61. Van Goethem JW, Maes M, Ozsarlar O, et al. Imaging in spinal trauma. *Eur Radiol*. 2005;15:582. [PubMed: 15696292] □
-
62. Richards PJ. Cervical spine clearance: a review. *Injury*. 2005;36:248; discussion 270. [PubMed: 15664589] □
-
63. Sliker CW, Mirvis SE, Shanmuganathan K. Assessing cervical spine stability in obtunded blunt trauma patients: review of medical literature. *Radiology*. 2005;234:733. [PubMed: 15734929] □
-
64. Miller LA. Chest wall, lung and pleural space trauma. *Radiol Clin North Am*. 2006;44(2):213. [PubMed: 16500204] □

-
65. Holmes JF, Sokolove PE, Brant WE, et al. A clinical decision rule for identifying children with thoracic injuries after blunt torso trauma. *Ann Emerg Med.* 2002;39:492. [PubMed: 11973556] □
66. Blackmore CC, Zweibel A, Mann FA. Determining risk of traumatic aortic injury: how to optimize imaging strategy. *AJR Am J Roentgenol.* 2000;174:343. [PubMed: 10658702] □
67. Steenburg SD, Ravenel JG. Acute traumatic thoracic aortic injuries: experience with 64-MDCT. *AJR Am J Roentgenol.* 2008;191:1564. [PubMed: 18941102] □
68. Malhotra AK, Fabian TC, Croce MA, Weiman DS, Gavant ML, Pate JW. Minimal aortic injury: a lesion associated with advancing diagnostic techniques. *J Trauma.* 2001;51(6):1042. [PubMed: 11740248] □
69. Gunn ML, Lehnert BE, Lungren RS, et al. Minimal aortic injury of the thoracic aorta: imaging appearances and outcome. *Emerg Radiol.* 2014;21(3):227. [PubMed: 24414144] □
70. Omert L, Yeaney WW, Protetch J. Efficacy of thoracic computerized tomography in blunt chest trauma. *Am Surg.* 2001;67:660. [PubMed: 11450784] □
71. Desir A, Ghaye B. CT of blunt diaphragmatic rupture. *Radiographics.* 2012;32:477. [PubMed: 22411944] □
72. Holmes JF, Ngyuen H, Jacoby RC, et al. Do all patients with left costal margin injuries require radiographic evaluation for intraabdominal injury? *Ann Emerg Med.* 2005;46:232. [PubMed: 16126132] □
73. Shanmuganathan K, Mirvis SE, Chiu WC, Killeen KL, Hogan GJ, Scalea TM. Penetrating torso trauma: triple-contrast helical CT in peritoneal violation and organ injury—a prospective study in 200 patients. *Radiology.* 2004;231:775. [PubMed: 15105455] □
74. Brown CK, Dunn KA, Wilson K, et al. Diagnostic evaluation of patients with blunt abdominal trauma: a decision analysis. *Acad Emerg Med.* 2000;7:385. [PubMed: 10805630] □
75. Schurink GW, Bode PJ, van Luijt PA, van Vugt AB. The value of physical examination in the diagnosis of patients with blunt abdominal trauma: a retrospective study. *Injury.* 2007;28:261.
76. Bosnak AR, Shanmuganathan K, Mirvis SE, et al. Optimizing trauma multidetector CT protocol for blunt splenic injury: need for arterial and portal venous phase scans. *Radiology.* 2013;268(1):79. [PubMed: 23449955] □
77. Marmery H, Shanmuganathan K, Mirvis SE, et al. Correlation of MDCT findings with splenic arteriography and surgery: prospective study in 392 patients. *J Am Coll Surg.* 2008;206:685. [PubMed: 18387475] □
78. Ryan MF, Hamilton PA, Chu P, et al. Active extravasation of arterial contrast agent on post-traumatic abdominal computed tomography. *Can Assoc Radiol J.* 2004;55:160. [PubMed: 15237777] □
79. Sheridan MK, Blackmore CC, Linnau KF, et al. Can CT predict the source of arterial hemorrhage in patients with pelvic fractures? *Emerg Radiol.* 2002;9:188. [PubMed: 15290561] □
80. Brown CV, Kasotakis G, Wilcox A, et al. Does pelvic hematoma on admission computed tomography predict active bleeding at angiography for pelvic fracture? *Am Surg.* 2005;71:759. [PubMed: 16468513] □
81. Poletti PA, Mirvis SE, Shanmuganathan K, et al. CT criteria for management of blunt liver trauma: correlation with angiographic and surgical findings. *Radiology.* 2000;216:418. [PubMed: 10924563] □
82. Vaccaro JP, Brody JM. CT cystography in the evaluation of major bladder trauma. *Radiographics.* 2000;20(5):1373. [PubMed: 10992026] □

-
83. Horstman WG, McClellan BL, Heiken JP. Comparison of computed tomography and conventional cystography for detection of traumatic bladder rupture. *Urol Radiol.* 1991;12:188. [PubMed: 2042269] □
84. Watts DD, Fakhry SM, EAST Multi-Institutional Hollow Viscus Injury Research Group. Incidence of hollow viscus injury in blunt trauma: an analysis from 275,557 trauma admissions from the EAST multi-institutional trial. *J Trauma.* 2003;54:289. [PubMed: 12579054] □
85. Brofman N, Atri M, Hanson JM, et al. Evaluation of bowel and mesenteric blunt trauma with multidetector CT. *Radiographics.* 2006;26:1119. [PubMed: 16844935] □
86. Killeen KL, Shanmuganathan K, Poletti PA, Cooper C, Mirvis SE. Helical computed tomography of bowel and mesenteric injuries. *J Trauma.* 2001;51:26. [PubMed: 11468463] □
87. Steenburg SD, Petersen MJ, Shen C, Lin H. Multi-detector CT of blunt mesenteric injuries: usefulness of imaging findings for predicting surgically significant bowel injuries. *Abdom Imaging.* 2015;40(5):1026. [PubMed: 25296995] □
88. Yu J, Fulcher AS, Wang DB, et al. Frequency and importance of small amount of isolated pelvic free fluid detected with multidetector CT in male patients with blunt trauma. *Radiology.* 2010;256(3):799. [PubMed: 20720068] □
89. Fakhry SM, Brownstein M, Watts DD, Baker CC, Oller D. Relatively short diagnostic delays (<8 h) produce morbidity and mortality in blunt small bowel injury: an analysis of time to operative intervention in 198 patients from a multicenter experience. *J Trauma.* 2000;48:408; discussion 414. [PubMed: 10744277] □
90. Hunter JC, Brandser EA, Tran KA. Pelvic and acetabular trauma. *Radiol Clin North Am.* 1997;35:559. [PubMed: 9167663] □
91. Durkee NJ, Jacobson J, Jamadar D, Karunakar MA, Morag Y, Hayes C. Classification of common acetabular fractures: radiographic and CT appearances. *AJR Am J Roentgenol.* 2006;187(4):915. [PubMed: 16985135] □
92. Stiell IG, Greenberg GH, McKnight RD, et al. Decision rules for the use of radiography in acute ankle injuries. Refinement and prospective validation. *JAMA.* 1993;269:1127. [PubMed: 8433468] □
93. Stiell IG, Greenberg GH, Wells GA, et al. Prospective validation of a decision rule for the use of radiography in acute knee injuries. *JAMA.* 1996;275:611. [PubMed: 8594242] □
94. Stiell IG, Wells GA, Hoag RH, et al. Implementation of the Ottawa knee rule for the use of radiography in acute knee injuries. *JAMA.* 1997;278:2075. [PubMed: 9403421] □
95. Feliciano DV, Moore FA, West MA, et al. Evaluation and management of peripheral vascular injury. Part I. *J Trauma.* 2011;70:1551. [PubMed: 21817992] □
96. Jens S, Kerstens MK, Legemate DA, Reekers JA, Bipat S, Koelemay MJW. Diagnostic performance of CT angiography in peripheral arterial injury due to trauma: a systematic review and meta-analysis. *Eur J Vasc Endo Surg.* 2013;46(3):329.
97. Nguyen C, Saksobahavivat N, Steenburg SD, et al. MDCT diagnosis of post-traumatic hepatic arterio-portal fistulas. *Emerg Radiol.* 2013;20:225. [PubMed: 23238891] □
98. Haan JM, Biffl W, Knudson MM, et al. Splenic embolization revisited: a multicenter review. *J Trauma.* 2004;56:542. [PubMed: 15128125] □
99. Zarzaur BL, Koza R, Myers JG, et al. The splenic injury outcomes trial: an Association for the Surgery of Trauma multi-institutional study. *J Trauma Acute Care Surg.* 2015;79(3):335. [PubMed: 26307863] □
100. Marmery H, Shanmuganathan K, Alexander MT, Mirvis SE. Optimization of selection for nonoperative management of blunt splenic injury:

comparison of MDCT grading systems. *AJR Am J Roentgenol.* 2007;189(6):1421. [PubMed: 18029880] □

101. Saksobhavivat N, Shanmuganathan K, Chen HH, et al. Blunt splenic injury: use of a multidetector CT-based splenic injury grading system and clinical parameters for triage of patients at admission. *Radiology.* 2015;274(3):702. [PubMed: 25474179] □

102. White CE, Hsu JR, Holcomb JB. Haemodynamically unstable pelvic fractures. *Injury* 2009;40(10):1023. [PubMed: 19371871] □
